Mechanisms of phenazine-mediated extracellular electron transfer by *Pseudomonas aeruginosa*

Thesis by

Scott Harrison Saunders

In Partial Fulfillment of the Requirements for the
degree of
Doctor of Philosophy in Biology

CALIFORNIA INSTITUTE OF TECHNOLOGY
Pasadena, California

2020
(Defended March 26, 2020)

Scott Harrison Saunders
ORCID: 0000-0003-4224-9106

ACKNOWLEDGEMENTS

I am writing this during the coronavirus pandemic of 2020, and that puts some things in perspective. Caltech has now decreed that despite how important our science may be, our experiments are in fact non-essential when faced with a global emergency. It is a stark reminder that we sometimes take our science too seriously. Yet, in this time of need we also see the public turning to scientists for expert guidance and solutions. We are seeing that the scientific community has the power to help, and that collective mission to help society is our essential role. That said, I did not always know I would be part of that scientific community; there were many decisions and influences that could have put me on a different trajectory. Who knows what the outcome of those other timelines would have been – good, bad, or just different? Regardless, I feel that getting my PhD is certainly an accomplishment, and there is no way that this degree would have been possible without the guidance and support of countless people that have touched my life.

In order to properly acknowledge these people, I'd like to take a moment to explain how I have come to view research over the course of my PhD. First, let's admit that science is hard. Experiments do not work, biology is complicated, and solving problems is intellectually difficult. But beyond those academic challenges, there lie much deeper emotional challenges that I did not fully understand when I started graduate school. Though we as scientists and experimentalists try to be robotic dispassionate observers, we are not. We are messy, emotional, biased human beings. There were times I felt alone, but I never truly was. I absolutely would not have been able to deal with these challenges on my own, and whether they realized it or not, many of the people below helped keep me sane. So, for those moments of genuine human connection: big and small – thank you.

To my immediate and extended family, thank you for your constant love and support, and I'm sorry that I moved so far away for grad school – I have missed you all. To my parents, Amy and Ed Saunders, thank you for giving me every opportunity to succeed. You encouraged me to follow whatever career path I wanted, taught me to be kind, and told me to never give up. To my brother, Daniel Saunders, thank you for always being willing to talk

about science, technology, or politics and for the baked goods. To my grandmother, Joyce Harris, thank you for hosting countless family get-togethers and maintaining an endless supply of chocolate and candy. I was so lucky to grow up with such a tight-knit family. To my grandmother, Penny Saunders, thank you for teaching me about art and cooking – I use those skills quite often in science and in life. You inspire me to live life to the fullest. To my grandfather, Jeff Saunders, as a kid I didn't fully realize that you were training me to be a scientist. You taught me to question everything, remain curious, and to laugh at my own jokes. You'll be happy to know that I use microscopes periodically, and I often think of you and your basement laboratory. Thank you for making my childhood unique.

To my fiancée, Alicia Rogers, there's no one I'd rather be quarantined with. You put up with me and you support me every day and I'm really not sure I could have done this without you – I am forever grateful. Specific to this degree, I also admire you immensely as a scientist, and I can only aspire to achieve your organization, efficiency, and competence. My best memories of Caltech will always be getting coffee with you and walking to the turtle pond to see Peg (the turtle missing one foot). To our pets, Uma, Gimbel, and Ethel, thank you for supporting me with (mostly) unconditional love and cuteness through this period of my life.

To my advisor, Dianne Newman, thank you for always being on my team. You always understood that I was not a microbiology robot. We are different people and I will forever appreciate that you always tried to understand my perspective and exercised immense patience and compassion. Scientifically, you have given me the greatest gift – the courage to pursue a question no matter where it takes me. To this day, I feel that you and Caltech took a chance on me. We'll see how it works out, but no matter what, I will always owe so much of my career to you. Thank you.

To my collaborators, Jackie Barton and Lenny Tender, through our interactions I have grown scientifically and personally. Thank you for pushing me and supporting me. Thank you to the members of their labs that helped me over the years, particularly Matthew Yates, Edmund Tse, and Fernanda Jimenez Otero.

I must sincerely thank all of my wonderful lab mates for their scientific and non-scientific support over the years.

Current lab members

To Brittany Belin, thank you for being the best bay mate ever. I always appreciate your honest comments on science and life. To Lucas Andrade Mereilles, thank you for always being a friend. Your soccer skills are only matched by your science skillz. To Elena Perry, thank you for your insightful comments and for our wonderful trip to Brazil. To Elise Tookmanian, thank you for always being kind. To Melanie Spero, thank you for reminding me not to take science too seriously. To Lev Tyspin, thank you for giving me hope in the next generation. To John Ciemniecki, thank you for giving me an appreciation for some of the finer things in life – freshly ground coffee, fountain pens, and poetry. To Renee Wang, thank you for filling the lab with your sunny disposition and genuine curiosity. To Kurt Dahlstrom, thank you for filling the lab with your fungus and strange sense of humor. To Chelsea VanDrisse, thank you for your contagious enthusiasm especially regarding lab organization and genetics. To Darcy McRose, thank you for your helpful suggestions in lab and for making me appreciate my electrochemistry skills. To Daniel Dar, thank you for brainstorming crazy ideas with me. To Steven Wilbert, thank you for your beautiful images and delightful attitude. To Shannon Park, thank you for supporting everything we do in the lab. To Kristy Nguyen, thank you for supporting me in the lab, and for always lending a friendly ear.

Past lab members

To Megan Bergkessel, thank you for always taking the time to discuss science, pets, and life with me. Your scientific rigor and generosity are infectious, and I often try to imagine what you would say to me and others. To Kyle Costa, thank you for mentoring me in science and Catan as a young graduate student. To Will DePas, thank you for bringing both levity and Ruth to our side of the lab. To Nate Glasser, thank you for being my phenazine guide and inspiring me to invest the time and effort to solve worthwhile problems. To David Basta, thank you for showing me it's possible to be a meticulous experimentalist and not lose

enthusiasm, despite the challenges. To Lisa Racki, thank you for showing me that hard work and good scientific questions prevail. To Naomi Kreamer, thank you for warning me that I would hate my thesis project by the end of it. To Nick Shikuma, Christian Salgado, Ruth Lee, Elise Cowley, Sebastian Kopf, Gargi Kulkarni, Chia Wu, Jessica Ricci, and Peter Jorth, thank you for our many pleasant interactions. Thank you to alumni Suzanne Kern, Yun Wang, Lars Dietrich, Tracy Teal, Nora Sullivan, Andreas Kappler, whose work has helped me.

To Liz Ayala and Raina Beaven, thank you for all your support over the years. You have always been so kind and friendly to me, and I feel that I got to know the department much better while we planned graduate recruitment together. To the Marine Biological Laboratory Microbial Diversity Course 2017 staff and students, thank you for opening my eyes to new parts of the microbial world. To Justin Bois and Griffin Chure, thank you for inspiring me to up the rigor of my research by making my analyses reproducible.

To my undergraduate research mentor, Dr. Andrew Park, thank you for introducing me to the world of research. You gave me independence and the wonderful gift of R. To my NOAA summer internship mentor, Dr. Paul McElhany, thank you for introducing me to the world of experiments in all their messy glory.

To all my friends near and far that have supported me through this PhD directly and indirectly, thank you.

ABSTRACT

Extracellular electron transfer (EET), the process whereby cells access electron acceptors or donors that reside many cell lengths away, enables metabolic activity by microorganisms, particularly under oxidant-limited conditions that occur in multicellular bacterial biofilms. Although different mechanisms underpin this process in individual organisms, a potentially widespread strategy involves extracellular electron shuttles, redox-active metabolites that are secreted and recycled by diverse bacteria. Here, I first review general aspects of the electron shuttling strategy, such as the chemical diversity and potential distribution of electron shuttle producers and users, and the costs associated with electron shuttle biosynthesis. Then I address the long-standing question: how do these electron shuttles catalyze electron transfer within biofilms without being lost to the environment? I show that phenazine electron shuttles mediate efficient EET through interactions with extracellular DNA (eDNA) in *Pseudomonas aeruginosa* biofilms, which are important in nature and disease. Retention of pyocyanin (PYO) and phenazine carboxamide in the biofilm matrix is facilitated by binding to eDNA. In vitro, different phenazines can exchange electrons in the presence or absence of DNA and phenazines can participate directly in redox reactions through DNA; the biofilm eDNA can also support rapid electron transfer between redox-active intercalators. Electrochemical measurements of biofilms indicate that retained PYO supports an efficient redox cycle with rapid EET and slow loss from the biofilm. Together, these results establish that eDNA facilitates phenazine metabolic processes in *P. aeruginosa* biofilms, suggesting a model for how extracellular electron shuttles achieve retention and efficient EET in biofilms.

PUBLISHED CONTENT AND CONTRIBUTIONS

*Glasser, N. R., *Saunders, S. H., & Newman, D. K. (2017). The colorful world of extracellular electron shuttles. *Annual Review of Microbiology*, 71, 731–751. doi.org/10.1146/annurev-micro-090816-093913

SHS participated in writing the manuscript.

*Contributed equally

Saunders, S. H., Edmund, C. M., Yates, M. D., Otero, F. J., Trammell, S. A., Stemp, E. D, **Barton, J. K., **Tender, L. M. & **Newman, D. K. (2019). Extracellular DNA promotes efficient extracellular electron transfer by pyocyanin in *Pseudomonas aeruginosa* biofilms. *bioRxiv*. doi.org/10.1101/2019.12.12.872085

SHS participated in designing and performing experiments and writing the manuscript.

**Corresponding authors

TABLE OF CONTENTS

INTRODUCTION

"Life is the greatest ~~chemist~~ electrochemist."

-Adapted from Frances Arnold

How cells generate energy has been studied in detail for over a century, and broadly we understand that cells have exquisite mechanisms to capture energy as electrons move from high energy states to lower energy states. Therefore, energy is extracted from input molecules (i.e. food) through electron transfer reactions. One of the most beautiful examples of such a metabolic process is the mitochondrial electron transport chain (ETC) that generates most of the energy in our cells. This system is a set of membrane bound complexes that take high energy electrons stripped off of food molecules and facilitate sequential redox reactions to oxygen, the terminal electron acceptor. Each reaction cleverly captures the energy released by pumping protons across the membrane, and the resulting electrochemical proton gradient can be used directly or indirectly to power nearly every cellular process. However, the linear eukaryotic ETC we are taught from textbook diagrams is shockingly mundane compared to the diversity and complexity of bacterial and archaeal systems.

"Bacteria are the greatest chemists on the planet."

-Dianne Newman

Collectively, the Bacteria are capable of eating nearly all organic molecules and using them as high energy electron donors. Beyond oxygen, these organisms can use many different terminal electron acceptors like nitrate, sulfate and DMSO. For a given bacterium, there are often branched electron transport chains, containing different options for each step of the pathway, that allow for single cells to perform radically different metabolisms when needed. The bacterial ETC has long been appreciated, since much of this complexity exists in *Escherichia coli* – no exotic organisms required. However, in the last 20 years, a few relatively exotic organisms have taught us about an even more astonishing extension of electron transport systems in bacteria.

Unlike mitochondria or *E. coli*, *Shewanella* and *Geobacter* species can use insoluble terminal electron acceptors that cannot react with the ETC complexes at the inner membrane of the cell. Instead, these organisms possess extra ETC components that extend from the inner membrane, through the periplasm, to the outer membrane and beyond. These systems enable these organisms to respire solid minerals that only exist outside of the cell – this metabolism is known as extracellular electron transfer (EET). The common critical component of this pathway is an additional set of cytochromes – proteins containing redox-active heme groups. Specifically, there are multiheme cytochromes found in the outer membrane that provide a conduit for electrons to move to the outer edge of the cell. These proteins are fascinating, and their distinctive heme binding site motifs led to an explosion of discovery that revealed the existence of EET machinery in countless organisms found in genomic databases.

The outer membrane cytochrome system is striking, but it only transfers electrons to the very outer edge of the cell – no further. This works when single cells can attach directly onto minerals, but bacteria rarely live as single cells – they live as dense surface-attached communities known as biofilms. How can these systems function when cells are physically separated from their terminal electron acceptor, either because it is insoluble and distant or depleted locally? Much work has been done on "nanowires" in *Shewanella* and *Geobacter*, which may serve as physical extensions of the cell, connecting relatively distant electron acceptors back to the outer membrane cytochrome complexes. The mechanism and importance of these structures is still being clarified, but cells can also access electron acceptors via a different EET pathway. Instead of creating physical extensions of the cells, certain organisms seem to be capable of secreting small redox-active molecules that can carry electrons to distant electron acceptors. These molecules are called electron shuttles.

Chapter 1 explores this electron shuttling strategy for EET based on literature and uses that foundation to speculate on general principles and prevalence. It reviews literature on two relatively characterized electron shuttles – flavins used by *Shewanella oneidensis* and phenazines used by *Pseudomonas aeruginosa.* Apart from those two examples, this work

tries to identify other potential electron shuttling systems among known redox-active metabolites and redox-sensing transcription factors in the Bacteria. More generally, the feasibility of an electron shuttling strategy is discussed in terms of biosynthetic cost and diffusive flux. Lastly, this review provides an experimental roadmap to characterize new electron shuttles.

Chapter 2 dives into the phenazine-based electron shuttling system used by *P. aeruginosa.* Broadly, this manuscript tries to understand how phenazines can support electron transfer through the biofilm matrix. This is a complicated question, but it is broken down into two simpler questions. 1) Are phenazines retained in the biofilm matrix? 2) What is the mechanism of electron transfer? By starting to answer these questions, a more specific and complicated model of multi-phenazine EET could be proposed. This model and the supporting data are the author's primary scientific contributions to the field.

While Chapter 2 focuses on extracellular processes, the appendix discusses a preliminary attempt to characterize the cell-associated genetic determinants of phenazine electron shuttling. A pooled transposon-based screen was performed in a liquid culture system to assay phenazine dependent survival metabolism. Therefore, the screen identified genes important for single cells to survive using phenazines in this condition. The dataset contains many fascinating effects and may be useful for future phenazine aficionados.

Like the ETC, phenazines have also been studied (on and off) for over a century. Although we know a good deal about these molecules' genetics and chemistry, there is so much we don't know. Maybe one day there will be a satisfying textbook diagram of a phenazine electron transport system. Maybe then phenazine EET will seem mundane compared to the next discovery of microbial ingenuity. Certainly, the microbial world is full of many more surprises.

C h a p t e r 1

THE COLORFUL WORLD OF EXTRACELLULAR ELECTRON SHUTTLES

This work was first published as:

*Glasser, N. R., *Saunders, S. H., & Newman, D. K. (2017). The colorful world of extracellular electron Shuttles. *Annual Review of Microbiology*, 71, 731–751. doi.org/10.1146/annurev-micro-090816-093913

*Contributed equally

Abstract

Descriptions of the changeable, striking colors associated with secreted natural products date back well over a century. These molecules can serve as extracellular electron shuttles (EES) that permit microbes to access substrates at a distance. In this review, we argue that the colorful world of EES has too-long been neglected. Rather than simply serving as a diagnostic attribute of a particular microbial strain, redox-active natural products likely play fundamental, underappreciated roles in the biology of their producers, particularly those that inhabit biofilms. Here, we describe the chemical diversity and potential distribution of EES producers and users, discuss the costs associated with their biosynthesis, and critically evaluate strategies for their economical usage. We hope this review will inspire efforts to identify and explore the importance of EES cycling by a wide range of microorganisms, so that their contributions to shaping microbial communities can be better assessed and exploited.

1. Introduction

The microbial world is nothing if not colorful. Colorful figuratively, in that microbes accomplish stunning metabolic feats, which, increasingly, are being recognized for their important roles in promoting human health (20, 118), shaping the composition of the atmosphere, lithosphere and hydrosphere (59), and biotechnological potential (72), to list only a few examples. Colorful literally, in that they produce a spectacular range of pigments, representing every rainbow hue. This latter aspect of microbial identity is often the first thing one notices about a strain when it is streaked upon a plate, whether its pigments are tightly associated with its colonies or rapidly diffuse away. Flipping through Bergey's Manual of Systematic Bacteriology (43), one can find numerous examples of organisms that have been named after the colors they produce (*e.g. Pseudomonas aeruginosa (131), Pseudoalteromonas luteoviolacia (44), Streptomyces coelicolor (19)*, etc.), yet the biological functions of these defining pigments are seldom discussed. Both old (40) and emerging evidence (49, 56, 95), however, suggests that literal colorfulness may underpin figurative colorfulness, particularly when the pigment in question has the property of *changing* color.

Color changes are often indicative of redox-reactions, and the redox properties of many colorful excreted metabolites confer upon them rich potential (bio)chemical reactivity. Such reactivity, when combined with their ability to cycle in and out of the cells that produce them, permit these molecules to serve as extracellular electron shuttles (EES). While we use the word "extracellular" to draw attention to the fact that these metabolites can leave the cell in their reduced state to transfer electrons to a distant extracellular oxidant, equally important to the definition of microbial electron shuttles is that they can return to the cell in the oxidized state, whereupon they are re-reduced (Fig. 1a). It is the cycling of EES and their facilitation of electron transfer both within and without the cell that underpins their important physiological functions. Several years ago, we made a distinction between two types of EES, classifying them according to whether microorganisms produce them (endogenous) or whether they are already present in an environment (exogenous) (56). Endogenous EES, for example, include microbial metabolites that are often considered to be redox-active antibiotics (95); exogenous EES include a chemically heterogeneous fraction of organic compounds that derive from the degradation of microbial and plant matter (61, 99).

EES are particularly relevant to situations where microbes have limited access to a critical substrate. For example, an electron acceptor for catabolism might be poorly soluble, as is the case for minerals in many groundwater and sedimentary systems or electrodes in biofuel applications. Alternatively, the substrate might be locally depleted due to rapid consumption by other cells, outpacing its diffusion, as is the case for oxygen in biofilms, be they on the surface of a corroding steel pipeline or in the mucus-filled lungs of an individual living with cystic fibrosis (23, 68, 112, 126). Finally, the substrate might be utilized by another organism in an intimate syntrophic partnership, requiring the passage of electrons between different cell types to catalyze an important biogeochemical reaction, such as the anaerobic oxidation of methane achieved by mixed archaeal-bacterial aggregates (76, 102). In all of these cases, extracellular electron transfer permits the microbes at a distance from the terminal electron acceptor to remain metabolically active.

Cycling of EES represent a strategy whereby microbes can facilitate extracellular electron transfer, yet is by no means the only one. Over the past three decades, investigations into how organisms transfer electrons to or from minerals have revealed that many possess outer membrane cytochromes that are critically important for these processes (106). Whether and/or how electrons traverse through "nanowires" or "cables" or some type of extracellular matrix is still being debated (74, 86, 115, 128). We simply note that in some organisms such as the mineral-reducing bacteria *Shewanella* and *Geobacter*, the proteinaceous machinery that is required for extracellular electron transfer can interact with and reduce EES of different types (16, 66, 71, 110, 117). Thus, it is important to be mindful of the potential involvement of EES in any context where extracellular electron transfer matters—be it the soil of the rhizophere or the inflamed tissues of chronic infections. Moreover, due to their versatile redox activity, EES can play other important biological roles, such as serving as signaling molecules and promoting iron acquisition (32, 55, 93, 122).

In this review, we focus our discussion primarily on colorful, endogenous EES, drawing upon our experience studying phenazines produced by *Pseudomonas aeruginosa* (21, 22, 31-34, 46, 47, 55, 56, 58, 93-96, 116, 120-122) (Fig. 1c). We use phenazines for illustrative purposes only, to pique the reader's curiosity about what other molecules may have similar physiological functions. We critically discuss costs of EES biosynthesis, as well as bioenergetic concerns related to the cell biology of their reduction and potential loss to the environment. Underpinning this review is the conviction that recent advances in mass spectrometry, imaging, and sequencing have the potential to enable dramatic progress in understanding the importance of endogenous EES across diverse microbial systems.

2. Diversity of Endogenous EES and Organisms

How many endogenous EES exist in nature and which organisms produce them? We are only at the threshold of being able to answer this question. The two most well-characterized EES-producing organisms are *Pseudomonas aeruginosa* and *Shewanella oneidensis*, known for their use of phenazines and flavins, respectively (13, 46, 66, 75, 120). Other putative EES-producing organisms, *Lactoccocus lactis, Sphingomonas xenophaga,* and *Klebsiella*

pneumonia, are reported to utilize quinone shuttles (see Table 1) (28, 39, 63, 83, 85). A few other observations in the literature hint at the production of EES by diverse organisms, including *Geothrix* and *Geobacter* species (11, 117), yet in most cases the molecular nature of the putative EES is unknown. Though many secreted redox-active natural products have been well known for decades, such as indigoidine, only recently have their physiological functions begun to be explored (25). Because these types of natural products are genetically encoded in biosynthetic clusters, bioinformatic analysis predicts that EES production by microorganisms may be extensive (Fig. 2). In this section, we discuss the chemical diversity and potential distribution of EES-producers and users as predicted by current bioinformatics platforms. We emphasize that these are *predictions*, which must be validated experimentally (Sidebar 1).

2A. Chemical diversity of EES

Much like their intracellular cousins (*e.g.* NAD(P)H, FAD, and quinones), EES are distinguished by the presence of conjugated bonds, often in the form of heterocyclic aromatic rings. It is this system of conjugated bonds that confers color upon EES. Generally, conjugated bonds are also the molecular origin of an electron shuttle's redox activity, as double bonds can be chemically reduced and rearranged at biologically-accessible reduction potentials. Rearrangement of the conjugated bond system necessarily entails a change in the molecule's absorption spectrum, and so a shuttle's redox activity is inextricably linked to its vibrant and interconvertible colors (Fig. 1c).

Unlike intracellular redox-active metabolites, the endogenous EES described in the literature to date generally lack modifications such as adenylation or lipidation. Instead, they can be decorated with functional groups (*e.g.* amines, carboxylic acids, amides) that tune physical and chemical properties such as the reduction potential, charge state, or solubility. Advances in mass spectrometry and natural product discovery are only beginning to unearth the rich combinatorial diversity of these modifications—as of February 2017, the Dictionary of Natural Products contains over 190 unique phenazine derivatives, 1200 quinones, 1600 napthoquinones, and 2200 anthraquinones (1). While the growth of natural products

databases has far outpaced our ability to empirically study the functions of these molecules, computational chemistry has shown recent progress in predicting their properties such as reduction potential (4). We anticipate that a convergence of metabolomics and computational chemistry, together with the on-going detailed study of select molecules such as phenazines, will implicate many of these redox-active natural products as ubiquitous and diverse EES.

2B. Phylogenetic Diversity

To predict which organisms may produce or utilize EES, we may consider the phylogenetic distribution of genes used to produce or interact with known EES. We might speculate that most organisms could shuttle electrons, since *S. oneidensis* uses a common cofactor, FMN (13). However, it is unclear how many could use flavins in a similar manner, so we will instead focus on more specialized natural products. As an example, we will see that biosynthetic clusters for phenazines are widespread, as well as the redox transcription factor, SoxR, which can sense phenazines.

Biosynthetic clusters. Biosynthetic clusters are organized sets of genes that encode enzymes to produce specific metabolites. Bioinformatic tools are rapidly improving our ability to identify specific natural products (e.g. AntiSmash) (123). The authors of the IMG-ABC database showcased their toolkit with phenazines by identifying ~1000 genomes that contained at least 6 of 7 genes required for phenazine biosynthesis. These species included the well-known phenazine producers Streptomyces and Pseudomonads, but also Alphaproteobacteria, Betaproteobacteria, and other Actinobacteria. It was suggested that a much wider set of species probably produces phenazines than previously thought, and that these new putative producers likely synthesize phenazines with novel chemical structures (52). As the accuracy of these types of bioinformatics tools advance, we may be able to predict an organism's ability to make EES from its genome with reasonable confidence.

SoxR redox sensors. One way to identify potential EES users is to search genomes for machinery that can sense them. Presently, the best-known example is the SoxR transcription factor. SoxR was originally studied in *E. coli* for its role in upregulating the oxidative stress response upon exposure to superoxide generating molecules. It was discovered that SoxR

sensed redox-active molecules through a Fe-S cluster bound by a unique cysteine motif, and its activation prompted sequence-specific binding and transcriptional activation (92). Studies outside of the Enterobacteriacae then showed that SoxR did not upregulate the oxidative stress response in *P. aeruginosa (82)* and *Streptomyces coelicolor (24)*, but that it responded to endogenous redox-active molecules (34, 109) and upregulated factors likely to be involved in their cycling. Comparative genomic analysis found that SoxR is widely distributed through the Bacteria, and it predicted that most organisms do not conform to the original *E. coli* oxidative stress paradigm (34).

Today the IMG database contains ~15,000 bacterial genomes with high-confidence SoxR homologues out of ~47,000 total bacterial genomes (14), approximately the same proportion as the stress sigma factor RpoS. Fig. 2 shows that SoxR homologues are present in 10 bacterial phyla, and that the most representatives are in orders of Proteobacteria and Actinobacteria (38, 69). It should be noted that homologues can be found in majorities of Pseudomonadales (2308 genomes) and Streptomycetes (402 genomes), which are well known for their production of natural products (often redox-active). Strikingly, SoxR homologues are also identified in the emerging and established pathogens of the Mycobacteria (~400 genomes), the agriculturally important Rhizobia (493 genomes) and Frankia (33 genomes), and recently discovered phyla (6 genomes). Whether these organisms use SoxR to sense endogenous EES remains to be determined, but it suggests they might sense exogenous EES at a minimum. It is even possible that organisms could upregulate their own EES processing machinery to "cheat," analogous to organisms that steal exogenous siderophores (51).

While the diversity of redox-active metabolites, biosynthetic clusters, and redox-sensing homologues satisfy important preconditions for potential widespread EES usage in the microbial world, the numbers we have presented come with two important caveats. First, not all secreted redox-active molecules can serve as EES due to redox-potential constraints (see Sidebar 2). Second, though we have good reason to think that SoxR is a robust predictor of an organism's ability to sense EES, it is just one of many possible transcription factors used

to sense, modify, and transport small redox-active molecules (34, 101). Our bioinformatic analysis only *suggests* the potential for widespread production and usage of EES in the microbial world, which we hope will stimulate experimental follow-up (Sidebar 1).

3. Costs of EES biosynthesis

At first glance, electron shuttles might appear expensive to produce, especially for a molecule that can be lost to diffusion or used by competitors in a microbial community. We discuss strategies for overcoming diffusive losses later, but here we wish to critically ask whether shuttles are 'expensive.' While a cell certainly loses carbon material by secreting a shuttle, the cost should not be compared to the energy that might be gained from fully oxidizing it to CO_2. It is, after all, precisely the condition of oxidant-limitation where EES are important. In a microenvironment where organic carbon is abundant, but oxidants are limited or absent, there is essentially no opportunity cost to discarding carbon. Based on biosynthetic pathways, what is the cost of producing EES?

All the known phenazine-producing bacteria use the same biosynthetic pathway, reviewed in detail elsewhere (9), in which two molecules of chorismate are modified and condensed to produce the core phenazine ring. Chorismate synthesis begins with two ATP equivalents and requires two additional ATP equivalents for completion (29), and so the core phenazine molecule requires a total of 8 ATP. Some quinones require only a single ATP in their conversion from chorismate (29). Riboflavin synthesis requires only one ATP in its conversion from guanosine triphosphate (5), and including the precursors, its cost has been estimated at up to 25 ATP per molecule (75). For these representative examples, the energy required to synthesize a shuttle is on the order of 5 to 25 ATP per molecule. How does this compare to other cellular processes? In protein synthesis, the addition of a single amino acid to a nascent peptide chain requires an estimated 4.5–7.9 ATP per amino acid (3), while RNA transcription further requires one ATP equivalent per nucleotide, and so the biosynthetic proteins themselves may represent a significant portion of a shuttle's cost. A quantitative analysis in *Shewanella* illustrates that its endogenous shuttles, flavin derivatives, cost less

than 0.1% of a cell's energy budget to secrete at the necessary concentration (as low as 250 nM) (75).

The striking conclusion is that for a redox-limited microbial community, shuttle synthesis may pose only a minor metabolic cost. Furthermore, bacteria are known to carefully regulate production of secreted molecules. Xavier et al. coined the term metabolic prudence to describe how *P. aeruginosa* specifically secretes carbon-rich rhamnolipids (used for swarming motility) when excess carbon is available and the cost of production is low (125). This regulation ensures that secreting cells are more fit than cheaters in competition experiments because cost is minimized while the benefit of swarming remains high. Examples from *P. aeruginosa* and *Salmonella typhimurium* suggest that metabolic prudence is a broadly-used strategy for regulating secretions under diverse nutritional conditions, such as iron, phosphate, or nitrogen limitation (45, 48). We expect that metabolically prudent regulation could further reduce the effective cost of EES under oxidant limitation.

4. Cell biology of electron shuttling

The biochemical reduction of EES poses a unique topological challenge. Perhaps the best-elucidated mechanism of extracellular electron transport (EET) is in *Shewanella oneidensis* MR-1, which has been reviewed in detail elsewhere (13, 107). This organism uses the Mtr pathway, which is distinguished by a set of proteins that directly transfer electrons through the inner membrane, across the periplasm, and to the outside of the outer membrane where they directly reduce extracellular shuttles (Fig. 3a). The reduction of quinone by NADH dehydrogenase can be accompanied by the translocation of up to four protons across the inner-membrane (42), thus directly contributing to the proton motive force. In contrast, many other membrane-bound quinone reductases, such as succinate dehydrogenase or lactate dehydrogenase, are not known to translocate protons, and so the direct benefit of EET depends on the particular metabolism of a cell.

In contrast to *Shewanella*, specific pathways of extracellular electron transfer in other systems, such as phenazine shuttling in *P. aeruginosa*, remain ambiguous. Recent work from our laboratory shows that cytoplasmic (flavo)proteins can catalyze phenazine reduction in *P.*

aeruginosa (47). Specifically, the enzyme dihydrolipoamide dehydrogenase enables phenazines to substitute for NAD^+ in the pyruvate and α-ketoglutarate dehydrogenase complexes. This activity may allow phenazines to promote ATP synthesis during glucose oxidation by increasing the flux through pyruvate dehydrogenase and acetate kinase (47) (Fig. 3b). Similar findings have been observed in fermenting organisms, where the presence of humic substances or analogs increases the ratio of oxidized-to-reduced products (7), presumably increasing the ATP yield of fermentation.

The invocation of cytoplasmic EES reduction has interesting implications with respect to the proton-motive force. Upon reduction, phenazines, quinones, and flavins all take on two protons at circumneutral pH (Fig. 1c). The subsequent secretion and oxidation of the reduced shuttle would therefore release those two protons outside the cell, essentially translocating two protons across the inner membrane (Fig. 3b). If this shuttle does not require active transport into or out of the cell, redox cycling of a shuttle could drive the generation of a proton motive force. Conversely, shuttles that accept electrons from the cytoplasmic face of NADH dehydrogenase might consume the proton motive force, such as the artificial compound paraquat (18) (Fig. 3c). Though progress is being made on phenazine transport systems (101), where different phenazines are reduced and how they enter the appropriate efflux pump machinery remain open questions. The take-away message is that the subcellular localization of shuttle reduction greatly influences the energy that can be conserved, and we expect that future work will elucidate new and interesting mechanisms to accompany the Mtr system.

Finally, while we have focused here on the mechanisms of EES reduction, electron transfer entails a subtler point with respect to the terminal electron acceptor. The reduction potential of minerals, and the kinetics of their reduction by shuttles (121), depends strongly on pH, and so the free energy available to a cell necessarily depends on its microenvironment. Moreover, mineral reduction is accompanied by alkalization (Fig. 3c), which further inhibits the available free energy and may even negatively affect the proton motive force if it happens close to the cell. From a cell's perspective, the energy that can be conserved via electron

shuttling may depend on the pH-buffering capacity of its environment and the rate of proton diffusion.

5. EES in the extracellular environment

In addition to defining the constraints that shape intracellular EES biosynthesis and processing, central to any predictive understanding of EES usage is knowledge of what happens to EES once they leave the cell. Because most bacteria live in biofilms (81, 113), we will consider the extracellular environment to be a self-produced matrix of EPS and water. Here, we explore under what conditions EES can be efficiently recycled.

5A. Shuttle diffusion

Two studies have shown that diffusion can theoretically explain electron shuttling-supported metabolism in a closed system (64, 89). In any environment, the flux of reduced EES away from cells (J_{red}) (toward electron acceptor) is driven by the concentration gradient that forms as cells reduce EES and the electron acceptor oxidizes them. Simultaneously, the concentration gradient of oxidized EES drives flux (J_{ox}) back to the cells that use EES to run their metabolism (Fig. 4a). We adapted a simple model of 3D diffusion, where an inner sphere of cells shuttle electrons to an outer sphere of electron acceptor, analogous to *P. aeruginosa* biofilms limited for oxygen (Fig. 4c) (73, 77, 79, 87). Using realistic values of phenazine diffusion coefficients (~10^{-9}–10^{-10} m^2/s), concentrations (>10 μM), and metabolic requirements (M_{min}), the model produces redox gradients that can drive sufficient flux of oxidized EES to support survival (Fig. 4d), in agreement with observed phenazine mediated survival (33, 46, 64).

5B. Electron hopping as an alternative to shuttle diffusion

But what about in an open system, which more accurately models environments where EES operate? An attractive mechanism that might prevent EES loss in an open system is electron hopping among EES's bound in the biofilm matrix (12, 89). Such conduction would avoid the conflict between turnover and loss within the shuttle diffusion model and might better

explain electron shuttling in open systems. The flux of hopping electrons from the cells to the acceptor is considered a diffusive process, which is driven by the concentration gradient of electrons (*i.e.* redox gradient) (111). In this scenario, EES are bound within the extracellular matrix, and electrons propagate from cells to the terminal metabolic electron acceptor (*e.g.* O_2) by sequential electron-transfer reactions among the EES, allowing EES retention and reuse (Fig. 4b). Hopping steps (k_{hop}) are expected to happen rapidly compared to shuttle diffusion (D) (100, 119).

Significant theoretical and experimental work has already been done to describe electron hopping in electrode-grown biofilms of *Geobacter sulfurreducens*. Such biofilms, which can exceed tens of microns in thickness, utilize the underlying electrode, poised at a sufficiently oxidizing potential, as the terminal metabolic acceptor. Cells not in direct contact with the electrode can transport their respired electrons to the electrode via hopping through a proposed network of c-type cytochromes as opposed to EES. This model is supported experimentally by measurements of biofilm electrical conductivity (12, 88, 98, 111, 114, 127-130). Much of the theory comes from models of synthetic redox polymers and proteins that contain bound redox cofactors (10, 12, 50, 91, 115). This work provides a proof-of-principle that motivates experiments to test for electron hopping in other biofilms where EES may dominate extracellular electron transfer.

5C. Evolutionary strategies that maintain EES in open environments

Regardless of the electron transfer mechanism, sufficient concentrations of EES must be maintained for viability. What strategies do microbes take in producing and maintaining public goods in open environments? We view EES as public goods because they are secreted molecules that benefit nearby individuals as well as the producer cell (124). Kin selection theory posits that public good production can evolve when individuals' actions increase not only their own reproductive success, but also the success of genetically related individuals (124). Microbes are therefore more likely to produce public goods when they are highly related to their neighbors, the direct and indirect benefits are high, and the cost of production is low (78).

In this context, it makes sense that EES would be regulated by quorum sensing (QS) molecules, signals that direct population behaviors when cell numbers are high. QS molecules can provide cells with information on nearby relatives and diffusion conditions (54). By dividing quickly and producing an extracellular matrix, many bacteria can establish highly-related microcolonies that favor the evolution of public goods (78). Laboratory studies show that producers of the siderophore, pyoverdin, outcompete non-producer mutants when populations are highly related, but not when strains are mixed (35, 51). Because QS molecules are secreted into the environment and subject to diffusion, they enable cells to distinguish between closed and open systems (97). A good example of QS-regulation of EES production can be found in how *Pseudomonas* species regulate phenazine production (32).

Other strategies that can facilitate the viability of EES utilization relate to mechanisms of privatization, such as physical retention or a requirement for special machinery to utilize the secreted molecule (124). Physical retention can be achieved via noncovalent interactions between small molecule and biofilm components, which in the case of EES, could conceivably also provide a scaffold for electron hopping. Marine microbes that retain siderophores by embedding them in the outer membrane with lipophilic sidechains (67) provide an example of selective retention of a secreted metabolite near producing cells. Other chemical mechanisms may facilitate retention, however, such as electrostatic attraction between EES and specific components of a biofilm matrix. This may help rationalize co-regulation of EES and exopolymeric substances (EPS), as in the case of phenazines, eDNA, and particular types of EPS (26, 27, 33). Discrimination can be achieved with highly specific receptors for siderophores and QS molecules that enable only producers to uptake their secreted products (80, 104, 124). Another strategy is to make the public good itself toxic, which requires specialized detoxification systems (103). Interestingly, many EES were first identified as antibiotics (25, 95), and special proteins are required to deal with their toxic byproducts (53).

6. Outlook

This is an exciting time to care about microbes that change color. The explosion of computational platforms that can predict structures and properties of natural products, combined with the exponential growth of genomic databases, is ushering in a golden age for EES discovery. Based on these databases and lessons learned from experimental systems where redox-active pigment production and utilization have been well documented, the available evidence suggests that EES are likely to be widespread and play underappreciated roles in the physiology of diverse microbes.

Going forward, it will be important to prioritize systematic screens to test for EES production and usage. Sidebar 1 provides an example of how one can approach this, yet innovations that would enable high-throughput screens are needed to stimulate the search process. While such technologies could be developed by individual labs at universities, an opportunity for efficient scale-up exists if national labs that are interested in metabolomics, such as the Joint Genome Institute (6, 14, 108), take on this challenge. The creation of pipelines to interface metabolomics with complementary bioinformatics and physiological screens would greatly accelerate EES discovery. In our view, the identification of genetically-tractable EES-producing microbes should be a priority for future research. Genetically-tractable systems are now more achievable than ever before (17, 84), thus the isolation of EES-producing or utilizing microbes has the potential to quickly reach a mechanistic level of understanding.

Identification of machinery that sense and process EES across diverse microorganisms will permit the type of comparative analysis needed to enable general principles to be resolved. For example, the better we understand the conservation of EES transporters or sensors, the more confidently we will be able to scan genomes to predict EES production or usage by new isolates. In this way, we will be able to learn whether the strategies that govern EES cycling by the handful of organisms that have been studied in detail to date represent special cases or broader paradigms. Generally, metabolic strategies fall into a limited number of categories that are viable for cells, thus it will be exciting to discovery the range of strategies that can be used by organisms that employ EES for energy generation and other purposes.

Finally, we end by noting that much of what we understand about microbial metabolism springs from research that has been done when nutrients are replete. Yet microbial existence in the natural world is usually limited by a variety of substrates (8), and it is in this context that we believe EES will prove to be important. Not only can EES enable energy generation in oxidant-limited biofilms, which are ubiquitous (81, 113), but the broader reactivity of EES can impact the fate and transport of pollutants in soils and sediments (60-62). From both fundamental and applied viewpoints, a broader and deeper understanding of EES production, sensing, and utilization thus stands to improve our ability to rationalize and control the composition and activities of microbial communities across a variety of natural, engineered, and clinical environments.

Glossary

1. Extracellular electron shuttles (EES): A self-produced small molecule that enables a microbe to perform EET by *reversibly* accepting metabolic electrons and donating them to extracellular electron acceptors. Note that these molecules can also act as electron donors to metabolism (15).

2. Biosynthetic clusters: organized sets of genes that encode enzymes to produce specific metabolites.

3. Redox gradient: A concentration gradient of electrons across a field of redox-active molecules. This gradient can drive physical diffusion of the molecules in different redox states, or electron diffusion via electron transfer between redox-active molecules.

4. Public goods: Secreted molecules that benefit nearby individuals that did not originally produce the molecules.

Acknowledgements

We thank Leonard Tender and Matthew Yates for helpful comments, and Muir Morrison, Tal Einav, and Manuel Razo for guidance in deriving the 3D diffusion model.

References

1. 2017. Dictionary of Natural Products 25.2. http://dnp.chemnetbase.com/: Taylor and Francis
2. Alberty RA. 1994. Thermodynamics of the nitrogenase reactions. *Journal of Biological Chemistry* 269: 7099-102
3. Amthor JS. 2000. The McCree–de Wit–Penning de Vries–Thornley respiration paradigms: 30 years later. *Annals of Botany* 86: 1-20
4. Assary RS, Brushett FR, Curtiss LA. 2014. Reduction potential predictions of some aromatic nitrogen-containing molecules. *RSC Advances* 4: 57442-51
5. Bacher A, Eberhardt S, Fischer M, Kis K, Richter G. 2000. Biosynthesis of vitamin B2 (riboflavin). *Annual Review of Nutrition* 20: 153-67
6. Baran R, Ivanova NN, Jose N, Garcia-Pichel F, Kyrpides NC, et al. 2013. Functional genomics of novel secondary metabolites from diverse cyanobacteria using untargeted metabolomics. *Marine Drugs* 11: 3617-31
7. Benz M, Schink B, Brune A. 1998. Humic acid reduction by *Propionibacterium freudenreichii* and other fermenting bacteria. *Applied and Environmental Microbiology* 64: 4507-12
8. Bergkessel M, Basta DW, Newman DK. 2016. The physiology of growth arrest: uniting molecular and environmental microbiology. *Nature Reviews Microbiology* 14: 549-62
9. Blankenfeldt W, Parsons JF. 2014. The structural biology of phenazine biosynthesis. *Current Opinion in Structural Biology* 0: 26-33
10. Blauch DN, Saveant JM. 1992. Dynamics of electron hopping in assemblies of redox centers. Percolation and diffusion. *Journal of the American Chemical Society* 114: 3323-32
11. Bond DR, Lovley DR. 2005. Evidence for involvement of an electron shuttle in electricity generation by *Geothrix fermentans*. *Applied and Environmental Microbiology* 71: 2186-89
12. Boyd DA, Snider RM, Erickson JS, Roy JN, Strycharz-Glaven SM, Tender LM. 2015. Measuring electron transport rates through electrochemically active biofilms In *Biofilms in Bioelectrochemical Systems: From Laboratory Practice to Data Interpretation*, ed. JB Haluk Beyenal: John Wiley & Sons, Inc.
13. Brutinel ED, Gralnick JA. 2012. Shuttling happens: soluble flavin mediators of extracellular electron transfer in *Shewanella*. *Applied Microbiology and Biotechnology* 93: 41-48
14. Chen I-MA, Markowitz VM, Chu K, Palaniappan K, Szeto E, et al. 2016. IMG/M: integrated genome and metagenome comparative data analysis system. *Nucleic Acids Research*: gkw929
15. Coates JD, Cole KA, Chakraborty R, O'Connor SM, Achenbach LA. 2002. Diversity and ubiquity of bacteria capable of utilizing humic substances as electron donors for anaerobic respiration. *Applied and Environmental Microbiology* 68: 2445-52

16. Coates JD, Ellis DJ, Blunt-Harris EL, Gaw CV, Roden EE, Lovley DR. 1998. Recovery of humic-reducing bacteria from a diversity of environments. *Applied and Environmental Microbiology* 64: 1504-09
17. Cobb RE, Wang Y, Zhao H. 2014. High-efficiency multiplex genome editing of *Streptomyces* species using an engineered CRISPR/Cas system. *ACS Synthetic Biology* 4: 723-28
18. Cochemé HM, Murphy MP. 2008. Complex I Is the major site of mitochondrial superoxide production by paraquat. *Journal of Biological Chemistry* 283: 1786-98
19. Conn JE. 1943. The pigment production of *Actinomyces coelicolor* and *A. violaceus-ruber*. *Journal of Bacteriology* 46: 133
20. Consortium HMP. 2012. Structure, function and diversity of the healthy human microbiome. *Nature* 486: 207-14
21. Costa KC, Bergkessel M, Saunders S, Korlach J, Newman DK. 2015. Enzymatic degradation of phenazines can generate energy and protect sensitive organisms from toxicity. *mBio* 6: e01520-15
22. Costa KC, Glasser NR, Conway SJ, Newman DK. 2017. Pyocyanin degradation by a tautomerizing demethylase inhibits *Pseudomonas aeruginosa* biofilms. *Science* 355: 170-73
23. Cowley ES, Kopf SH, LaRiviere A, Ziebis W, Newman DK. 2015. Pediatric cystic fibrosis sputum can be chemically dynamic, anoxic, and extremely reduced due to hydrogen sulfide formation. *mBio* 6
24. Cruz RD, Gao Y, Penumetcha S, Sheplock R, Weng K, Chander M. 2010. Expression of the *Streptomyces coelicolor* SoxR regulon is intimately linked with actinorhodin production. *Journal of Bacteriology* 192: 6428-38
25. Cude WN, Mooney J, Tavanaei AA, Hadden MK, Frank AM, et al. 2012. Production of the antimicrobial secondary metabolite indigoidine contributes to competitive surface colonization by the marine roseobacter *Phaeobacter* sp. strain Y4I. *Applied and Environmental Microbiology* 78: 4771-80
26. Das T, Kutty SK, Tavallaie R, Ibugo AI, Panchompoo J, et al. 2015. Phenazine virulence factor binding to extracellular DNA is important for *Pseudomonas aeruginosa* biofilm formation. *Scientific Reports* 5: 8398
27. Das T, Manefield M. 2012. Pyocyanin promotes extracellular DNA release in *Pseudomonas aeruginosa*. *PLoS One* 7: e46718
28. Deng L, Li F, Zhou S, Huang D, Ni J. 2010. A study of electron-shuttle mechanism in *Klebsiella pneumoniae* based-microbial fuel cells. *Chinese Science Bulletin* 55: 99-104
29. Dewick PM. 1994. The biosynthesis of shikimate metabolites. *Natural Product Reports* 11: 173-203
30. Dhall S, Do DC, Garcia M, Kim J, Mirebrahim SH, et al. 2014. Generating and reversing chronic wounds in diabetic mice by manipulating wound redox parameters. *Journal of Diabetes Research* 2014: 562625
31. Dietrich LE, Price-Whelan A, Petersen A, Whiteley M, Newman DK. 2006. The phenazine pyocyanin is a terminal signalling factor in the quorum sensing network of *Pseudomonas aeruginosa*. *Molecular Microbiology* 61: 1308-21

32. Dietrich LE, Price-Whelan A, Petersen A, Whiteley M, Newman DK. 2006. The phenazine pyocyanin is a terminal signalling factor in the quorum sensing network of *Pseudomonas aeruginosa*. *Molecular Microbiology* 61: 1308-21
33. Dietrich LEP, Okegbe C, Price-Whelan A, Sakhtah H, Hunter RC, Newman DK. 2013. Bacterial community morphogenesis is intimately linked to the intracellular redox state. *Journal of Bacteriology* 195: 1371-80
34. Dietrich LEP, Teal TK, Price-Whelan A, Newman DK. 2008. Redox-active antibiotics control gene expression and community behavior in divergent bacteria. *Science* 321: 1203-06
35. Diggle SP, Griffin AS, Campbell GS, West SA. 2007. Cooperation and conflict in quorum-sensing bacterial populations. *Nature* 450: 411-14
36. Emde R, Swain A, Schink B. 1989. Anaerobic oxidation of glycerol by *Escherichia coli* in an amperometric poised-potential culture system. *Applied Microbiology and Biotechnology* 32: 170-75
37. Farrington JA, Ebert M, Land EJ, Fletcher K. 1973. Bipyridylium quaternary salts and related compounds. V. Pulse radiolysis studies of the reaction of paraquat radical with oxygen. Implications for the mode of action of bipyridyl herbicides. *Biochimica et Biophysica Acta (BBA) - Bioenergetics* 314: 372-81
38. Federhen S. 2012. The NCBI taxonomy database. *Nucleic Acids Research* 40: D136-D43
39. Freguia S, Masuda M, Tsujimura S, Kano K. 2009. *Lactococcus lactis* catalyses electricity generation at microbial fuel cell anodes via excretion of a soluble quinone. *Bioelectrochemistry* 76: 14-18
40. Friedheim E, Michaelis L. 1931. Potentiometric study of pyocyanine. *Journal of Biological Chemistry* 91: 355-68
41. Fuller SJ, McMillan DG, Renz MB, Schmidt M, Burke IT, Stewart DI. 2014. Extracellular electron transport-mediated Fe(III) reduction by a community of alkaliphilic bacteria that use flavins as electron shuttles. *Applied and Environmental Microbiology* 80: 128-37
42. Galkin AS, Grivennikova VG, Vinogradov AD. 1999. →H+/2e stoichiometry in NADH-quinone reductase reactions catalyzed by bovine heart submitochondrial particles. *FEBS Letters* 451: 157-61
43. Garrity GM, Bell JA, Lilburn TG. 2004. Taxonomic outline of the prokaryotes. Bergey's manual of systematic bacteriology. *Springer, New York, Berlin, Heidelberg*
44. Gauthier M, Flatau G. 1976. Antibacterial activity of marine violet-pigmented Alteromonas with special reference to the production of brominated compounds. *Canadian Journal of Microbiology* 22: 1612-19
45. Gerstel U, Römling U. 2001. Oxygen tension and nutrient starvation are major signals that regulate *agfD* promoter activity and expression of the multicellular morphotype in *Salmonella typhimurium*. *Environmental Microbiology* 3: 638-48
46. Glasser NR, Kern SE, Newman DK. 2014. Phenazine redox cycling enhances anaerobic survival in *Pseudomonas aeruginosa* by facilitating generation of ATP and a proton-motive force. *Molecular Microbiology* 92: 399-412

47. Glasser NR, Wang BX, Hoy JA, Newman DK. 2017. The pyruvate and α-ketoglutarate dehydrogenase complexes of *Pseudomonas aeruginosa* catalyze pyocyanin and phenazine-1-carboxylic acid reduction via the subunit dihydrolipoamide dehydrogenase. *Journal of Biological Chemistry*: jbc. M116. 772848
48. Glick R, Gilmour C, Tremblay J, Satanower S, Avidan O, et al. 2010. Increase in rhamnolipid synthesis under iron-limiting conditions influences surface motility and biofilm formation in *Pseudomonas aeruginosa*. *Journal of Bacteriology* 192: 2973-80
49. Grahl N, Kern SE, Newman DK, Hogan DA. 2013. The yin and the yang of phenazine physiology. In *Microbial Phenazines*, ed. S Chincholkar, LS Thomashow, pp. 43-70: Springer
50. Gray HB, Winkler JR. 1996. Electron transfer in proteins. *Annual Review of Biochemistry* 65: 537-61
51. Griffin AS, West SA, Buckling A. 2004. Cooperation and competition in pathogenic bacteria. *Nature* 430: 1024-27
52. Hadjithomas M, Chen I-MA, Chu K, Ratner A, Palaniappan K, et al. 2015. IMG-ABC: a knowledge base to fuel discovery of biosynthetic gene clusters and novel secondary metabolites. *mBio* 6: e00932-15
53. Hassan HM, Fridovich I. 1979. Intracellular production of superoxide radical and of hydrogen peroxide by redox active compounds. *Archives of Biochemistry and Biophysics* 196: 385-95
54. Hense BA, Kuttler C, Müller J, Rothballer M, Hartmann A, Kreft J-U. 2007. Does efficiency sensing unify diffusion and quorum sensing? *Nature Reviews Microbiology* 5: 230-39
55. Hernandez ME, Kappler A, Newman DK. 2004. Phenazines and other redox-active antibiotics promote microbial mineral reduction. *Applied and Environmental Microbiology* 70: 921-8
56. Hernandez ME, Newman DK. 2001. Extracellular electron transfer. *Cell and Molecular Life Sciences* 58: 1562-71
57. Herrmann G, Jayamani E, Mai G, Buckel W. 2008. Energy conservation via electron-transferring flavoprotein in anaerobic bacteria. *Journal of Bacteriology* 199: 784-91
58. Hunter RC, Klepac-Ceraj V, Lorenzi MM, Grotzinger H, Martin TR, Newman DK. 2012. Phenazine content in the cystic fibrosis respiratory tract negatively correlates with lung function and microbial complexity. *American Journal of Respiratory Cell and Molecular Biology* 47: 738-45
59. Jelen BI, Giovannelli D, Falkowski PG. 2016. The role of microbial electron transfer in the coevolution of the biosphere and geosphere. *Annual Review of Microbiology* 70: 45-62
60. Jiang J, Kappler A. 2008. Kinetics of microbial and chemical reduction of humic substances: implications for electron shuttling. *Environmental Science & Technology* 42: 3563-69

61. Kappler A, Benz M, Schink B, Brune A. 2004. Electron shuttling via humic acids in microbial iron(III) reduction in a freshwater sediment. *FEMS Microbiology Ecology* 47: 85-92
62. Kappler A, Haderlein SB. 2003. Natural organic matter as reductant for chlorinated aliphatic pollutants. *Environmental Science & Technology* 37: 2714-19
63. Keck A, Rau J, Reemtsma T, Mattes R, Stolz A, Klein J. 2002. Identification of quinoide redox mediators that are formed during the degradation of naphthalene-2-sulfonate by *Sphingomonas xenophaga* BN6. *Applied and Environmental Microbiology* 68: 4341-49
64. Kempes CP, Okegbe C, Mears-Clarke Z, Follows MJ, Dietrich LE. 2014. Morphological optimization for access to dual oxidants in biofilms. *Proceedings of the National Academy of Sciences* 111: 208-13
65. Khan MT, Duncan SH, Stams AJ, Van Dijl JM, Flint HJ, Harmsen HJ. 2012. The gut anaerobe *Faecalibacterium prausnitzii* uses an extracellular electron shuttle to grow at oxic–anoxic interphases. *The ISME journal* 6: 1578-85
66. Kotloski NJ, Gralnick JA. 2013. Flavin electron shuttles dominate extracellular electron transfer by *Shewanella oneidensis*. *mBio* 4: e00553-12
67. Kümmerli R, Schiessl KT, Waldvogel T, McNeill K, Ackermann M. 2014. Habitat structure and the evolution of diffusible siderophores in bacteria. *Ecology Letters* 17: 1536-44
68. Lee A, Newman D. 2003. Microbial iron respiration: impacts on corrosion processes. *Applied Microbiology and Biotechnology* 62: 134-39
69. Letunic I, Bork P. 2016. Interactive tree of life (iTOL) v3: an online tool for the display and annotation of phylogenetic and other trees. *Nucleic Acids Research* 44: W242-W45
70. Li F, Hinderberger J, Seedorf H, Zhang J, Buckel W, Thauer RK. 2008. Coupled ferredoxin and crotonyl coenzyme A (CoA) reduction with NADH catalyzed by the butyryl-CoA dehydrogenase/Etf complex from *Clostridium kluyveri*. *Journal of Bacteriology* 190: 843-50
71. Lies DP, Hernandez ME, Kappler A, Mielke RE, Gralnick JA, Newman DK. 2005. *Shewanella oneidensis* MR-1 uses overlapping pathways for iron reduction at a distance and by direct contact under conditions relevant for biofilms. *Applied and Environmental Microbiology* 71: 4414-26
72. Lovley DR. 2006. Bug juice: harvesting electricity with microorganisms. *Nature Reviews Microbiology* 4: 497-508
73. Lukacs GL, Haggie P, Seksek O, Lechardeur D, Freedman N, Verkman A. 2000. Size-dependent DNA mobility in cytoplasm and nucleus. *Journal of Biological Chemistry* 275: 1625-29
74. Malvankar NS, Rotello VM, Tuominen MT, Lovley DR. 2016. Reply to 'Measuring conductivity of living *Geobacter sulfurreducens* biofilms'. *Nature Nanotechnology* 11: 913-14
75. Marsili E, Baron DB, Shikhare ID, Coursolle D, Gralnick JA, Bond DR. 2008. Shewanella secretes flavins that mediate extracellular electron transfer. *Proceedings of the National Academy of Sciences* 105: 3968-73

76. McGlynn SE, Chadwick GL, Kempes CP, Orphan VJ. 2015. Single cell activity reveals direct electron transfer in methanotrophic consortia. *Nature* 526: 531-35
77. Murray AG, Jackson GA. 1992. Viral dynamics: A model of the effects size, shape, motion and abundance of single-celled planktonic organisms and other particles. *Marine Ecology Progress Series. Oldendorf* 89: 103-16
78. Nadell CD, Xavier JB, Foster KR. 2009. The sociobiology of biofilms. *FEMS Microbiology Reviews* 33: 206-24
79. Nauman JV, Campbell PG, Lanni F, Anderson JL. 2007. Diffusion of insulin-like growth factor-I and ribonuclease through fibrin gels. *Biophysical Journal* 92: 4444-50
80. Neilands J. 1981. Iron absorption and transport in microorganisms. *Annual Review of Nutrition* 1: 27-46
81. O'Toole G, Kaplan HB, Kolter R. 2000. Biofilm formation as microbial development. *Annual Reviews in Microbiology* 54: 49-79
82. Palma M, Zurita J, Ferreras JA, Worgall S, Larone DH, et al. 2005. *Pseudomonas aeruginosa* SoxR does not conform to the archetypal paradigm for SoxR-dependent regulation of the bacterial oxidative stress adaptive response. *Infection and Immunity* 73: 2958-66
83. Pence HE, Williams A. 2010. ChemSpider: an online chemical information resource. *ACS Publications*
84. Peters JM, Silvis MR, Zhao D, Hawkins JS, Gross CA, Qi LS. 2015. Bacterial CRISPR: accomplishments and prospects. *Current Opinion in Microbiology* 27: 121-26
85. Petrauskas AA, Kolovanov EA. 2000. ACD/Log P method description. *Perspectives in Drug Discovery and Design* 19: 99-116
86. Pfeffer C, Larsen S, Song J, Dong M, Besenbacher F, et al. 2012. Filamentous bacteria transport electrons over centimetre distances. *Nature* 491: 218-21
87. Phalak P, Chen J, Carlson RP, Henson MA. 2016. Metabolic modeling of a chronic wound biofilm consortium predicts spatial partitioning of bacterial species. *BMC Systems Biology* 10: 90
88. Phan H, Yates MD, Kirchhofer ND, Bazan GC, Tender LM, Nguyen T-Q. 2016. Biofilm as a redox conductor: a systematic study of the moisture and temperature dependence of its electrical properties. *Physical Chemistry Chemical Physics* 18: 17815-21
89. Picioreanu C, Head IM, Katuri KP, van Loosdrecht MC, Scott K. 2007. A computational model for biofilm-based microbial fuel cells. *Water Research* 41: 2921-40
90. Pierson III LS, Thomashow LS. 1992. Cloning and Heterologous Expression of the Phenazine Biosynthetic. *Molecular Plant-Microbe Interactions* 5: 330-39
91. Pirbadian S, El-Naggar MY. 2012. Multistep hopping and extracellular charge transfer in microbial redox chains. *Physical Chemistry Chemical Physics* 14: 13802-08
92. Pomposiello PJ, Demple B. 2001. Redox-operated genetic switches: the SoxR and OxyR transcription factors. *Trends in Biotechnology* 19: 109-14

93. Price-Whelan A, Dietrich LE, Newman DK. 2006. Rethinking 'secondary' metabolism: physiological roles for phenazine antibiotics. *Nature Chemical Biology* 2: 71-8
94. Price-Whelan A, Dietrich LE, Newman DK. 2007. Pyocyanin alters redox homeostasis and carbon flux through central metabolic pathways in *Pseudomonas aeruginosa* PA14. *Journal of Bacteriology* 189: 6372-81
95. Price-Whelan A, Dietrich LEP, Newman DK. 2006. Rethinking 'secondary' metabolism: physiological roles for phenazine antibiotics. *Nature Chemical Biology* 2: 221-21
96. Ramos I, Dietrich LE, Price-Whelan A, Newman DK. 2010. Phenazines affect biofilm formation by *Pseudomonas aeruginosa* in similar ways at various scales. *Research in Microbiology* 161: 187-91
97. Redfield RJ. 2002. Is quorum sensing a side effect of diffusion sensing? *Trends in Microbiology* 10: 365-70
98. Robuschi L, Tomba JP, Schrott GD, Bonanni PS, Desimone PM, Busalmen JP. 2013. Spectroscopic slicing to reveal internal redox gradients in electricity-producing biofilms. *Angewandte Chemie International Edition* 52: 925-28
99. Roden EE, Kappler A, Bauer I, Jiang J, Paul A, et al. 2010. Extracellular electron transfer through microbial reduction of solid-phase humic substances. *Nature Geoscience* 3: 417-21
100. Rosso KM, Smith DM, Wang Z, Ainsworth CC, Fredrickson JK. 2004. Self-exchange electron transfer kinetics and reduction potentials for anthraquinone disulfonate. *The Journal of Physical Chemistry A* 108: 3292-303
101. Sakhtah H, Koyama L, Zhang Y, Morales DK, Fields BL, et al. 2016. The *Pseudomonas aeruginosa* efflux pump MexGHI-OpmD transports a natural phenazine that controls gene expression and biofilm development. *Proceedings of the National Academy of Sciences*: 201600424
102. Scheller S, Yu H, Chadwick GL, McGlynn SE, Orphan VJ. 2016. Artificial electron acceptors decouple archaeal methane oxidation from sulfate reduction. *Science* 351: 703-07
103. Schertzer JW, Boulette ML, Whiteley M. 2009. More than a signal: non-signaling properties of quorum sensing molecules. *Trends in Microbiology* 17: 189-95
104. Schuster M, Joseph Sexton D, Diggle SP, Peter Greenberg E. 2013. Acyl-homoserine lactone quorum sensing: from evolution to application. *Annual Review of Microbiology* 67: 43-63
105. Scott DT, McKnight DM, Blunt-Harris EL, Kolesar SE, Lovley DR. 1998. Quinone moieties act as electron acceptors in the reduction of humic substances by humics-reducing microorganisms. *Environmental Science & Technology* 32: 2984-89
106. Shi L, Dong H, Reguera G, Beyenal H, Lu A, et al. 2016. Extracellular electron transfer mechanisms between microorganisms and minerals. *Nature Reviews Microbiology*

107. Shi L, Rosso KM, Clarke TA, Richardson DJ, Zachara JM, Fredrickson JK. 2012. Molecular underpinnings of Fe(III) oxide reduction by *Shewanella oneidensis* MR-1. *Frontiers in Microbiology*: 46
108. Silva LP, Northen TR. 2015. Exometabolomics and MSI: deconstructing how cells interact to transform their small molecule environment. *Current Opinion in Biotechnology* 34: 209-16
109. Singh AK, Shin JH, Lee KL, Imlay JA, Roe JH. 2013. Comparative study of SoxR activation by redox-active compounds. *Molecular Microbiology* 90: 983-96
110. Smith JA, Tremblay P-L, Shrestha PM, Snoeyenbos-West OL, Franks AE, et al. 2014. Going wireless: Fe(III) oxide reduction without pili by *Geobacter sulfurreducens* strain JS-1. *Applied and Environmental Microbiology* 80: 4331-40
111. Snider RM, Strycharz-Glaven SM, Tsoi SD, Erickson JS, Tender LM. 2012. Long-range electron transport in *Geobacter sulfurreducens* biofilms is redox gradient-driven. *Proceedings of the National Academy of Sciences* 109: 15467-72
112. Stewart PS. 2003. Diffusion in biofilms. *Journal of Bacteriology* 185: 1485-91
113. Stewart PS, Franklin MJ. 2008. Physiological heterogeneity in biofilms. *Nature Reviews Microbiology* 6: 199-210
114. Strycharz-Glaven SM, Snider RM, Guiseppi-Elie A, Tender LM. 2011. On the electrical conductivity of microbial nanowires and biofilms. *Energy & Environmental Science* 4: 4366-79
115. Subramanian P, Pirbadian S, El-Naggar MY, Jensen GJ. 2017. The ultrastructure of *Shewanella oneidensis* MR-1 nanowires revealed by electron cryo-tomography. *bioRxiv*
116. Sullivan NL, Tzeranis DS, Wang Y, So PT, Newman D. 2011. Quantifying the dynamics of bacterial secondary metabolites by spectral multiphoton microscopy. *ACS Chemical Biology* 6: 893-9
117. Tan Y, Adhikari RY, Malvankar NS, Ward JE, Nevin KP, et al. 2016. The low conductivity of *Geobacter uraniireducens* pili suggests a diversity of extracellular electron transfer mechanisms in the genus *Geobacter*. *Frontiers in Microbiology* 7
118. Turnbaugh PJ, Ley RE, Hamady M, Fraser-Liggett C, Knight R, Gordon JI. 2007. The human microbiome project: exploring the microbial part of ourselves in a changing world. *Nature* 449: 804
119. Uchimiya M, Stone AT. 2009. Reversible redox chemistry of quinones: Impact on biogeochemical cycles. *Chemosphere* 77: 451-58
120. Wang Y, Kern SE, Newman DK. 2010. Endogenous phenazine antibiotics promote anaerobic survival of *Pseudomonas aeruginosa* via extracellular electron transfer. *Journal of Bacteriology* 192: 365-9
121. Wang Y, Newman DK. 2008. Redox reactions of phenazine antibiotics with ferric (hydr)oxides and molecular oxygen. *Environmental Science and Technology* 42: 2380-6
122. Wang Y, Wilks JC, Danhorn T, Ramos I, Croal L, Newman DK. 2011. Phenazine-1-carboxylic acid promotes bacterial biofilm development via ferrous iron acquisition. *Journal of Bacteriology* 193: 3606-17

123. Weber T, Blin K, Duddela S, Krug D, Kim HU, et al. 2015. antiSMASH 3.0—a comprehensive resource for the genome mining of biosynthetic gene clusters. *Nucleic Acids Research* 43: W237-W43
124. West SA, Griffin AS, Gardner A, Diggle SP. 2006. Social evolution theory for microorganisms. *Nature Reviews Microbiology* 4: 597-607
125. Xavier JB, Kim W, Foster KR. 2011. A molecular mechanism that stabilizes cooperative secretions in *Pseudomonas aeruginosa*. *Molecular Microbiology* 79: 166-79
126. Xu KD, Stewart PS, Xia F, Huang CT, McFeters GA. 1998. Spatial physiological heterogeneity in *Pseudomonas aeruginosa* biofilm is determined by oxygen availability. *Applied and Environmental Microbiology* 64: 4035-9
127. Yates MD, Golden JP, Roy J, Strycharz-Glaven SM, Tsoi S, et al. 2015. Thermally activated long range electron transport in living biofilms. *Physical Chemistry Chemical Physics* 17: 32564-70
128. Yates MD, Strycharz-Glaven SM, Golden JP, Roy J, Tsoi S, et al. 2016. Measuring conductivity of living *Geobacter sulfurreducens* biofilms. *Nature Nanotechnology* 11: 910-13
129. Yates MD, Strycharz-Glaven SM, Tender LM. 2016. Understanding long-distance extracellular electron transport in an electroautotrophic microbial community. *Energy & Environmental Science (in press)*
130. Yates MD, Tender LM. 2016. Electrochemical gating measurements of living electrode-grown *Geobacter sulfurreducens* biofilms *Nature Nanotechnology (in press)*
131. Young G. 1947. Pigment production and antibiotic activity in cultures of *Pseudomonas aeruginosa*. *Journal of Bacteriology* 54: 109

Sidebars

Sidebar 1. How to characterize a putative EES?

What criteria establish that a molecule functions as an EES? Based on our definition, the molecule must 1) facilitate extracellular electron transfer, 2) undergo multiple redox cycles, and 3) provide a physiological benefit to its producer via cycling. The following steps can be used to determine whether a particular secreted metabolite is an EES.

Find a tractable extracellular electron transfer phenotype and implicate a soluble EES. Quantifiable extracellular electron transfer phenotypes can be detected in assays with minerals (55), electrodes (36, 46, 120), or soluble electron acceptors (65, 95). Secreted EES can be implicated by demonstrating electron acceptor reduction in the absence of direct cell contact using different strategies, such as separation by agar, permeable membranes, glass frits, or compartments in microfluidic devices.

Isolate and characterize the EES molecule. Once an EES phenotype is established, the responsible molecule can be purified using chromatography and other standard separation methods from organic chemistry. Its spectral properties, biotic and abiotic reactivity, and redox potential can then be measured using different types of spectroscopy (UV-VIS, EPR) and cyclic voltammetry, respectively (*e.g.*(40, 105, 121)).

Genetically inhibit EES biosynthesis. Because EES are not essential under all conditions, it is possible to isolate mutants defective in their production. Such mutants can offer insights into EES biosynthesis, regulation, and even cycling mechanisms (*e.g.*(31, 90, 120)). Control over EES production, which is enabled by mutant strains, is necessary to rigorously determine the physiological benefits of an EES.

Measure EES turnover. EES uptake and reduction can be quantified using biosynthetic mutants in the presence of a defined EES concentration and oxidant (*e.g.*(120)). The molecule can be defined as an EES if it enables a super-stoichiometric reaction with the distal electron acceptor.

Sidebar 2. How does redox-potential define an EES?

The essence of a shuttle is summarized by its midpoint reduction potential, a broad generalization of a compound's ability to act as electron acceptor or donor. To avoid misusing this parameter, one must remain cognizant that it is descriptive of standard conditions for reactions heading towards thermodynamic equilibrium, conditions that rarely describe biological systems. Importantly, many redox reactions involve proton exchange, and so the true reduction potential depends on the environmental pH. A distinction must also be drawn between the one- and two-electron potentials of a shuttle, which can vary by hundreds of millivolts—this difference has even been exploited by some microorganisms to drive the reduction of low-potential acceptors in a process known as electron bifurcation (57, 70). Moreover, the reduction potential says nothing about the kinetics or chemical sensibility of the reaction. A striking example of this distinction is the thermodynamic favorability of biological nitrogen fixation (2), a process that nonetheless requires catalysis and energy input to proceed at rates that support life. Conversely, the artificial redox cycling drug paraquat has a midpoint potential below that of most intracellular donors, rendering paraquat reduction thermodynamically unfavorable *at standard conditions*; even so, the paraquat radical reacts with oxygen at a rate that is nearly diffusion-limited (37), allowing paraquat to drive redox cycling under biological conditions. And so, while a shuttle's reduction potential is a core physical parameter that captures the essence of redox cycling, it must be carefully considered with respect to the environmental conditions, reaction kinetics, and other chemical properties. A rigorous quantitative prediction of these effects remains an ongoing challenge, but further advancements will undoubtedly enrich the already informative natural products databases.

Figures

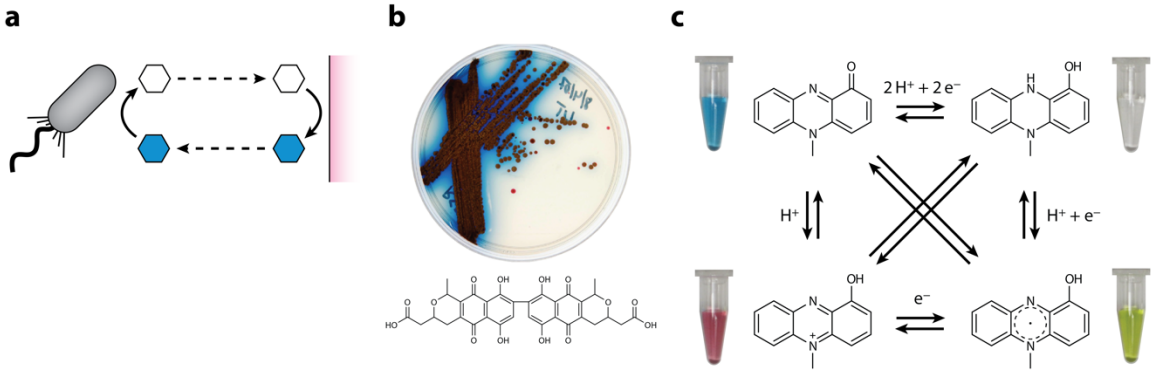

Figure 1. The colorful world of EES. (a) Action at a distance. Cells can perform redox chemistry on small molecules, which then diffuse or electrically conduct to extracellular substrates that can be many cell lengths away. (b) The colorful world of microbes as illustrated by *Streptomyces coelicolor*, producing the blue molecule actinorhodin whose structure is shown. (c) One molecule, four colors. The color of pyocyanin depends on both the pH and reduction potential. The tubes pictured each contain approximately 200 µM pyocyanin in water. The radical and fully reduced forms can be prepared by titrating pyocyanin with sodium dithionite, producing to an immediate and stunning color change.

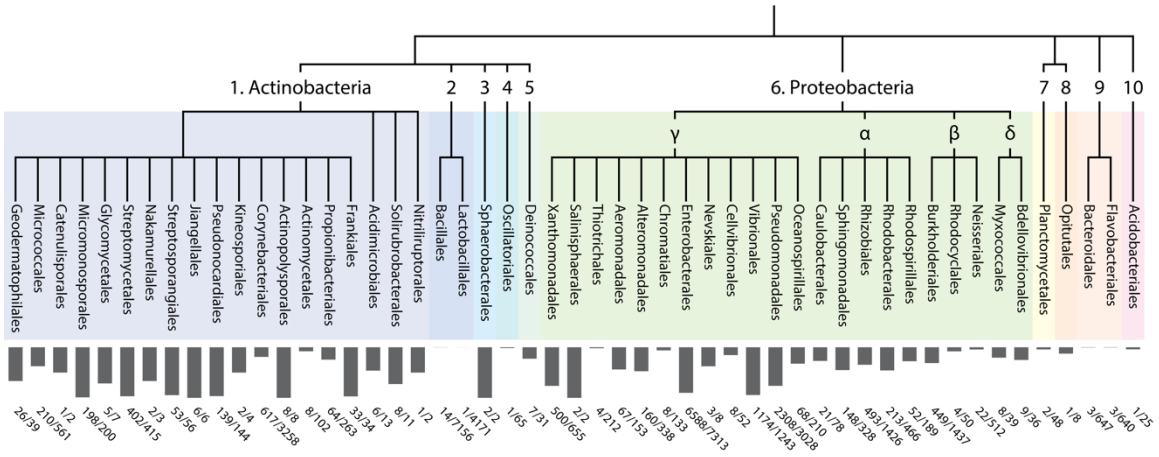

Figure 2. Phylogenetic distribution of SoxR, a transcription factor that senses redox-active metabolites. The phylogenetic tree shows all bacterial orders containing at least one genome with a SoxR homolog in the IMG database (SoxR TIGRfam 01950 (14)). The gray bars represent the percentage of genomes from each order that contain SoxR, with the absolute numbers listed below. The phyla represented are: (1) Actinobacteria, (2) Fermicutes, (3) Chloroflexi, (4) Cyanobacteria, (5) Deinococcus, (6) Proteobacteria, with each subphylum labeled separately, (7) Planctomycetes, (8) Verrumicrobia, (9) Bacteroidetes, (10) Acidobacteria. The tree was generated using the NCBI taxinomic classification with PhyloT and the IToL (38, 69).

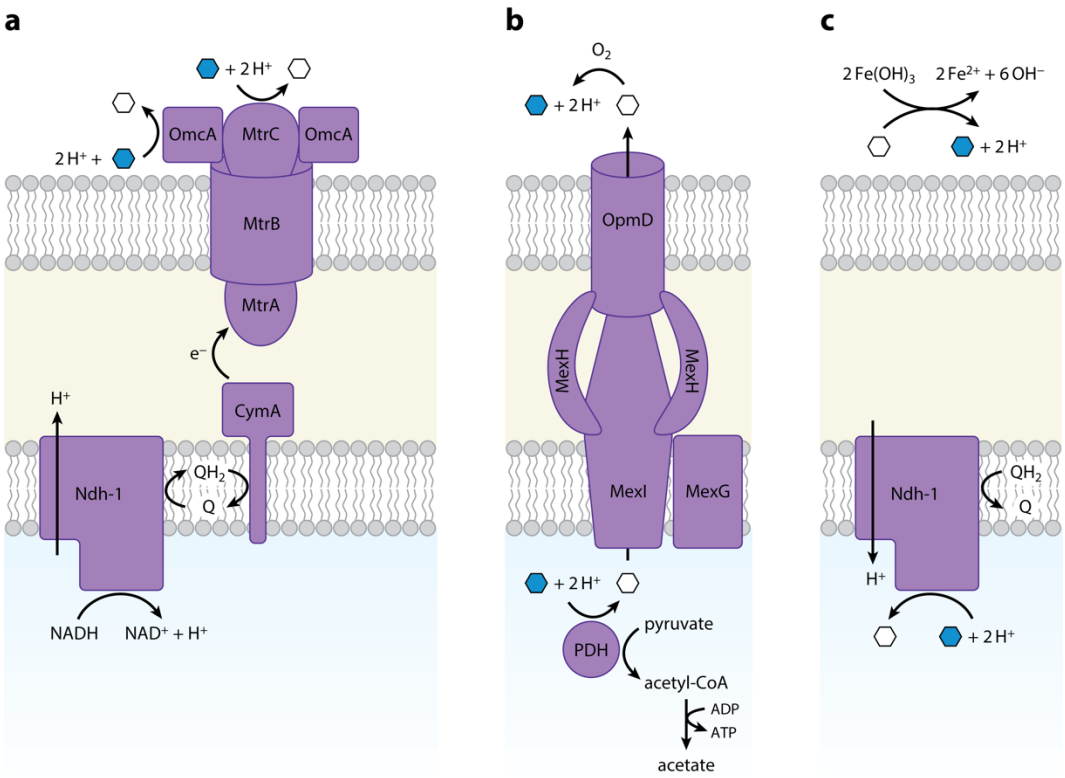

Figure 3. The topology of electron shuttle reduction and oxidation. Filled blue hexagons represent oxidized shuttle, and open white hexagons represent reduced shuttle. (a) The Mtr system in *S. oneidensis* MR-1. Shuttles are reduced extracellulary and do not need to re-enter the cell. (b) A model of phenazine reduction in *P. aeruginosa* that allows for energy conservation by electron shuttling. By substituting for NAD^+ in the pyruvate dehydrogenase complex (PDH), phenazines enable the synthesis of acetyl-CoA, which can drive ATP synthesis through the enzymes phosphate transacetylase and acetate kinase (46, 47). Efflux of reduced phenazines by MexGHI-OpmD (101) may be coupled to proton translocation. (c) A condition where electron shuttling is costly. Operating the NADH dehydrogenase in reverse can consume the protonmotive force to drive shuttle reduction. Extracellular reduction of some minerals, such as $Fe(OH)_3$, can alkalize the medium, possibly depleting the protonmotive force further and causing pH stress for the cell.

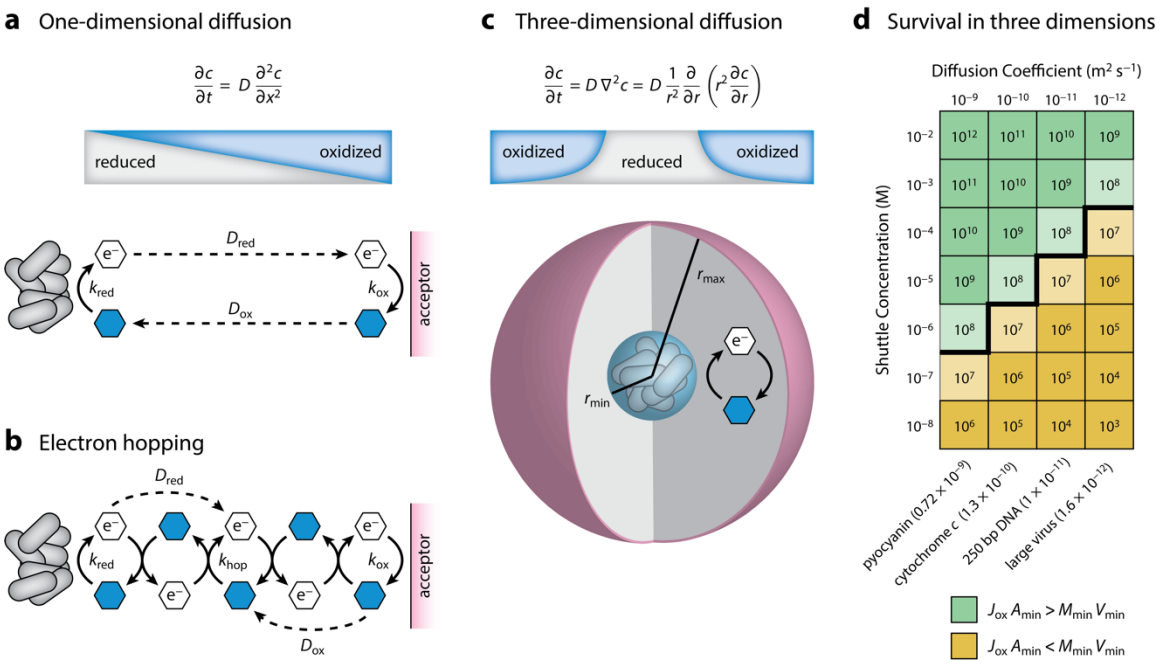

Figure 4. Mechanisms of electron transfer by EES. (a) Diffusion only. The reduced EES can diffuse down its concentration gradient to an electron acceptor, while the oxidized form simultaneously returns along its own concentration gradient. At steady state ($\partial c/\partial t = 0$), the concentration gradients are linear in this closed one-dimensional system. (b) The self-exchange rate (k_{hop}) allows electrons to hop between oxidized and reduced EES. If k_{hop} is significantly faster than the rate of diffusion, electron hopping will accelerate the apparent diffusion of electrons. EES diffusion can also co-occur. (c) In three dimensions, with an inner sphere of cells and an outer sphere of electron acceptor, the concentration gradient at steady state is *non-linear*. The gradient is steeper near the inner sphere, allowing for higher flux than in the one-dimensional case. (d) Results of a closed steady-state model of EES diffusion in three dimensions, with different EES concentrations and diffusion coefficients. Representative aqueous diffusion coefficients are listed below the plot (30, 73, 77, 79). The numbers in each box correspond to the modeled flux of oxidized EES (J_{ox}) through the surface area (A_{min}) of the inner sphere, in units of molecules per second. Green indicates regions where diffusion can account for the minimum flux needed for cells to survive, while orange indicates regions where diffusion is too slow. The number of molecules per second needed to support the inner sphere with volume V_{min} was calculated to be 1.5×10^7 molecules/s based on published parameters for M_{min}, the minimum energy required for survival in *P. aeruginosa* (64). The inner sphere radius was $r_{min} = 10$ µm and the outersphere radius was $r_{max} = 100$ µm. For simplification, we have taken the diffusion constants of the oxidized and reduced EES (D_{red} and D_{ox}) to be equivalent, and the rates of EES reduction and oxidation (k_{red} and k_{ox}) to be instant.

C h a p t e r 2

EXTRACELLULAR DNA PROMOTES EFFICIENT EXTRACELLULAR ELECTRON TRANSFER BY PYOCYANIN IN *PSEUDOMONAS AERUGINOSA* BIOFILMS

This work was first published as:

Saunders, S. H., Edmund, C. M., Yates, M. D., Otero, F. J., Trammell, S. A., Stemp, E. D, *Barton, J. K., *Tender, L. M. & *Newman, D. K. (2019). Extracellular DNA promotes efficient extracellular electron transfer by pyocyanin in *Pseudomonas aeruginosa* biofilms. *bioRxiv*. doi.org/10.1146/annurev-micro-090816-093913

* Corresponding authors

Abstract

Extracellular electron transfer (EET), the process whereby cells access electron acceptors or donors that reside many cell lengths away, enables metabolic activity by microorganisms, particularly under oxidant-limited conditions that occur in multicellular bacterial biofilms. Although different mechanisms underpin this process in select organisms, a widespread strategy involves extracellular electron shuttles: redox-active metabolites that are secreted and recycled by diverse bacteria. How these shuttles catalyze electron transfer within biofilms without being lost to the environment has been a long-standing question. Here, we show that phenazine electron shuttles mediate efficient EET through interactions with extracellular DNA (eDNA) in *Pseudomonas aeruginosa* biofilms, which are important in nature and disease. Retention of pyocyanin (PYO) and phenazine carboxamide in the biofilm matrix is facilitated by binding to eDNA. In vitro, different phenazines can exchange electrons in the presence or absence of DNA and phenazines can participate directly in redox reactions through DNA; the biofilm eDNA can also support rapid electron transfer between redox-active intercalators. Electrochemical measurements of biofilms indicate that retained PYO supports an efficient redox cycle with rapid EET and slow loss from the biofilm. Together, these results establish that eDNA facilitates phenazine metabolic processes in *P. aeruginosa* biofilms, suggesting a model for how extracellular electron shuttles achieve retention and efficient EET in biofilms.

Introduction

Microbial biofilms are ubiquitous in natural and engineered contexts, spanning plant roots to chronic human infections to anaerobic digestors (Watnick and Kolter, 2000). As biofilms develop, metabolic stratification occurs, driven by steep concentration gradients of substrates, such as oxygen, that are consumed by cells at the biofilm periphery faster than the substrates can diffuse into the biofilm interior (Stewart, 2003; Stewart and Franklin, 2008; Xu et al., 1998). Indeed, oxidant limitation is a generic challenge for cells that inhabit biofilm microenvironments where electron donors are abundant, yet electron acceptors are not. One widespread strategy microbes employ to overcome this challenge is to channel electrons derived from intracellular metabolism to extracellular oxidants at a distance (Shi et al., 2016).

Known as extracellular electron transfer (EET), this process requires electron carriers to bridge the gap, be they outer membrane-associated or extracellular cytochromes (Jiménez Otero et al., 2018; Richter et al., 2009; Xu et al., 2018), cytochrome-replete "nanowires" (Subramanian et al., 2018; Wang et al., 2019), cable bacteria conductive filaments (Cornelissen et al., 2018), or redox-active small molecules (Glasser et al., 2017a; Hernandez and Newman, 2001). While the putative molecular components underpinning different EET processes have been described in a variety of organisms, a detailed understanding of how these components achieve EET remains an important research goal across diverse systems.

In contrast to the intense study of microbial nanowires (Malvankar et al., 2011; Reguera et al., 2005; Wang et al., 2019), less attention has been paid to how small soluble (physically diffusive) extracellular electron shuttles facilitate EET beyond interactions at the cell surface (Light et al., 2018; Marsili et al., 2008; Xu et al., 2016). In part, this neglect is due to the challenges involved in identifying and studying small molecule metabolites, compared to the multiheme cytochromes observed in many genomes of organisms known to engage in EET. Accordingly, to study extracellular electron shuttling, we have chosen to work with a model system that employs a relatively well studied and tractable set of shuttles called phenazines. Phenazines are colorful redox-active molecules that are produced by numerous microbial species, including the bacterium *Pseudomonas aeruginosa* (Turner and Messenger, 1986). *P. aeruginosa* strains are ubiquitous yet perhaps most well-known for their roles in chronic infections where their growth as biofilms renders them antibiotic tolerant and contributes to patient morbidity and mortality (Costerton et al., 1999); importantly, phenazines support the development of anoxic, antibiotic tolerant biofilm regions (Dietrich et al., 2013a; Jo et al., 2017; Schiessl et al., 2019). While significant progress has been made in defining the composition of the *P. aeruginosa* biofilm matrix (Colvin et al., 2012) and mapping the zones of phenazine production within it (Bellin et al., 2014, 2016), we still have much to learn about how phenazines facilitate EET within the matrix.

Intriguingly, while the *P. aeruginosa* biofilm matrix comprises a heterogeneous group of polymers, extracellular DNA (eDNA) from dead cells is a significant contributor (Allesen-

Holm et al., 2006; Whitchurch et al., 2002), accounting for the majority of the matrix polymers in some cases (Matsukawa and Greenberg, 2004; Steinberger and Holden, 2005). Phenazines have long been known to intercalate into double stranded DNA *in vitro* (Hollstein and Van Gemert, 1971), and more recently, it was suggested that the phenazine pyocyanin (PYO) can participate in DNA-mediated charge transfer (DNA CT) chemistry *in vitro* (Das et al., 2015). Together with the observation that PYO promotes eDNA release by stimulating cell lysis (Das and Manefield, 2012), these facts led to speculation that phenazine-eDNA interactions might facilitate biofilm EET (Das et al., 2015). Notably, the ability of PYO to stimulate cell lysis changes according to the environment: when cells are oxidatively stressed (*i.e.* oxidant replete, but reductant limited) and ATP limited, PYO is toxic; whereas when they are reductively stressed (*i.e.* reductant replete, but oxidant limited), PYO promotes viability and biofilm aggregate expansion (Costa et al., 2017; Meirelles and Newman, 2018). This observation suggests the intriguing possibility that cell lysis by a small percentage of the population early on might later promote EET once biofilms have developed anoxic zones where extracellular electron shuttles support metabolism. Though a variety of roles for eDNA in biofilms have been proposed, including serving as a structural support, nutrient and/or genetic reservoir (Flemming and Wingender, 2010), to our knowledge, that eDNA may stimulate biofilm metabolism by facilitating EET has not been tested.

The current model of the phenazine redox cycle in biofilms can be broadly defined (Fig. 1A). In anoxic regions, oxidized phenazines are reduced intracellularly by metabolic reactions that support these cells (Glasser et al., 2014, 2017b; Jo et al., 2017; Wang et al., 2010). These reduced phenazines physically diffuse through the extracellular matrix toward the oxic region where they react abiotically with molecular oxygen. Upon re-oxidation, phenazines return to the anoxic region of the biofilm to complete the redox cycle. Although studies have begun to characterize the reactions on either side of the redox cycle, very little is known about how phenazines operate in the intervening extracellular matrix. Theoretical studies suggest that physical diffusion of oxidized phenazine towards the biofilm interior and reduced phenazine towards the biofilm periphery may be fast enough to support the metabolism of the oxidant limited cells (Glasser et al., 2017a; Kempes et al., 2014). However,

these studies assume a closed system, and it has been an unresolved paradox how diffusible extracellular molecules could function in a redox cycle without being lost from the biofilm to the environment. Here, we explore how phenazine electron transfer may be reconciled with phenazine retention. Specifically, we ask: Are phenazines retained? What mechanisms of electron transfer are compatible with phenazine retention? Is phenazine electron transfer *in vivo* fast compared to phenazine loss? Our motivation to answer these questions arises not only from a desire to constrain the model of phenazine redox cycling within *P. aeruginosa* biofilms, but more broadly, to identify a potentially generalizable strategy for how diverse electron shuttles enable EET.

Results

We studied three major phenazine derivatives made by *P. aeruginosa* strain UCBPP PA14 (Schroth et al., 2018): phenazine carboxylate (PCA), phenazine carboxamide (PCN), and pyocyanin (PYO) (Fig. 1B). Beyond studying wild type (WT) produced phenazines, we also explore the effects of individual synthetic phenazines on a mutant that does not produce phenazines, Δ*phz* (Δ*phzA1-G1*, Δ*phzA2-G2*), or on a mutant that is also incapable of modifying PCA, Δ*phz* (*Δ*phz,* Δ*phzMS,* Δ*phzH*). Experiments were performed with two different types of biofilms: macroscopic colony biofilms grown on nutrient agar surfaces (Fig. 1C, Fig. S1A) and microscopic biofilms attached to the surface of an interdigitated microelectrode array suspended in liquid medium. Phenazine-dependent biofilm phenotypes operate similarly at both scales (Ramos et al., 2010), so we selected the biofilm cultivation method for any given experiment based on which was best suited to answering our specific research question.

Colony biofilms retain PCN and PYO, but not PCA

First, we sought to quantify phenazine retention by colony biofilms (Fig 1C-D). In contrast to previous work that used an electrode array to electrochemically measure the spatial distribution of phenazines that physically diffuse into agar underneath colony biofilms (Bellin et al., 2014, 2016), we used liquid chromatography-mass spectrometry (LC-MS) to quantify extracted endogenous phenazines from the biofilms and compare their

concentrations to that in the underlying agar (Fig 1D-F). Colony biofilms could be cleanly separated from the agar because they were separated by a 0.2 μm membrane filter, which did not affect the results (Fig. S1B-C). Overall, PCA, PCN, and PYO concentrations varied by more than 10-fold in the biofilms reaching concentrations of ~15 μM PCA, ~ 400 μM PCN, and ~80 μM PYO. Comparing biofilm to agar concentrations showed that PCN and PYO were enriched in the biofilm 10-fold and 30-fold, respectively, while PCA reached similar concentrations in the biofilm and the agar (Fig. 1E-F). This suggested that PCN and PYO were strongly retained by the biofilm and PCA was not. Importantly, lysing resuspended biofilm cells by sonication prior to phenazine quantification did not strongly affect the results (Fig. S1D), indicating that the measured pools of phenazines were predominantly retained in the extracellular matrix rather than intracellularly.

To test if differential phenazine retention was caused by a spatial or temporal difference in biosynthesis, we grew *Δphz** colony biofilms with synthetic phenazines in the agar and quantified phenazines taken up by the biofilm. Incubation with ≥ 10μM PYO resulted in >200 μM PYO accumulation in the biofilm (Fig. 1G). PCN accumulated to a lesser extent, and PCA biofilm uptake was minimal (<50 μM) even with 200 μM added to the agar (Fig. 1G). *Δphz** colonies transferred from phenazine agar to fresh agar after 3 days of growth retained phenazines in the same pattern as the wild type (WT) over 24h (Fig. 1H), demonstrating that the observed phenazine retention does not depend on endogenous phenazine production. Wild-type colony biofilms exhibit relatively thick and smooth morphologies that contain deep anoxic regions that are thought to be supported by phenazines. Δ*phz** colony biofilms exhibit different colony morphologies that are thin and highly wrinkled, which is thought to be a physiological adaptation to maximize surface area and oxygen penetration in the absence of phenazines as shown for Δ*phz* (Dietrich et al., 2013b). Notably, only incubation of *Δphz** colonies with exogenous PYO appreciably complemented the colony wrinkling phenotype (Fig. S1A). *P. aeruginosa* colony biofilms thus appear able to take up and use significant amounts of exogenous PYO, and PCN to a lesser extent. These results predict that colony biofilms contain an extracellular matrix component that binds and effectively retains PYO and PCN, but not PCA.

Phenazines differentially bind extracellular DNA

The extracellular matrix in *P. aeruginosa* PA14 biofilms is known to be primarily composed of two polymers: DNA from dead cells (eDNA) and the polysaccharide Pel (Colvin et al., 2011; Das and Manefield, 2012). To test the hypothesis that eDNA in the biofilm matrix was responsible for binding phenazines, we quantified the binding affinity of oxidized PCA, PCN, and PYO for double-stranded (ds) DNA *in vitro* using isothermal titration calorimetry (Fig. 2A). As expected, oxidized PCA showed no detectable binding because it is negatively charged, as is the phosphate backbone of DNA at pH 7. In contrast, oxidized PCN (K_D = 194 μM; 95% C.I. 148 – 305 μM) and PYO (K_D = 13 μM; 95% C.I. 6.5 – 49 μM) both bind ds DNA, and these results were consistent with ethidium bromide displacement and microscale thermophoresis binding assays (Fig. S2A-B) (Das et al., 2015). Notably, these *in vitro* phenazine-DNA binding affinities correlate with their *in vivo* retention ratio ([biofilm]/[agar]), where PYO is retained in the biofilm significantly more than PCN, and PCA is not retained. Reduced PYO showed no change in endogenous fluorescence upon addition of calf thymus DNA (Fig. S2C), which is unexpected for strong intercalative binding. Therefore, the DNA binding affinity of PYO is likely redox-dependent.

To determine whether phenazine-eDNA binding occurs *in vivo*, we treated 3-day old WT biofilms with DNase I for 24 hrs. These experiments were performed with DNase I spotted on tryptone agar medium rather than its optimal buffer, as controls showed that buffer alone significantly disturbed the biofilm (Fig. S3A-C). Despite a low activity for DNase under these conditions, DNase-treated biofilms showed significantly lower biofilm PCN and PYO concentrations than their untreated counterparts; moreover, PCA concentration was unchanged (Fig. 2B). *P. aeruginosa* eDNA originates from the genomic DNA of dead cells and is therefore high molecular weight and may be bound by other biomolecules (e.g. proteins) (Kavanaugh et al., 2019). Therefore, DNase treatment was likely only partially effective because it could not cleave ds DNA in the presence of other bound matrix components, and/or because it did not have enough activity to degrade the eDNA completely to eliminate phenazine binding sites. We also compared the phenazine retention in the WT to a Pel mutant *(Δpel*) and found that biofilms without Pel retained significantly more PYO

(Fig. 2C). Because Pel is known to bind eDNA (Jennings et al., 2015), these results suggest that Pel may partially block access to eDNA by PYO, although this remains to be tested *in vitro*.

To probe the eDNA binding sites within the biofilm using a different approach, we competed phenazines against ethidium bromide, a classical DNA intercalator. Since PCN and PYO compete for DNA binding sites with ethidium *in vitro*, and ethidium is largely excluded from cells (Jernaes and Steen, 1994), we reasoned that these intercalators could compete for binding sites in the biofilm eDNA. We grew Δ*phz** biofilms with 50 μM PCN and PYO and increasing amounts of ethidium in the underlying agar. Figure 2D shows that increasing concentrations of ethidium resulted in successively less PYO accumulating in the biofilms, while PCN accumulated to a similar lower level in the presence of any amount of added ethidium.

Confocal microscopy of WT and Δ*phz** colony biofilms with a cell-impermeable ds DNA dye, TOTO-1 (Okshevsky and Meyer, 2014), showed abundant eDNA localized in dead cells and in between cells (Fig. S3D). We quantified the bulk concentration of eDNA in colony biofilms by incubating biofilm suspensions with TOTO-1 and measuring dye fluorescence. Both WT and Δ*phz** biofilm suspensions yielded large fluorescence values when incubated with TOTO-1. These values fall within the range of 60–500 μM bp ds DNA in the colony biofilms, when calibrated against standards of calf thymus DNA (Fig. 2E). However, adding calf thymus DNA to the biofilm suspensions did not yield the expected increase in dye fluorescence (Fig. S3E), which suggests that the dye may be partially inhibited by biofilm components. Therefore, this order of magnitude estimate of biofilm eDNA should be interpreted as a lower bound on the true value. Given this estimate, the biofilm eDNA (>100 μM bp) is in excess of PYO (~80 μM), but it may not be in excess of PCN (>300 μM). Due to its poor aqueous solubility, it is probable that PCN crystallizes extracellularly at the observed biofilm concentrations, which could lead to its measured retention (Hernandez et al., 2004). Together, our *in vivo* and *in vitro* results are consistent with eDNA providing binding sites for oxidized PCN and oxidized PYO in the biofilm extracellular matrix.

Constraints on phenazine electron transfer mechanisms in vitro and in vivo

Given that phenazines are differentially bound and retained in biofilm eDNA, we next sought to constrain how electron transfer might be achieved in this context. Previous research has shown distinct localization patterns for different phenazines within biofilms, with the lowest potential phenazines (*e.g.* PCA) in the interior, and the highest potential phenazine (*e.g.* PYO) at the oxic periphery (Bellin et al., 2014, 2016). To test whether electron transfer could occur between these molecules in solution, we mixed different oxidized and reduced phenazines under anoxic conditions and monitored the absorbance spectra before and after mixing (Fig. 3A-B). Because PYO exhibited the largest changes in absorbance upon reduction, we monitored different mixtures of PYO with PCA or PCN at 690 nm (unique PYO absorbance maximum) starting one minute after mixing, at which point equilibrium had been achieved. Reactions proceeded as expected from the redox potentials of the phenazines, where PYO was almost completely reduced by the lower potential PCA and PCN, but reduction of PCA and PCN by the higher potential PYO was minimal (Fig. 3B, Fig. S4A). In addition to establishing that electron transfer can occur between different phenazines, given their similar structures, these results suggest that electron transfer between like phenazines (*e.g.,* PYO-PYO electron self-exchange) can occur within a redox gradient. Moreover, reactions between reduced PCA or PCN and oxidized PYO proceeded faster than oxidation of any of these phenazines by molecular oxygen (Fig. 3C). We next wondered whether the presence of eDNA would affect the extent of PYO reduction. PYO reduction by PCA or PCN proceeded to completion in the presence of eDNA (Fig. 3B). Because PCA does not bind eDNA, this result suggests that electron transfer is occurring in solution between PCA and unbound PYO. For PCN and PYO that both bind eDNA, it is also possible that electron transfer is achieved by their unbound counterparts in solution. However, it has long been known that DNA can facilitate electron transfer between bound redox molecules (Genereux and Barton, 2010), motivating us to test whether such a process could also occur within our *P. aeruginosa* biofilms.

DNA facilitates charge transfer (DNA CT) through the π-stacked base pairs (Genereux and Barton, 2010), and recent studies have shown that DNA CT can occur over kilobase distances

(Tse et al., 2019). A previous study suggested that PYO might be able to transport electrons via DNA (Das et al., 2015), but given the preliminary nature of these experiments, we decided to revisit these experiments more rigorously. To better test the ability of phenazines to carry out DNA CT, we covalently attached a phenazine via a flexible linker to one DNA strand and then made DNA-modified gold electrodes with a thiol linker on the complementary strand according to standard protocols (Kelley et al., 1997; Slinker et al., 2010, 2011). Specifically, short ds DNA molecules (17 bp) were covalently linked to the gold surface to form a packed monolayer, and the distal 5' end of each duplex contained a covalently linked PCN, the phenazine derivative most amenable to synthesis (see Materials and Methods) (Fig. 3D). Thus, we established a well-defined chemical system to test if a phenazine could participate in electron transfer to the electrode through the ds DNA.

Because the efficiency of DNA CT depends upon the integrity of the π-stacking of base pairs within the DNA duplex (Genereux and Barton, 2010), we compared well-matched duplex DNA monolayers to duplex DNAs containing a single base mismatch that stacks less efficiently (Fig. 3D). We utilized multiplexed DNA chips to facilitate replicate comparisons between well-matched and mismatched DNA monolayers (Fig. S4B-D); measurements with a non-intercalating control probe showed that these different monolayers had very similar surface coverages (Fig. S4E-F) (Slinker et al., 2010). Figure 3E shows that the mismatched construct yielded diminished current in the phenazine redox peak, consistent with the charge transfer being DNA-mediated; the presence of the intervening mismatch inhibits DNA CT. This mismatch effect was consistent across replicate low density (32-54% decrease) and high density (36-69% decrease) DNA monolayers (Fig. S4C and supp. text). These results displayed mismatch attenuation similar to that observed for well-characterized small molecules shown to stack with the DNA duplex and carry out DNA-mediated CT (Slinker et al., 2011). Strikingly, in the presence of oxygen, a classic voltammetric signal characteristic of electrocatalysis was obtained (Fig. 3F) centered on the phenazine redox peak. Hence, the DNA-tethered phenazine is able to accept electrons from the electrode through the DNA π-stack and then reduce oxygen in a catalytic fashion. Together, these results demonstrate that a *P. aeruginosa* phenazine can participate in DNA CT *in vitro*.

To test if biofilm eDNA could support DNA CT, we incubated Δ*phz** colony biofilms suspended in PBS with well-characterized intercalators that can perform DNA CT reactions, which can be monitored by time-resolved spectroscopy (Arkin et al., 1996a). The quenching of photoexcited $Ru(phen)_2dppz^{2+}$ by $Rh(phi)_2bpy^{3+}$ is well-characterized and known to occur by a redox mechanism (Stemp et al., 1995) and not energy transfer (e.g. FRET), with both the forward and back electron transfers occurring predominantly on the picosecond timescale (Fig. 3G, Fig. S4G) (Arkin et al., 1996b). Both of these intercalators bind to ds DNA more than an order of magnitude more tightly than do phenazines. Moreover, $Ru(phen)_2dppz^{2+}$ is luminescent in aqueous solution only when intercalated in DNA (or otherwise protected from water), precluding a 2nd order reaction between the complexes in solution. Thus, in time-resolved emission experiments on the nanosecond timescale, static quenching, where quenching is fast and occurs without a change in the $Ru(phen)_2dppz^{2+}$ excited state lifetime, is consistent with DNA-mediated CT (Arkin et al., 1996a), while slower dynamic quenching, which leads to a change in emission lifetime, is consistent with a slower diffusive process. We first compared the $Ru(phen)_2dppz^{2+}$ signals of liquid grown and biofilm suspensions (of the same optical density) to determine if the signal was specific to eDNA; the ruthenium complex is not expected to be taken up by the cells and bind to genomic DNA on the time scale of this experiment (Fig. 3H). We only observed ruthenium luminescence in the presence of the biofilm suspension, consistent with ruthenium luminescence being associated with binding to eDNA. We then examined the pattern of quenching of $Ru(phen)_2dppz^{2+}$ by $Rh(phi)_2bpy^{3+}$. Figure 3I shows static quenching where the intensity of the $Ru(phen)_2dppz^{2+}$ signal decreases, while the observed decay kinetics are unchanged (Fig. S4H). Therefore, we conclude that biofilm eDNA can support rapid DNA CT between these two metal complexes faster than the timescale for diffusion.

Electrode-grown biofilms retain PYO capable of extracellular electron transfer

Having explored phenazine retention and electron transfer separately, we next wanted to establish a system in which we could monitor both of these processes simultaneously in vivo. We took an electrochemical approach to achieve this, growing *P. aeruginosa* biofilms on interdigitated microelectrode arrays (IDA) (Fig. 4A). Biofilms were grown by incubating

IDAs in bioelectrochemical reactors with planktonic cultures under oxic conditions and stirring (Fig. 4B). After 4 days, with medium replaced daily, mature biofilms were transferred to anoxic reactors with fresh medium for electrochemical measurements. Confocal and SEM imaging revealed that the IDA biofilms were heterogeneous in composition, but consistently contained multicellular structures of live cells and abundant eDNA (Fig. 4C-E, Fig. S5A-B). Under these conditions, the cells predominately produced PYO, as measured by LC-MS (Fig. S5C). Because PYO was the most tightly retained phenazine in colony biofilms and in vitro, we focused on this phenazine for the remainder of these experiments.

Originally used to measure conductivity of abiotic materials, the IDA has a 2-working electrode geometry and recently was adapted to study EET through microbial biofilms (Boyd et al., 2015; Snider et al., 2012; Xu et al., 2018; Yates et al., 2015). Measurements are made by driving electron transfer between the two electrode bands across a 5 μm gap (Fig. 4F), which treats the biofilm like an abiotic material, resulting in EET that is decoupled from the cells' metabolic activity. Specifically, we used a generator-collector (GC) strategy to measure EET through the biofilm, where the "generator" electrode is swept from an oxidizing potential (E = 0 mV vs. Ag/AgCl) to a reducing potential (E = -500 mV), while the "collector" electrode maintains a fixed oxidizing potential (E = 0 mV). In this GC arrangement, electron transfer into the biofilm from the generator occurs as the potential of the generator is swept negatively, reducing PYO (E_0 = -250 mV) at the biofilm/generator interface. Electrons are conducted across the gap through the biofilm due to EET, either by physical diffusion of PYO or other mechanisms. The electron transfer at both the generator and collector is measured as current (I_{gc}) and plotted against the potential of the generator electrode. Implicit in generating a sustained I_{gc} is recycling of the redox molecules that support the observed current. Figure 4G shows that WT and *Δphz** + PYO biofilms supported current (above background), while *Δphz** alone did not. This current occurs across the 5 μm gap over a ~3 min scan as the generator potential approached PYO's redox potential (-250 mV vs. Ag/AgCl), consistent with PYO-mediated EET. Dependency of current on the generator potential observed here is consistent with PYO-mediated EET being a diffusive

process. Reduction of PYO at the generator and oxidation of PYO at the collector generates a redox gradient that drives EET through the intervening biofilm, resulting in current centered on the PYO midpoint potential that saturates at strongly reducing generator potentials (Snider et al., 2012). Here, the diffusive nature of EET would reflect either physical diffusion of PYO through the biofilm (reduced PYO from the generator to collector, oxidized PYO from the collector to the generator) or the effective diffusion of electrons through bound PYO (Strycharz-Glaven et al., 2011a).

To test whether these short-term GC measurements of biofilm EET indicate long-term ability to support metabolic activity, we poised the IDA electrodes at an oxidizing potential (+100mV vs. Ag/AgCl) and monitored the current produced by the biofilm over 4 days in the presence of 40 mM succinate as the electron donor for cellular metabolism under anoxic conditions. In this configuration, the observed current would be due to cellular oxidation of succinate coupled with PYO-catalyzed EET to the poised electrode, where the electrode acts as the terminal electron acceptor instead of oxygen (Fig. 4H). Figure 4I shows that both WT biofilms relying solely on endogenous PYO and *Δphz** biofilms + exogenous PYO generate robust current over many days, while *Δphz** alone does not. The daily periodic rise in current likely reflects the impact of slight temperature or light fluctuations in the room on the cells' metabolic activity over the course of the experiment (Kahl et al., 2016, 2019). Differences in current magnitude between the WT and *Δphz** + PYO runs are likely due to differences in PYO abundance in the biofilms and/or efficiency of cellular PYO reduction. Together, these results demonstrate that the IDA biofilms can use retained PYO for EET to support metabolic activity.

To determine whether our IDA biofilms retained phenazines in the same manner as colony biofilms, *Δphz** IDA biofilms were soaked in PYO in one reactor and then transferred to another reactor with fresh medium lacking PYO (Fig. 5A). The equilibration of PYO (from the IDA biofilm) with the fresh medium was monitored by square wave voltammetry (SWV) (Fig. 5B), for which peak current (I_{swv}) is proportional to the concentration of the PYO remaining in the biofilm at each time interval (Bard et al., 1980). Thus, the rate of decay of

I_{swv} provides a means to assess the loss rate of PYO from the biofilm, a measure of how tightly PYO is retained. Upon transfer, the biofilm PYO peak current (I_{swv}) decays in 30-45 min, while for a blank IDA (no biofilm) dipped in PYO, I_{swv} decays in 2-3 min (Fig. 5E). We compared PYO and PCA soaks and found that PCA immediately became undetectable by SWV or GC in the transfer reactor (Fig. S5D-E) because it quickly diffuses out of the biofilm, as expected, because it does not bind eDNA. Thus, like colony biofilms, IDA biofilms appear to tightly retain PYO but not PCA.

Electron transfer through biofilms is faster than PYO loss

Next, we sought to understand the efficiency of PYO-mediated EET in the biofilm. We reasoned that a determination of "efficiency" would compare the rate of electron transfer (which supports the metabolism of the O_2 limited cells) to the loss rate of PYO from the biofilm (which limits the utility of each PYO molecule). These two processes can both be described by diffusion coefficients, so in a single electrochemical experiment we measured the apparent diffusion coefficient for the PYO-mediated EET, D_{ap}, which characterizes all of the redox processes with the electrode, and the diffusion coefficient for PYO as it is lost from the biofilm, D_{loss}.

We determined D_{ap} for EET by PYO in an IDA Δ*phz** biofilm to avoid confounding PYO retention with production, although WT biofilms with endogenous PYO yielded similar results (Fig. S6A-B). Each Δ*phz** biofilm was soaked with PYO in one reactor, then transferred to a second reactor lacking PYO (Fig. 5A), and the equilibration of the biofilm PYO into the fresh medium was monitored by paired SWV and GC measurements over time (Fig. 5B and Fig. 5C). Noting that I_{swv} is proportional to $C * \sqrt{D_{ap}}$, where C is the effective PYO concentration (Bard et al., 1980), whereas I_{gc} is proportional to $C * D_{ap}$ (Strycharz-Glaven et al., 2011b), plotting I_{gc} vs. I_{swv} for each time point is expected to yield a linear dependency with a slope (m) proportional to $\sqrt{D_{ap}}$ (Fig. 5D) when D_{ap} is independent of the concentration of PYO in the biofilm (Akhoury et al., 2013; White et al., 1982a). In this manner, it is possible to measure D_{ap} for PYO remaining in the biofilm at any given instance when its concentration is unknown.

Applying this approach, for two biological replicates of Δ*phz** biofilms (three technical replicates each), we found that the mean D_{ap} for PYO is 6.4 x10^{-6} cm^2/sec over a wide range of PYO biofilm concentrations (Fig. 5F, Fig. S6C). To validate our approach, we measured D_{ap} using a blank IDA with no biofilm, only solution PYO for which we expect $D_{ap} \approx D_{loss}$. Using known PYO concentrations with a blank IDA (no biofilm), we obtained nearly identical estimates (D_{ap} = 6.8x10^{-6} cm^2/sec) using our I_{gc} vs. I_{swv} method (concentration unknown) or established methods (I_{gc} vs. [PYO] and I_{swv} vs. [PYO]) that depend on known concentrations (Fig. 5F, Supplementary text, Fig. S6D-G) (Bard et al., 1980). We further validated our measurement scheme by comparing it to an established chronocoulometry technique with two other redox molecules (Hexaammineruthenium(III) and ferrocenemethanol) in the presence and absence of the polymer Nafion. In all cases, estimates of D_{ap} by the two methods were within ~2x (Fig. S6H).

To estimate the upper limit for D_{loss} of PYO lost from *P. aeruginosa* biofilms, we applied a semi-infinite one-dimensional diffusion model (Supplemental Text) to fit the decay of the same I_{swv} measurements used above (Fig. 5B, 5E). Although each SWV scan depends on D_{ap}, the decay process of I_{swv} results from loss of PYO out of the biofilm (D_{loss}). This calculation requires a scan time constant, whose value we constrain by using the blank control where we assume $D_{ap} = D_{loss}$, allowing us to solve for this constant (see Supplemental Text and Fig. S7A). For *Δphz** biofilms, this diffusion model yields a mean D_{loss} of 2.0x10^{-7} cm^2/sec (Fig. S7B). Hence, D_{ap} for PYO-mediated biofilm EET is more than 25-fold higher than D_{loss} (Fig. 5F). While this model simplifies the actual physical system, it provides a means to estimate an upper limit for the rate of PYO loss from the biofilm. Such a low D_{loss} is consistent with the relatively long time it takes for I_{swv} to decay when transferred to fresh medium for PYO in a biofilm (~45min) compared to PYO for a blank IDA (<2min) (Fig. 5E) or to PCA in a biofilm (< 1 min) (Fig. S5E). Moreover, the conservative assumptions of our model make it likely that we have underestimated the true difference between D_{loss} and D_{ap} in the biofilm. Collectively, these observations support the idea that PYO EET occurs rapidly compared to the loss of PYO diffusing out of the IDA biofilms.

Discussion

The redox activity of phenazine metabolites produced by *P. aeruginosa* has intrigued researchers since the 1930's (Friedheim, 1934), and over the last twenty years a model has emerged that links phenazine electron transfer to biofilm metabolism (Dietrich et al., 2013b; Hernandez and Newman, 2001; Jo et al., 2017). Using the well-characterized *P. aeruginosa*-phenazine system as a model for studying EET mediated by extracellular electron shuttles, here we addressed the conundrum of how phenazines complete their redox cycle within the biofilm matrix without being lost to the environment. Our results point to eDNA as being a critical component of the matrix that facilitates phenazine cycling for EET.

Quantifying phenazine retention in a simple biofilm system was our first goal. While past work has measured phenazines in culture supernatants and in agar underlying colony biofilms (Bellin et al., 2014, 2016; Dietrich et al., 2006), phenazine concentrations within any type of biofilm system were unknown. We found that the degree of retention varied dramatically between the three studied phenazines in colony biofilms, with PCN and PYO being strongly enriched in the biofilm, in contrast to PCA, which readily diffuses away. We observed a similar trend for biofilms grown in liquid medium attaching to IDAs. Notably, oxidized PCN and PYO bind ds DNA *in vitro*, and perturbing extracellular DNA binding sites disrupt PYO retention (and PCN to a lesser extent) *in vivo*. Previous studies have shown that PYO actually promotes eDNA release via cell lysis, so PYO retention by eDNA suggests a connection between eDNA production and utilization. To our knowledge, PYO retention in eDNA is the first example of a metabolically helpful (as opposed to biofilm structural) molecule being bound by the extracellular matrix of a biofilm. Because eDNA is found in biofilms made by diverse species and many small molecules exhibit DNA binding capacity, our results may be broadly relevant to diverse biofilm functions involving extracellular metabolites.

Recognizing that a primary function for phenazines is extracellular electron transfer, we characterized this process *in vivo*. Our IDA experiments suggest that PYO simultaneously can be retained (low D_{loss}) and facilitate fast EET (high D_{ap}), establishing the efficiency of

this process. To understand the mechanism that underpins this efficient EET, we can interpret our results in the context of electron transfer theory from the study of redox polymers (Dalton and Murray, 1990). This theory holds that the measured D_{ap} is the sum of the effective diffusion coefficient of electrons due to self-exchange reactions among bound shuttles (D_e) and the physical diffusion coefficient (D_{phys}) of any unbound shuttles ($D_{ap} = D_e + D_{phys}$). In this context, we think that there are two ways to explain our electrochemical results that biofilm PYO D_{ap} (~6.4 x10^{-6} cm^2/sec) is higher than biofilm PYO D_{loss} (~2.0 x10^{-7} cm^2/sec), and similar to solution PYO D_{phys} (6.8 x10^{-6} cm^2/sec) (Fig. 5F). First, if we assume that our measured D_{loss} is the same as PYO D_{phys} within the biofilm, the difference between D_{ap} and D_{phys} can be explained by D_e. Our *in vitro* data suggest that such self-exchange reactions (D_e) could be DNA-mediated. In the case of very rapid electron transfer among eDNA-bound PYO, D_{ap} would still be limited by counter ion diffusion, consistent with a measured D_{ap} similar to that of a small molecule in solution (~7 x 10^{-6} cm^2/s) (White et al., 1982b). Alternatively, the measured loss of PYO from the biofilm, D_{loss}, may not accurately reflect physical diffusion of PYO within the biofilm, D_{phys}. Because the IDA biofilms do not completely cover the electrodes, PYO may be able to physically diffuse in solution adjacent to them. In this case, diffusion in solution would be consistent with the measured D_{ap}, and the low D_{loss} measurement would reflect the slow release of PYO from the IDA biofilm due to its retention by eDNA. Regardless, the striking measured difference between D_{ap} and D_{loss} indicates that PYO electron transfer promotes efficient biofilm EET metabolism because electron transfer occurs rapidly, while loss of PYO to the environment is slow.

Together, our results allow us to refine our model for how phenazine EET may operate within biofilms (Fig. 6). Intriguingly, PYO biosynthesis requires O_2, whereas PCN and PCA do not, and electrochemical imaging underneath colony biofilms has shown lower potential phenazines in the anoxic interior (PCA, PCN) and the higher potential phenazine (PYO) near the oxic periphery (Bellin et al., 2014, 2016). Reduced PYO is also known to react with oxygen significantly faster than PCA and PCN (Wang and Newman, 2008). As such, it is tempting to speculate that phenazines are ordered in the biofilm matrix in a sequence akin to a large extracellular electron transport chain—from reduced PCA/PCN in the anoxic interior,

to eDNA bound PYO at the oxic periphery, and ultimately to molecular oxygen (Fig. 6A). How then do phenazines exchange electrons within this framework? Noting that the heterogeneity of the biofilm matrix makes it possible that different electron transfer pathways could occur in these complex systems, we favor two mechanisms mediated by eDNA for how phenazine EET may operate in the matrix (Fig. 6B). Both mechanisms assume that reduced PCA and PCN will diffuse from the anoxic zone to the oxic zone (i), where PYO_{ox} is bound to eDNA. In one model (Fig. 6B top), PYO's binding equilibrium will result in some PYO_{ox} unbinding from the eDNA, allowing it to react with PCA_{red} or PCN_{red} (ii). PYO_{red} then reacts with oxygen generating PYO_{ox} (iii), which rebinds DNA. In the other model (Fig. 6B bottom), reduced phenazines (likely PCN) intercalate into eDNA and reduce PYO_{ox} via DNA CT (ii). PYO_{red} unbinds DNA, reacts with oxygen (iii), and PYO_{ox} rebinds DNA. Given that PCA_{red} and PCN_{red} react more quickly with PYO_{ox} than O_2, then both models would facilitate the re-oxidation of the interior phenazines and promote diffusion back toward the anoxic interior (iv). These non-mutually exclusive models integrate what is known about phenazine O_2 reactivities, redox potentials, and biosynthesis zones, and help explain how PYO and eDNA interactions enhance EET in *P. aeruginosa* biofilms by facilitating retention and electron transfer. Testing these models in physicochemically well-defined matrixes in addition to complex biofilms represents an exciting challenge for future research.

In conclusion, our findings illustrate that eDNA binding provides a mechanism to resolve how otherwise diffusible extracellular electron shuttles can catalyze efficient EET in real world, open systems. Beyond serving as a structural support, carbon source, or genetic reservoir, our studies reveal that interactions between extracellular electron shuttles and eDNA in biofilms underpin their metabolic vitality. It is noteworthy that eDNA is abundant in many biofilms (Flemming and Wingender, 2010) and diverse biofilm-forming bacteria have the potential to produce extracellular electron shuttles (Glasser et al., 2017a). Accordingly, eDNA retention of these electron shuttles—and perhaps of other biologically useful molecules—may represent a widespread strategy whereby a reactive extracellular matrix supports bacterial biofilms in unexpected and physiologically significant ways.

Acknowledgments

We thank Jeanyoung Jo, Lars Dietrich, and Matthew Parsek for providing strains. This work was supported by grants to D.K.N. from NIH (1R01AI127850- 01A1) and ARO (W911NF-17-1-0024), to J.K.B. from NIH (GM126904), and to S.H.S., D.K.N, and J.K.B. from the Rosen Bioengineering Center at Caltech. E.C.M.T. was supported by a Croucher Foundation Research Fellowship.

Author contributions

Conceptualization, S.H.S., J.K.B., L.M.T., and D.K.N.; Methodology, S.H.S., E.C.M.T., M.D.Y., F.J.O., S.A.T., E.D.A.S., J.K.B., L.M.T., D.K.N.; Formal Analysis, S.H.S. and L.M.T.; Investigation, S.H.S., E.C.M.T., M.D.Y., F.J.O., S.A.T., E.D.A.S.; Resources, J.K.B., L.M.T. and D.K.N.; Writing – Original Draft, S.H.S. and D.K.N.; Writing – Reviewing & Editing, S.H.S., E.C.M.T., M.D.Y., F.J.O., S.A.T., E.D.A.S., J.K.B., L.M.T., D.K.N.; Visualization, S.H.S.; Supervision, J.K.B., L.M.T. and D.K.N.; Funding Acquisition, J.K.B., L.M.T. and D.K.N.

Competing interests

Authors declare no competing interests.

Data and materials availability

Data and strains used in this study are available on request. Data and code are available at github.com/DKN-lab/phz_eDNA_2019.

References

Akhoury, A., Bromberg, L., and Hatton, T.A. (2013). Interplay of electron hopping and bounded diffusion during charge transport in redox polymer electrodes. J Phys Chem B *117*, 333–342.

Allesen-Holm, M., Barken, K.B., Yang, L., Klausen, M., Webb, J.S., Kjelleberg, S., Molin, S., Givskov, M., and Tolker-Nielsen, T. (2006). A characterization of DNA release in *Pseudomonas aeruginosa* cultures and biofilms. Mol Microbiol *59*, 1114–1128.

Arkin, M.R., Stemp, E.D.A., Turro, C., Turro, N.J., and Barton, J.K. (1996a). Luminescence Quenching in Supramolecular Systems: A Comparison of DNA- and SDS Micelle-Mediated Photoinduced Electron Transfer between Metal Complexes. J Am Chem Soc *118*, 2267–2274.

Arkin, M.R., Stemp, E.D., Holmlin, R.E., Barton, J.K., Hörmann, A., Olson, E.J., and Barbara, P.F. (1996b). Rates of DNA-mediated electron transfer between metallointercalators. Science *273*, 475–480.

Atlas, R. (2004). Handbook of microbiological media, third edition (CRC Press).

Bard, A.J., Faulkner, L.R., Leddy, J., and Zoski, C.G. (1980). Electrochemical methods: fundamentals and applications (New York: Wiley).

Bellin, D.L., Sakhtah, H., Rosenstein, J.K., Levine, P.M., Thimot, J., Emmett, K., Dietrich, L.E.P., and Shepard, K.L. (2014). Integrated circuit-based electrochemical sensor for spatially resolved detection of redox-active metabolites in biofilms. Nat Commun *5*, 3256.

Bellin, D.L., Sakhtah, H., Zhang, Y., Price-Whelan, A., Dietrich, L.E.P., and Shepard, K.L. (2016). Electrochemical camera chip for simultaneous imaging of multiple metabolites in biofilms. Nat Commun *7*, 10535.

Boyd, D.A., Snider, R.M., Erickson, J.S., Roy, J.N., Strycharz-Glaven, S.M., and Tender, L.M. (2015). Theory of Redox Conduction and the Measurement of Electron Transport Rates Through Electrochemically Active Biofilms. In Biofilms in Bioelectrochemical Systems, H. Beyenal, and J. Babauta, eds. (John Wiley & Sons, Inc), p.

Colvin, K.M., Gordon, V.D., Murakami, K., Borlee, B.R., Wozniak, D.J., Wong, G.C.L., and Parsek, M.R. (2011). The pel polysaccharide can serve a structural and protective role in the biofilm matrix of *Pseudomonas aeruginosa*. PLoS Pathog *7*, e1001264.

Colvin, K.M., Irie, Y., Tart, C.S., Urbano, R., Whitney, J.C., Ryder, C., Howell, P.L., Wozniak, D.J., and Parsek, M.R. (2012). The Pel and Psl polysaccharides provide *Pseudomonas aeruginosa* structural redundancy within the biofilm matrix. Environ Microbiol *14*, 1913–1928.

Cornelissen, R., Bøggild, A., Thiruvallur Eachambadi, R., Koning, R.I., Kremer, A., Hidalgo-Martinez, S., Zetsche, E.-M., Damgaard, L.R., Bonné, R., Drijkoningen, J., et al. (2018). The cell envelope structure of cable bacteria. Front Microbiol *9*, 3044.

Costa, K.C., Glasser, N.R., Conway, S.J., and Newman, D.K. (2017). Pyocyanin degradation by a tautomerizing demethylase inhibits *Pseudomonas aeruginosa* biofilms. Science *355*, 170–173.

Costerton, J.W., Stewart, P.S., and Greenberg, E.P. (1999). Bacterial biofilms: a common cause of persistent infections. Science *284*, 1318–1322.

Das, T., and Manefield, M. (2012). Pyocyanin promotes extracellular DNA release in *Pseudomonas aeruginosa*. PLoS ONE *7*, e46718.

Das, T., Kutty, S.K., Tavallaie, R., Ibugo, A.I., Panchompoo, J., Sehar, S., Aldous, L., Yeung, A.W., Thomas, S.R., Kumar, N., et al. (2015). Phenazine virulence factor binding to extracellular DNA is important for *Pseudomonas aeruginosa* biofilm formation. Sci. Rep. *5*, 8398.

Dietrich, L.E.P., Price-Whelan, A., Petersen, A., Whiteley, M., and Newman, D.K. (2006). The phenazine pyocyanin is a terminal signalling factor in the quorum sensing network of *Pseudomonas aeruginosa*. Mol Microbiol *61*, 1308–1321.

Dietrich, L.E.P., Okegbe, C., Price-Whelan, A., Sakhtah, H., Hunter, R.C., and Newman, D.K. (2013a). Bacterial community morphogenesis is intimately linked to the intracellular redox state. J Bacteriol *195*, 1371–1380.

Dietrich, L.E.P., Okegbe, C., Price-Whelan, A., Sakhtah, H., Hunter, R.C., and Newman, D.K. (2013b). Bacterial community morphogenesis is intimately linked to the intracellular redox state. J Bacteriol *195*, 1371–1380.

Duvvuri, H., Wheeler, L.C., and Harms, M.J. (2018). pytc: Open-Source Python Software for Global Analyses of Isothermal Titration Calorimetry Data. Biochemistry *57*, 2578–2583.

Flemming, H.-C., and Wingender, J. (2010). The biofilm matrix. Nat Rev Microbiol *8*, 623–633.

Friedheim, E.A. (1934). The effect of pyocyanine on the respiration of some normal tissues and tumours. Biochem J *28*, 173–179.

Genereux, J.C., and Barton, J.K. (2010). Mechanisms for DNA charge transport. Chem Rev *110*, 1642–1662.

Glasser, N.R., Kern, S.E., and Newman, D.K. (2014). Phenazine redox cycling enhances anaerobic survival in *Pseudomonas aeruginosa* by facilitating generation of ATP and a proton-motive force. Mol Microbiol *92*, 399–412.

Glasser, N.R., Saunders, S.H., and Newman, D.K. (2017a). The colorful world of extracellular electron shuttles. Annu Rev Microbiol *71*, 731–751.

Glasser, N.R., Wang, B.X., Hoy, J.A., and Newman, D.K. (2017b). The Pyruvate and α-Ketoglutarate Dehydrogenase Complexes of *Pseudomonas aeruginosa* Catalyze Pyocyanin

and Phenazine-1-carboxylic Acid Reduction via the Subunit Dihydrolipoamide Dehydrogenase. J Biol Chem *292*, 5593–5607.

Hernandez, M.E., and Newman, D.K. (2001). Extracellular electron transfer. Cell Mol Life Sci *58*, 1562–1571.

Hernandez, M.E., Kappler, A., and Newman, D.K. (2004). Phenazines and other redox-active antibiotics promote microbial mineral reduction. Appl Environ Microbiol *70*, 921–928.

Hollstein, U., and Van Gemert, R.J. (1971). Interaction of phenazines with polydeoxyribonucleotides. Biochemistry *10*, 497–504.

Jennings, L.K., Storek, K.M., Ledvina, H.E., Coulon, C., Marmont, L.S., Sadovskaya, I., Secor, P.R., Tseng, B.S., Scian, M., Filloux, A., et al. (2015). Pel is a cationic exopolysaccharide that cross-links extracellular DNA in the *Pseudomonas aeruginosa* biofilm matrix. Proc Natl Acad Sci U S A *112*, 11353–11358.

Jernaes, M.W., and Steen, H.B. (1994). Staining of Escherichia coli for flow cytometry: influx and efflux of ethidium bromide. Cytometry *17*, 302–309.

Jiménez Otero, F., Chan, C.H., and Bond, D.R. (2018). Identification of Different Putative Outer Membrane Electron Conduits Necessary for Fe(III) Citrate, Fe(III) Oxide, Mn(IV) Oxide, or Electrode Reduction by *Geobacter sulfurreducens*. J Bacteriol *200*.

Jo, J., Cortez, K.L., Cornell, W.C., Price-Whelan, A., and Dietrich, L.E. (2017). An orphan cbb3-type cytochrome oxidase subunit supports *Pseudomonas aeruginosa* biofilm growth and virulence. Elife *6*.

Kahl, L.J., Morales, D., and Dietrich, L. (2016). Light- and Temperature-Controlled Redox Cycling in *Pseudomonas aeruginosa* Biofilms. Free Radical Biology and Medicine *100*, S185.

Kahl, L.J., Price-Whelan, A., and Dietrich, L.E.P. (2019). Light-mediated decreases in cyclic di-GMP levels are potentiated by pyocyanin and inhibit structure formation in *Pseudomonas aeruginosa* biofilms. BioRxiv.

Kavanaugh, J.S., Flack, C.E., Lister, J., Ricker, E.B., Ibberson, C.B., Jenul, C., Moormeier, D.E., Delmain, E.A., Bayles, K.W., and Horswill, A.R. (2019). Identification of Extracellular DNA-Binding Proteins in the Biofilm Matrix. MBio *10*.

Kelley, S.O., Barton, J.K., Jackson, N.M., and Hill, M.G. (1997). Electrochemistry of methylene blue bound to a DNA-modified electrode. Bioconjug Chem *8*, 31–37.

Kempes, C.P., Okegbe, C., Mears-Clarke, Z., Follows, M.J., and Dietrich, L.E.P. (2014). Morphological optimization for access to dual oxidants in biofilms. Proc Natl Acad Sci U S A *111*, 208–213.

Light, S.H., Su, L., Rivera-Lugo, R., Cornejo, J.A., Louie, A., Iavarone, A.T., Ajo-Franklin, C.M., and Portnoy, D.A. (2018). A flavin-based extracellular electron transfer mechanism in diverse Gram-positive bacteria. Nature *562*, 140–144.

Lovrić, M. (2010). Square-Wave Voltammetry. In Electroanalytical Methods, F. Scholz, A.M. Bond, R.G. Compton, D.A. Fiedler, G. Inzelt, H. Kahlert, Š. Komorsky-Lovrić, H. Lohse, M. Lovrić, F. Marken, et al., eds. (Berlin, Heidelberg: Springer Berlin Heidelberg), pp. 121–145.

Malvankar, N.S., Vargas, M., Nevin, K.P., Franks, A.E., Leang, C., Kim, B.-C., Inoue, K., Mester, T., Covalla, S.F., Johnson, J.P., et al. (2011). Tunable metallic-like conductivity in microbial nanowire networks. Nat Nanotechnol *6*, 573–579.

Marsili, E., Baron, D.B., Shikhare, I.D., Coursolle, D., Gralnick, J.A., and Bond, D.R. (2008). *Shewanella* secretes flavins that mediate extracellular electron transfer. Proc Natl Acad Sci U S A *105*, 3968–3973.

Matsukawa, M., and Greenberg, E.P. (2004). Putative exopolysaccharide synthesis genes influence *Pseudomonas aeruginosa* biofilm development. J Bacteriol *186*, 4449–4456.

Meirelles, L.A., and Newman, D.K. (2018). Both toxic and beneficial effects of pyocyanin contribute to the lifecycle of *Pseudomonas aeruginosa*. Mol Microbiol *110*, 995–1010.

Müller, K. (2018). hms: Pretty Time of Day (CRAN).

Niesner, R., and Heintz, A. (2000). Diffusion coefficients of aromatics in aqueous solution. J. Chem. Eng. Data *45*, 1121–1124.

Okshevsky, M., and Meyer, R.L. (2014). Evaluation of fluorescent stains for visualizing extracellular DNA in biofilms. J Microbiol Methods *105*, 102–104.

R Core Team (2018). R: A Language and Environment for Statistical Computing (Vienna, Austria: R Foundation for Statistical Computing).

Ramos, I., Dietrich, L.E., Price-Whelan, A., and Newman, D.K. (2010). Phenazines affect biofilm formation by *Pseudomonas aeruginosa* in similar ways at various scales. Res Microbiol *161*, 187–191.

Reguera, G., McCarthy, K.D., Mehta, T., Nicoll, J.S., Tuominen, M.T., and Lovley, D.R. (2005). Extracellular electron transfer via microbial nanowires. Nature *435*, 1098–1101.

Richter, H., Nevin, K.P., Jia, H., Lowy, D.A., Lovley, D.R., and Tender, L.M. (2009). Cyclic voltammetry of biofilms of wild type and mutant *Geobacter sulfurreducens* on fuel cell anodes indicates possible roles of OmcB, OmcZ, type IV pili, and protons in extracellular electron transfer. Energy Environ. Sci. *2*, 506.

Robinson, D., and Hayes, A. (2018). broom: Convert Statistical Analysis Objects into Tidy Tibbles (CRAN).

Schiessl, K.T., Hu, F., Jo, J., Nazia, S.Z., Wang, B., Price-Whelan, A., Min, W., and Dietrich, L.E.P. (2019). Phenazine production promotes antibiotic tolerance and metabolic heterogeneity in *Pseudomonas aeruginosa* biofilms. Nat Commun *10*, 762.

Schindelin, J., Arganda-Carreras, I., Frise, E., Kaynig, V., Longair, M., Pietzsch, T., Preibisch, S., Rueden, C., Saalfeld, S., Schmid, B., et al. (2012). Fiji: an open-source platform for biological-image analysis. Nat Methods *9*, 676–682.

Schroth, M.N., Cho, J.J., Green, S.K., Kominos, S.D., and Microbiology Society Publishing (2018). Epidemiology of *Pseudomonas aeruginosa* in agricultural areas. J Med Microbiol *67*, 1191–1201.

Shi, L., Dong, H., Reguera, G., Beyenal, H., Lu, A., Liu, J., Yu, H.-Q., and Fredrickson, J.K. (2016). Extracellular electron transfer mechanisms between microorganisms and minerals. Nat Rev Microbiol *14*, 651–662.

Slinker, J.D., Muren, N.B., Gorodetsky, A.A., and Barton, J.K. (2010). Multiplexed DNA-modified electrodes. J Am Chem Soc *132*, 2769–2774.

Slinker, J.D., Muren, N.B., Renfrew, S.E., and Barton, J.K. (2011). DNA charge transport over 34 nm. Nat Chem *3*, 228–233.

Snider, R.M., Strycharz-Glaven, S.M., Tsoi, S.D., Erickson, J.S., and Tender, L.M. (2012). Long-range electron transport in *Geobacter sulfurreducens* biofilms is redox gradient-driven. Proc Natl Acad Sci U S A *109*, 15467–15472.

Steinberger, R.E., and Holden, P.A. (2005). Extracellular DNA in single- and multiple-species unsaturated biofilms. Appl Environ Microbiol *71*, 5404–5410.

Stemp, E.D.A., Arkin, M.R., and Barton, J.K. (1995). Electron transfer between metallointercalators bound to DNA: Spectral identification of the transient intermediate. J Am Chem Soc *117*, 2375–2376.

Stewart, P.S. (2003). Diffusion in biofilms. J Bacteriol *185*, 1485–1491.

Stewart, P.S., and Franklin, M.J. (2008). Physiological heterogeneity in biofilms. Nat Rev Microbiol *6*, 199–210.

Strycharz-Glaven, S.M., Snider, R.M., Guiseppi-Elie, A., and Tender, L.M. (2011a). On the electrical conductivity of microbial nanowires and biofilms. Energy Environ. Sci. *4*, 4366.

Strycharz-Glaven, S.M., Snider, R.M., Guiseppi-Elie, A., and Tender, L.M. (2011b). On the electrical conductivity of microbial nanowires and biofilms. Energy Environ. Sci. *4*, 4366.

Subramanian, P., Pirbadian, S., El-Naggar, M.Y., and Jensen, G.J. (2018). Ultrastructure of *Shewanella oneidensis* MR-1 nanowires revealed by electron cryotomography. Proc Natl Acad Sci U S A *115*, E3246–E3255.

Tse, E.C.M., Zwang, T.J., Bedoya, S., and Barton, J.K. (2019). Effective Distance for DNA-Mediated Charge Transport between Repair Proteins. ACS Cent. Sci. *5*, 65–72.

Turner, J.M., and Messenger, A.J. (1986). Occurrence, biochemistry and physiology of phenazine pigment production. Adv Microb Physiol *27*, 211–275.

Wang, Y., and Newman, D.K. (2008). Redox reactions of phenazine antibiotics with ferric (hydr)oxides and molecular oxygen. Environ Sci Technol *42*, 2380–2386.

Wang, F., Gu, Y., O'Brien, J.P., Yi, S.M., Yalcin, S.E., Srikanth, V., Shen, C., Vu, D., Ing, N.L., Hochbaum, A.I., et al. (2019). Structure of Microbial Nanowires Reveals Stacked Hemes that Transport Electrons over Micrometers. Cell *177*, 361–369.e10.

Wang, Y., Kern, S.E., and Newman, D.K. (2010). Endogenous phenazine antibiotics promote anaerobic survival of *Pseudomonas aeruginosa* via extracellular electron transfer. J Bacteriol *192*, 365–369.

Watnick, P., and Kolter, R. (2000). Biofilm, city of microbes. J Bacteriol *182*, 2675–2679.

Whitchurch, C.B., Tolker-Nielsen, T., Ragas, P.C., and Mattick, J.S. (2002). Extracellular DNA required for bacterial biofilm formation. Science *295*, 1487.

White, H.S., Leddy, J., and Bard, A.J. (1982a). Polymer films on electrodes. 8. Investigation of charge-transport mechanisms in Nafion polymer modified electrodes. J Am Chem Soc.

White, H.S., Leddy, J., and Bard, A.J. (1982b). Polymer films on electrodes. 8. Investigation of charge-transport mechanisms in Nafion polymer modified electrodes. J Am Chem Soc *104*, 4811–4817.

Wickham, H. (2017). tidyverse: Easily Install and Load the "Tidyverse" (CRAN).

Xu, K.D., Stewart, P.S., Xia, F., Huang, C.T., and McFeters, G.A. (1998). Spatial physiological heterogeneity in *Pseudomonas aeruginosa* biofilm is determined by oxygen availability. Appl Environ Microbiol *64*, 4035–4039.

Xu, S., Jangir, Y., and El-Naggar, M.Y. (2016). Disentangling the roles of free and cytochrome-bound flavins in extracellular electron transport from *Shewanella oneidensis* MR-1. Electrochim Acta *198*, 49–55.

Xu, S., Barrozo, A., Tender, L.M., Krylov, A.I., and El-Naggar, M.Y. (2018). Multiheme Cytochrome Mediated Redox Conduction through Shewanella oneidensis MR-1 Cells. J Am Chem Soc *140*, 10085–10089.

Yates, M.D., Golden, J.P., Roy, J., Strycharz-Glaven, S.M., Tsoi, S., Erickson, J.S., El-Naggar, M.Y., Calabrese Barton, S., and Tender, L.M. (2015). Thermally activated long range electron transport in living biofilms. Phys Chem Chem Phys *17*, 32564–32570.

Main Figures

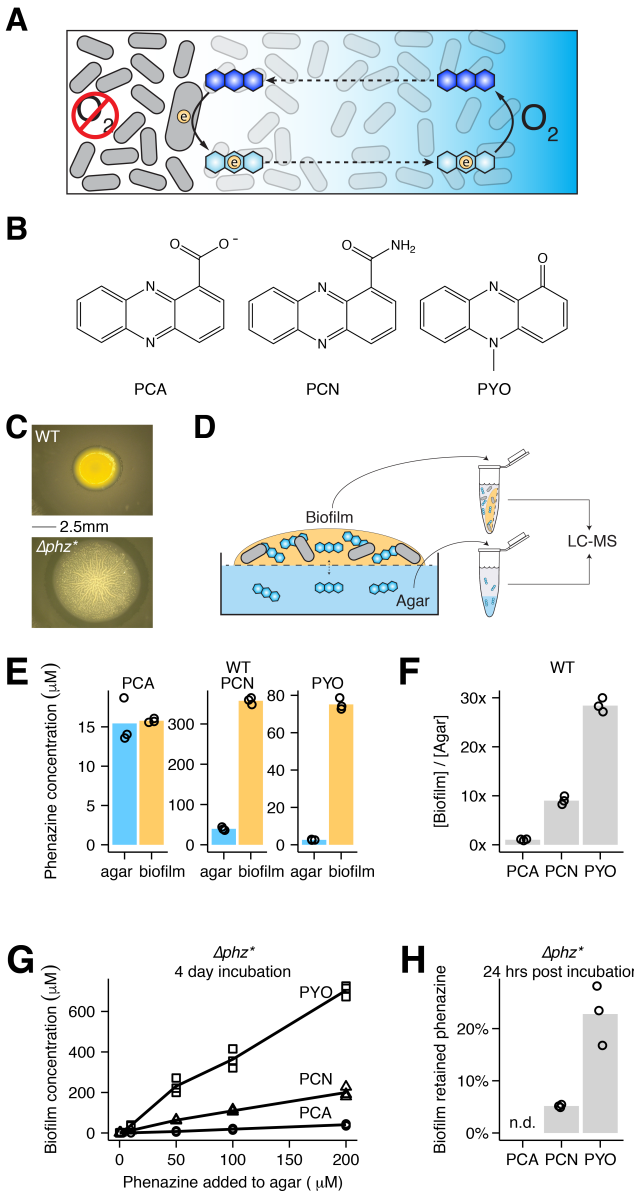

Figure 1. Colony biofilms retain PYO and PCN.

(A) Diagram of the phenazine redox cycle in a biofilm. Cells are shown as gray rods, phenazines are shown as blue hexagons, electrons are shown as circles, the oxygen gradient is shown as the blue background. (B) Structures of the three studied phenazines in their oxidized states produced by *P. aeruginosa* – phenazine carboxylate (PCA), phenazine carboxamide (PCN), and pyocyanin (PYO). (C) Images of WT (top) and Δ*phz** (bottom) colony biofilms. (D) Schematic of phenazine extractions from colony biofilms and agar. The

0.2 μm membrane is shown as the dashed line. (E) Biofilm and agar concentrations for PCA, PCN, and PYO from three WT biofilms. (F) The same data as C, represented as retention ratios ([Biofilm]/[Agar]). (G) Recovered phenazine concentrations from *Δphz** colony biofilms grown with different levels of synthetic phenazine in the underlying agar for 4 days. (H) Accumulated phenazine from three *Δphz** colony biofilms following three days of growth with synthetic phenazine (Day 3), and one day later after transfer to fresh agar (Day 4). Data are represented as the percentage Day 4/Day 3. PCA was not detected on Day 4. In panels E-H, values for individual biofilms are shown by open symbols, and lines or bars represent the mean.

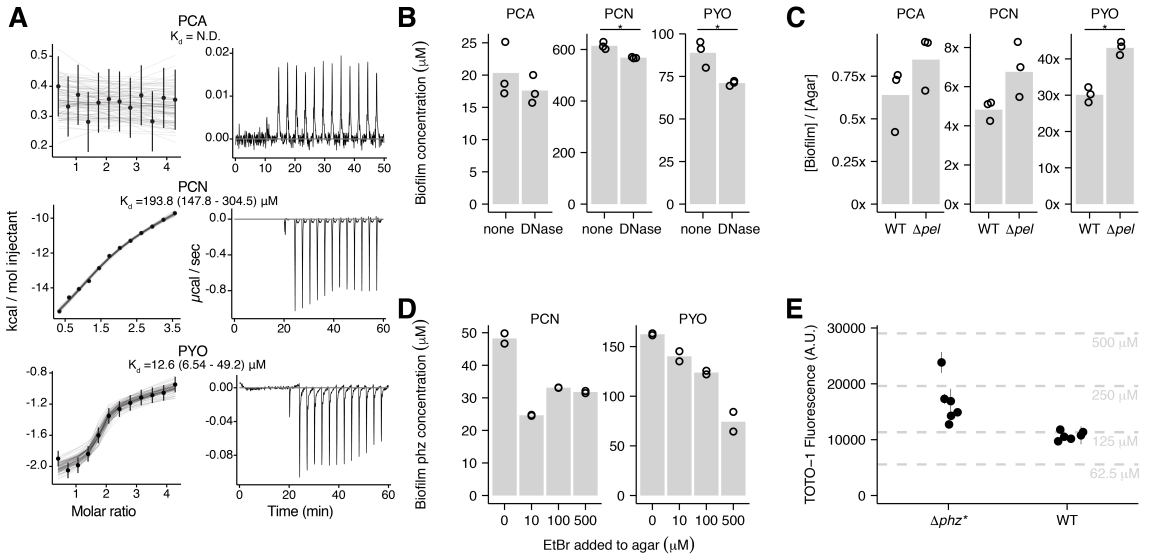

Figure 2. Phenazines interact with DNA in vitro *and* in vivo.

(A) Representative isothermal titration calorimetry (ITC) data for each phenazine injected into a solution of ds DNA (29 bp). Exothermic reactions are depicted as negative values. Integrated peak data was fit with a Bayesian model to calculate the K_d (in bp DNA) with 95% confidence intervals (values shown in parentheses) (Duvvuri et al., 2018). (B) Biofilm phenazine concentrations for WT biofilms treated with or without DNase I in the underlying agar for 24 hrs (n = 3 per condition). Bars with asterisks denote measurements that differ significantly ($p < 0.05$) by a Welch's single tailed t-test. (C) Phenazine retention ratios for WT and *Δpel* colony biofilms (n = 3 per condition). Statistical test same as in B. (D) Accumulated phenazine concentrations for Δ*phz** biofilms incubated with 50 µM PCN or PYO and increasing concentrations of the competitive intercalator, ethidium bromide, in the underlying agar. (E) eDNA quantified in six WT and Δ*phz** colony biofilms with the dye TOTO-1. Error bars show standard deviation from two technical replicates. Dashed lines show calf thymus DNA standards, with concentrations back calculated for the biofilm volume. In panels B-D, values for individual biofilms are shown by point symbols, and bars represent the mean.

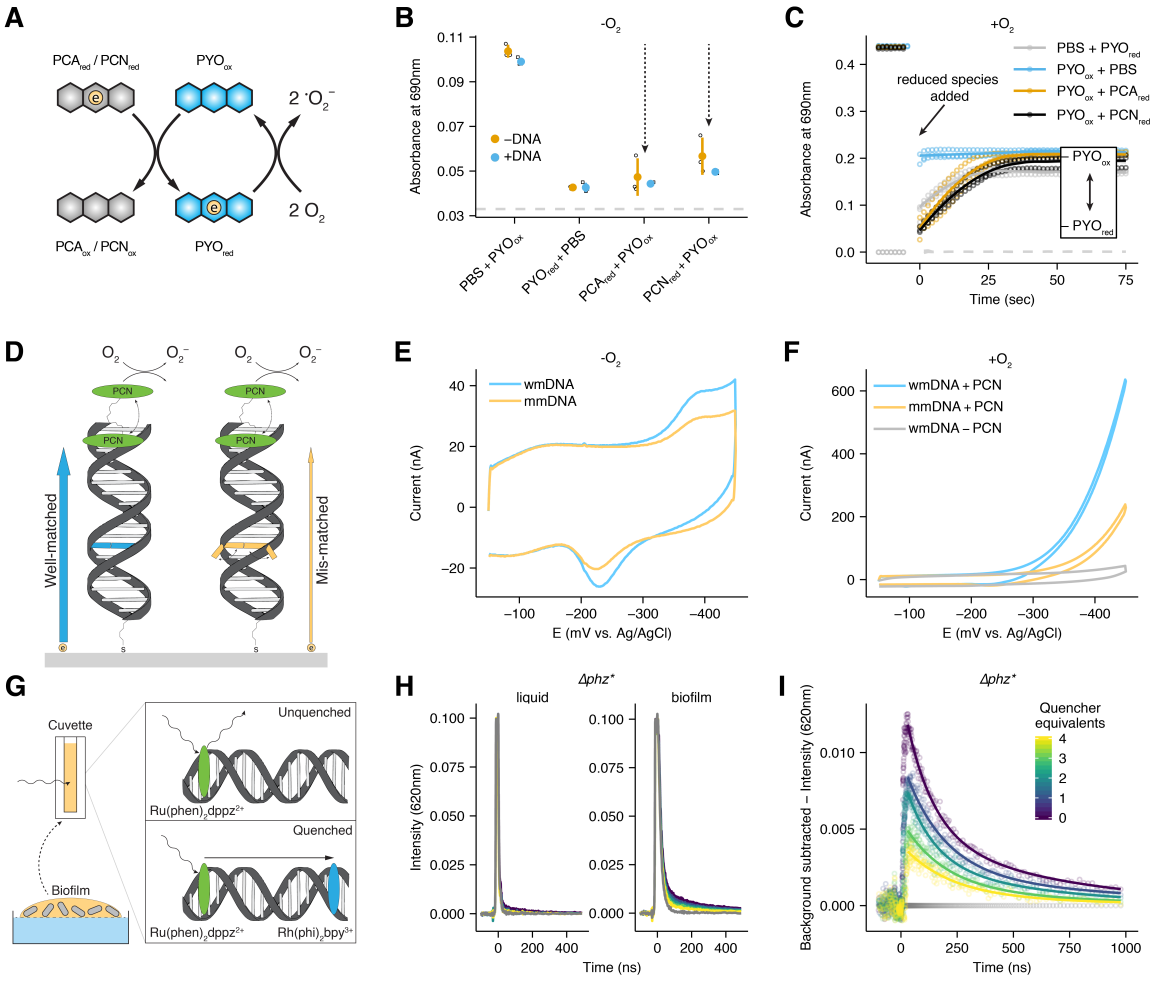

Figure 3. Inter-phenazine electron transfer and DNA CT.

(A) Diagram showing an electron transfer reaction in solution between a reduced phenazine and oxidized PYO and between reduced PYO and molecular oxygen. (B) Reaction progress after 1 min measured at 690 nm for mixtures of phenazines shown in A, compared to oxidized and reduced PYO alone. Each reaction was performed in the presence and absence of calf thymus DNA. For each condition, n=3 and error bars are one standard deviation. Dashed line shows the background signal from PBS alone or with PCN or PCA. (C) PYO oxidation state measured at 690 nm over time (diagnostic for oxidized PYO) for different reactions in the presence of oxygen. Points are individual measurements, lines are loess smoothed for each set of triplicate measurements. Dashed line shows the background signal from PBS with PCN_{red} or PCA_{red}. (D) Schematic showing a DNA modified electrode with tethered PCN (green oval) and the expected electron transfer for well-matched duplexes (blue arrow and bp) and duplexes containing a mismatch (orange arrow and bp). Mismatched bases are less likely to be in a well-stacked position, which is necessary for electron transfer through the DNA pi-stack. (E) Representative cyclic voltammetry of the well-matched (wmDNA) and mismatched (mmDNA) constructs shown in D under anoxic conditions. (F) Representative

cyclic voltammetry of the well-matched, mismatched, or no phenazine constructs under the aerobic conditions described in D. (G) Diagram of time-resolved spectroscopy of the photoexcited electron donor $Ru(phen)_2dppz^{2+}$ quenched by $Rh(phi)_2bpy^{3+}$ with biofilm eDNA. (H) Comparison of $Ru(phen)_2dppz^{2+}$ fluorescence in the presence of a concentrated liquid *P. aeruginosa* culture and a resuspended biofilm containing eDNA. Gray lines show background biological fluorescence before $Ru(phen)_2dppz^{2+}$ was added. The color map is the same as I. (I) The background subtracted data from the biofilm panel of H. The amount of $Rh(phi)_2bpy^{3+}$ is color-coded as quencher equivalents relative to $Ru(phen)_2dppz^{2+}$. Dots are raw data, lines are fit biexponential decays.

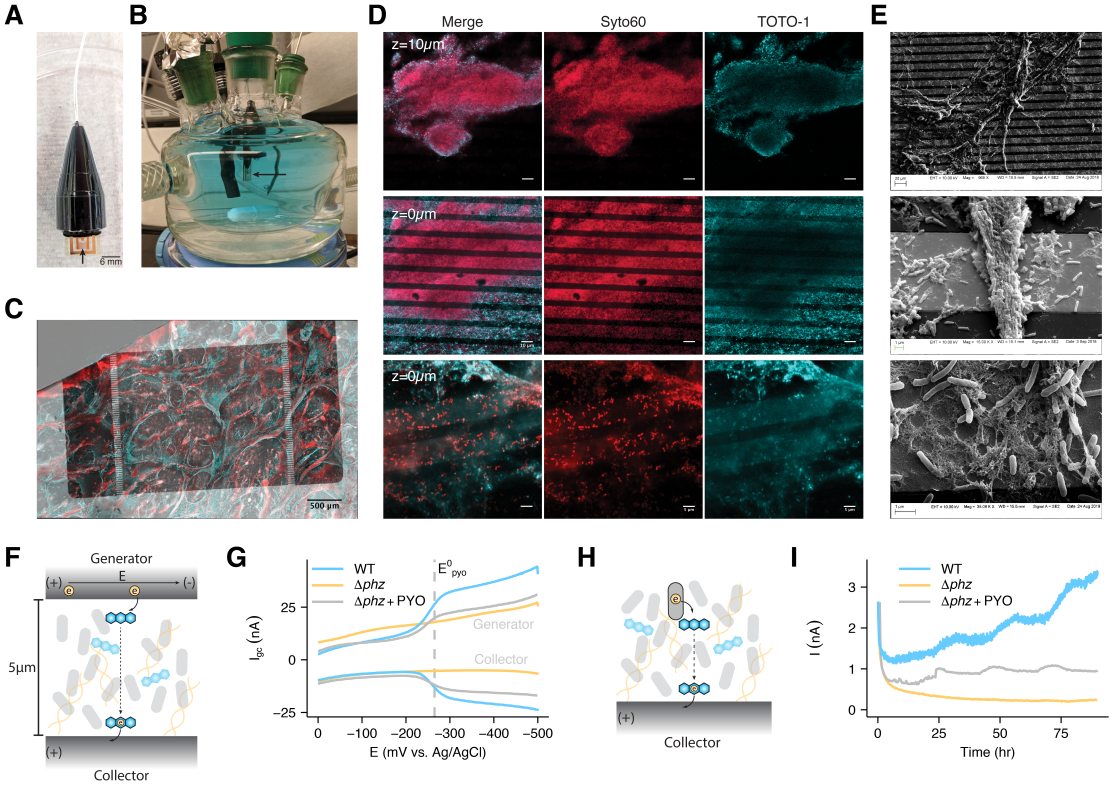

Figure 4. P. aeruginosa forms biofilms on electrodes and shows PYO dependent conductivity.

(A) Photograph of a sterile IDA. (B) Photograph of the growth/electrochemical reactor with a submerged IDA in a fresh medium + PYO solution. (C) A max intensity projection of a WT IDA biofilm imaged using Syto60 (cell permeable – all DNA), shown as red, and TOTO-1 (cell impermeable – eDNA), shown as cyan. Fluorescence channels are overlaid on a transmitted light channel showing the opaque gold regions of the electrode in gray scale. (D) Fluorescence microscopy of IDA biofilms with the same dyes as in C. Top: a 63x confocal image of a *Δphz** IDA biofilm from a zstack 10 μm above the electrode surface (scale bar = 10μm). Middle: a confocal image from the same zstack as top, but at the electrode surface (scale bar = 10 μm). Bottom: a confocal slice of a different *Δphz** biofilm from a 63x zoom with Airyscan, showing single live cells and eDNA on the electrode surface (scale bar = 5 μm). (E) SEM images at increasing magnification showing cells and extracellular matrix on the IDA electrode bands. (F) Diagram showing how a generator-collector (GC) two electrode system can generate current through PYO reduction. (G) GC data is displayed as the current at each electrode vs. the generator potential, E. Representative measurements are shown for WT, *Δphz* and *Δphz* + PYO biofilms. (H) Diagram showing how cells generate metabolism-dependent current through phenazine reduction. (I) Metabolic current described in H is measured by chronoamperometry for *Δphz* and WT biofilms over several days.

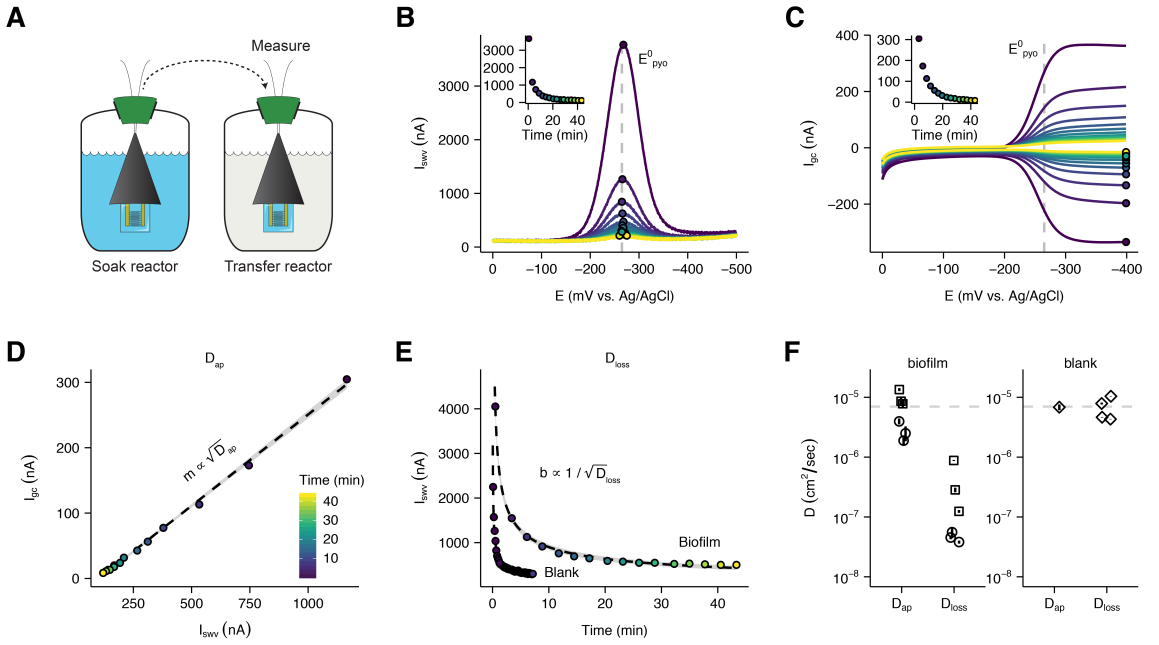

Figure 5. PYO mediated electron transfer is faster than PYO loss.

(A) Schematic showing how measurements are made to maximize biofilm specific PYO signals, by transferring IDAs to fresh medium. PYO is shown in blue. (B) Repeated SWV measurements were taken over time as the *Δphz** + PYO biofilm equilibrates with the solution in the transfer reactor. Points show peak current within each scan and inset shows the quantified peak currents vs. time. The color map is the same for panels B-E. (C) Repeated GC measurements were taken concurrently with SWV measurements over time as the same biofilm equilibrates. Points and inset are same as in B. (D) Plot of the peak GC vs. peak SWV currents fit with a line (gray area is 95% confidence interval). (E) Comparison of SWV signal over time in the transfer reactor from IDAs with or without a biofilm. Data are fit with a 1D diffusion model, as discussed in the supplementary text. Dashed lines are best fit models and gray regions show 95% confidence intervals. (F) Measurements of D_{ap} and D_{loss} for two *Δphz** biofilm IDAs soaked in 75μM PYO (shown as sets of open circles and squares) and a blank IDA soaked in different concentrations of PYO (open diamonds). A parameter for calculating D_{loss} (scan time - t_s) was solved by assuming that $D_{ap} = D_{loss}$ for the blank IDA (see supplementary text). Error bars for D_{ap} are 95% confidence intervals from the linear fit. Error bars for D_{loss} assume I_0 was the peak current in the soak reactor and high and low estimates were generated with the 95% confidence interval values from the SWV fit as well as the D_{ap} estimate. The dotted line is at 7 x 10^{-6} cm^2/sec, the measured D for the similarly sized small molecule, caffeine (Niesner and Heintz, 2000).

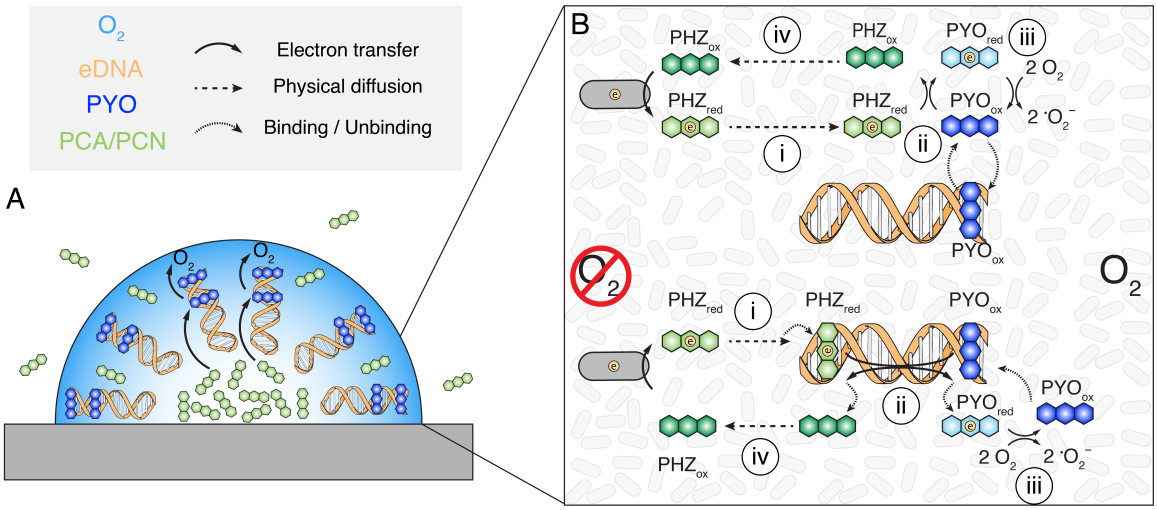

Figure 6. Proposed models of phenazine electron transfer and retention.

(A) Overview of phenazine electron transport to oxygen in the biofilm. Note that the DNA molecules are drawn radially for explanatory purposes only. (B) Proposed models for how the scheme shown in A occurs. The top model shows electron transfer in solution and the bottom model shows electron transfer via DNA CT. In both models, oxidized PYO is mostly bound and retained in the oxic region of the biofilm. PCN and PCA (PHZ) are reduced in the anoxic region of the biofilm and diffuse outward (i). The reduced phenazine reduces oxidized PYO (ii). Reduced PYO then reacts with molecular oxygen (iii), and the oxidized PYO re-equilibrates with the DNA binding sites. This facilitates the re-oxidation of PCA and PCN, allowing some diffusion back toward the interior (iv).

Materials and Methods

General

All strains were plated on LB from -80°C glycerol stocks and grown overnight at 37°C. Plates were stored at -4°C for up to a week and were used to inoculate liquid cultures. Liquid cultures were grown in 3 mL of medium in glass culture tubes (VWR #47729-583) in an orbital shaker (New Brunswick, Innova 44) at 37°C shaking at 250 rpm.

Chemicals were obtained from commercial sources (Sigma Aldrich, Fisher Scientific, VWR, and New England Biolabs) and used without further purification unless otherwise specified. All solutions were made with Milli-Q water (>18 MΩ cm). Phosphate buffered saline (PBS) used for resuspending cells or contacting biofilms (137 mM NaCl, 10 mM PO_4 (1.44 g/L Na_2HPO_4, 0.24 g/L KH_2PO_4), 2.7 mM KCl, pH 7.2) was different than PBS used for chemical stocks and in vitro assays (10 mM PO_4 (0.952 g/L Na_2HPO_4 , 0.592 g/L NaH_2PO_4), 50 mM NaCl, pH 7.0).

PCA was synthesized by Dr. Stuart Conway's Lab and was a gift. PCN was obtained from Princeton Biochem (#PBMR030086). PYO was synthesized by shining light on PMS (VWR #AAH56718-06) and purified with repeated organic (dichloromethane) and acid (HCl) extractions as described previously (Costa et al., 2017). PYO was further purified by reverse phase HPLC or repeated hexane precipitations. Stocks of PYO were either made in PBS (pH 7.0) to 1 mM or in 20 mM HCl to 10 mM and quantified by absorbance at 690 nm with the extinction coefficient $\varepsilon_{690} = 4306\ M^{-1}\ cm^{-1}$. Stocks of PCA were made in PBS to 1-2 mM or in 10 mM NaOH to 10 mM. Stocks of PCN were made in DMSO to 20 mM.

Colony Biofilms

Growth

Colony biofilms were grown on 1% tryptone (BD #211705), 1% agar (BD #214010) in 6-well plates (Fisher Scientific #08-772-49) at room temperature (~22°C) in the dark for 3 to 4 days. The medium was autoclaved and cooled to 60°C, then in a biosafety cabinet (The Baker Company #SG603A-HE) 5 mL of molten agar was transferred into each well of the 6-well plate and left to solidify for 60 min with no lid and constant airflow. When phenazines

were added to the medium, concentrated stocks were added first, then the medium, and then the wells were stirred with sterile pipettes until uniform. Membrane filters (Sigma-Aldrich # WHA110606) were gently placed shiny side down onto the center of each agar well, and colonies were inoculated by pipetting 10 µL of stationary phase culture (from LB liquid) onto the center of the membranes.

For DNase treated biofilms, after 3 days of growth membranes/biofilms were transferred to fresh agar wells containing 20 µL of DNase 1 (2 Kunitz units/µL) (Sigma-Aldrich #D4263) spotted directly underneath the biofilm. Biofilms then grew for another 24 hrs. DNase treatment was done with or without NEB Buffer 4.

Imaging

All colony biofilms were imaged in the 6-well plates at 20x zoom with a Keyence digital microscope (VHX-600) before extraction. Colonies were stained for confocal imaging by growing them with 1 µM TOTO-1 and 10 µM Syto60 in the underlying agar. Biofilms on their membranes were transferred to imaging dishes. High magnification images were taken by gently dropping coverslips (#1.5) onto the top surface of the colony and imaging through the coverslip with an upright confocal microscope, as described below (IDA biofilms – Fluorescence imaging). Colony biofilms on membranes were fixed for scanning electron microscopy (SEM) by floating the membrane on a paraformaldehyde solution, and then submerging. Upon submersion, the colony came off of the membrane mostly intact, leaving only a thin layer of cells fixed to the membrane. See SEM imaging section below for further details.

Extraction

Membranes, with the colony biofilms stably attached, were lifted off the agar with fine tweezers and carefully placed in microfuge tubes containing 800 µL or 1 mL of PBS. For colonies that were smaller in diameter than the microfuge tube, the membrane was placed upside down directly on top of the open tube, so that the colony sat above the PBS hanging from the membrane. Then, the colony was gently pushed down into the tube, by pushing with tweezers from the center. If the colony diameter was greater than the tube, the

membrane/biofilm was carefully held with the tweezers and allowed to flop over. While the membrane/biofilm was curved over, it was gently threaded into the tube. If any part of the colony touched the rim of the tube, the tweezers were used to scrape as much as possible into the inside.

Once the membrane/biofilm was in the tube, each tube was vortexed (Fisher Scientific #12-812) at maximum speed for 1 min, after which the vast majority of the biofilm was resuspended in the liquid and no longer associated with the membrane. The membrane was removed from each tube with tweezers. The biofilm suspension was then centrifuged (Eppendorf #5418) at 6000 rcf for 5 min. The supernatant was removed and immediately prepared for LC-MS or frozen at -20°C. This process was done for many biofilms at once, so biofilms typically sat for 30-60 min in PBS from the time the membrane was first added to the time the samples were centrifuged.

Biofilm volumes were estimated by comparing biofilm suspension volumes to controls that only had bare membranes added and removed. Volumes were measured with a p200 pipette. Significant variation was observed in volume measurements of replicate biofilms that looked identical, so the mean WT colony volume of 60 μL was used to normalize all colony measurements, although there are likely subtle volume differences between the differently treated colonies/strains.

The 6-well agar plates were extracted by adding 2 or 3 mL of PBS to the 5 mL of agar. The agar was scarred with a pipette tip to facilitate agar/liquid exchange. The 6-well plates were left on an orbital shaker at 250 rpm (Ika #KS-260) for 6 hours, which was determined to be optimal. Then, 1 mL of the liquid from each well was transferred to a microfuge tube and processed for LC-MS or frozen at -20°C.

For the sonication experiment, resuspended biofilms were treated for 1 min on ice (Fisher Scientific, Sonic Dismembrator 550), then processed normally. CFU counts showed that >65% of cells died. For the no-membrane experiment, 3 mL of PBS were added directly to the wells containing the biofilm. The biofilm was quickly resuspended in the liquid using a

cell scraper and 1 mL of liquid was saved, while the rest was removed. Then the agar was extracted as normal.

LC-MS

Samples were filtered with 0.2 µm spin filters (Corning #8160) and transferred to sample vials (Waters #600000668CV), and then loaded into the autosampler at 10°C. Samples were run on a Waters LC-MS system (Waters e2695 Separations Module, 2998 PDA Detector, QDA Detector). 10 µL of each sample was injected onto a reverse phase C-18 column (XBridge #186006035) running a gradient of 100% H_2O + 0.04% NH_4OH to 70% acetonitrile + 0.04% NH_4OH over 11 min (run times were 20 min total). UV-Vis and positive MS scans were acquired for each run. PCA, PCN, and PYO were distinguished by retention time (~3 min, 6 min, and 8.85 min, respectively), detected at 364 nm (PCA and PCN) or 313 nm (PYO), and manually verified by examining masses 225.2 (PCA), 224.2 (PCN) and 210.24 (PYO). Peaks were automatically identified in the UV-Vis channels by retention time, quantified using the apex track algorithm, converted to concentrations using standard curves (>6 points from 100 nM to 100 µM), and then exported as text files from the Empower software.

eDNA measurements

Resuspended colony biofilms were assayed for eDNA by measuring TOTO-1 fluorescence on a Tecan Spark 10M plate reader in black 96 well plates. Wells were prepared with 65 µL PBS and 10 µL of TOTO-1 (10 µM stock, 1 µM final), and 25 µL of biofilm suspension or calf thymus DNA was added to each well and gently mixed by pipetting. TOTO-1 fluorescence was monitored with 480 nm excitation and 535 nm emission after ~20 minutes of incubation at room temperature. Colony biofilms were measured with six biological replicates and technical triplicates. A standard curve was obtained by diluting a stock of calf thymus DNA twofold serially, yielding measurements from 500 µg/mL to 7 ng/mL.

DNA binding assays

Phenazine stocks were made in PBS (pH 7.0 10 mM PO_4, 50 mM NaCl) to 1 mM (PCA, PYO) or 500 µM (PCN with 5% DMSO). All assays were performed in the same PBS buffer

unless otherwise noted. Complementary 29 bp oligos from IDT were annealed (cooled incrementally over 1 hour following denaturation) to form the ds DNA for ITC and the ethidium displacement assays (see Table S2 for sequences). ds DNA for MST was prepared by PCR amplifying an 80 bp region from *P. aeruginosa* genomic DNA using the primers listed in table S2. One of the primers contained a Cy3 fluorophore for the MST readout.

Isothermal titration calorimetry (ITC)

ITC was performed with a MicroCal ITC200 (Malvern). Phenazine stocks were loaded directly into the ITC syringe. The cell was loaded with 10 to 50 μM ds DNA in PBS (or PBS + 5% DMSO for PCN). Results shown are representative of replicates taken at various ds DNA concentrations. Thermograms were recorded at 21°C with stirring at 300 rpm and reference power 2. There were 13 injections of 3.2 μL volume spaced by 240 seconds with 600 seconds of settle time.

Thermograms were integrated and baseline corrected in the Origin software. Peak integrations were then loaded into the GUI version of pytc (Duvvuri et al., 2018) with the default 0.1 units of uncertainty added to each measurement. Binding curves were plotted with the molar ratio phenazine/oligomer. The data were fit with the Bayesian model and parameter estimates with confidence intervals were generated. The K value was converted to a dissociation constant by taking the inverse and converted from the oligomer concentration to base-pair concentration by multiplying by 29 bp/fraction competent (f_x = 1.6 for PYO and 1.3 for PCN).

Ethidium bromide displacement

In black 96 well plates (Nunc #237105), 5 μM ethidium bromide (EtBr) was prepared in wells with increasing concentrations of PCA, PCN, or PYO. Fluorescence readings were taken on a Tecan Spark 10M plate reader with excitation 480 nm and emission 600 nm. Then a small volume of 29 bp ds DNA (prepared the same as for ITC) was added to a final concentration of 1 μM. The plates were mixed with rotary shaking and incubated at room temperature for at least 5 min protected from light. Then fluorescence was read again, and the bound ethidium signal was calculated by subtracting the pre-DNA reading from the post-

DNA reading. IC50 was calculated by fitting the data to the hill equation. IC50 was converted into K_i with the equation $K_i = IC50/(1 + [EtBr]/K_d)$, using an empirical K_d for ethidium (under the same -conditions) of 1 μM.

Microscale thermophoresis (MST)

Microscale thermophoresis was performed with a NanoTemper Monolith instrument following the manufacturer's protocol (capillaries – NanoTemper #MO-K022). Briefly, capillary solutions were prepared with 50 nM ds DNA and two-fold dilutions of phenazines starting at concentrations greater than or equal to 1 mM. Thermophoresis was performed at an ambient temperature of 22.5°C, with the thermophoresis laser power at 40% and the fluorescence excitation laser at 20% power. Thermophoresis was recorded for 30 seconds and evaluated using the T-jump strategy. Fluorescence peak shapes along the X-axis of each capillary were very uniform and peak intensity did not vary meaningfully between phenazine concentrations. K_d was calculated by fitting the quantified data to a hill equation. Results shown are representative of multiple MST runs with varied settings.

Endogenous fluorescence of reduced phenazines

The endogenous fluorescence of reduced phenazines was measured with different concentrations of calf thymus DNA with a BioTek Synergy 4 plate reader placed in an anaerobic chamber. Reduced phenazines (100 μM solutions) were prepared by bulk electrolysis of oxidized phenazine solutions in electrochemical chambers described previously (Wang et al., 2010). The solutions were transferred into stoppered serum bottles and moved to the anaerobic chamber containing the plate reader. 135 μL reduced phenazine was incubated with 15 μL PBS containing different amounts of calf thymus DNA, thus each well contained 90 μM phenazine. Fluorescence was monitored in a black 96-well plate with filter cubes to control excitation and emission wavelengths. PYO was excited using a 360 nm light and emission was monitored at 460 nm. For PCA and PCN, excitation was at 485 nm and emission was at 528 nm.

Phenazine to phenazine electron transfer in vitro

Electron transfer reactions between phenazines under anoxic conditions were monitored in the anaerobic plate reader described above. Reduced phenazines (described above) were mixed with oxidized phenazines (67.5 µL each) and 15 µL PBS with or without DNA (2 mg/mL) to yield mixtures containing 45 µM of each phenazine. Reactions in clear bottom, black walled 96-well plates were measured at 690 nm absorbance approximately one minute following mixing. For each well, an absorbance scan and fluorescence measurements (described above) were also taken, and these data matched the results obtained at 690 nm. Time series (2.5 min) of absorbance and fluorescence measurements were taken for each well, but no changes were observed, indicating that the reactions had reached equilibrium.

Phenazine redox reactions were monitored over time under oxic conditions with an aerobic Beckman Coulter DU 800 spectrophotometer. The instrument was blanked with PBS. Plastic cuvettes were filled with 500 µL PBS (oxic) or PYO_{ox} and placed inside the instrument and the lid was shut. Reduced phenazine or anoxic PBS was drawn (~500 µL) from stoppered serum bottles (anoxic) into needled 1 mL syringes. Absorbance measurements at 690 nm (1.5 sec intervals) were started on the cuvette and proceeded for 10 seconds to acquire baseline values. Then the lid was opened, the syringe was quickly emptied into the cuvette, and the lid was closed again. The measurement proceeded until 90 seconds had elapsed. Reactions were repeated in triplicate.

DNA modified electrodes

Preparation of thiol-modified oligonucleotide

A single-stranded DNA sequence with the 5' end modified with a C6 S-S phosphoramidite was purchased from Integrated DNA Technologies (see Table S1 for DNA sequences). The oligonucleotide was reduced using dithiothreitol (DTT, Sigma Aldrich, 100 mM) in a buffer solution (50 mM Tris-HCl, pH 8.4, 50 mM NaCl) for 2 h. The reduced thiol-modified DNA was then purified by size exclusion chromatography (Nap5 Sephadex, G-25, GE Healthcare) with phosphate buffer (pH 7.0, 5 mM NaH_2PO_4, 50 mM NaCl) as the eluent. Subsequently, high pressure liquid chromatography (HPLC, HP 1100, Agilent) was performed using a

reverse-phase PLRP-S column (Agilent) using a gradient of acetonitrile and 50 mM ammonium acetate (5-15% ammonium acetate over 35 minutes). After HPLC purification, the thiol-modified ssDNA was characterized using matrix-assisted laser desorption ionization (MALDI) characterization using an Autoflex MALDI TOF/TOF (Bruker), and quantified using a 100 Bio UV-visible spectrophotometer (Cary, Agilent). Another ssDNA strand for installing a CC mismatch near the interface between DNA duplexes and self-assembled monolayer (SAM) linker was prepared in an analogous manner as detailed above.

Preparation of amine-functionalized oligonucleotide

A single-stranded DNA sequence with the 5' end modified with a C6 NH_2 phosphoramidite was purchased from Integrated DNA Technologies. HPLC was performed using a reverse-phase PLRP-S column using a gradient of acetonitrile and 50 mM ammonium acetate (5-15% ammonium acetate over 35 minutes). After HPLC purification, the amine-modified oligonucleotide was characterized using MADLI-TOF-MS and quantified using UV-visible spectrophotometry.

Preparation of phenazine-functionalized oligonucleotide

Phenazine-1-carboxylic acid (PCA, 4.9 mg, 22 μmol) was added to dicyclohexylcarbodiimide (DCC, 9.3 mg, 45 mg) and *N*-hydroxysuccinimide (NHS, 5.2 mg, 45 μmol) in degassed, anhydrous dimethylformamide (DMF, 500 μL) at RT in a scintillation vial wrapped in aluminum foil. The barely soluble PCA turned from green to yellow upon stirring overnight in the dark under Ar. The NHS-activated PCA solution was reduced to low volume (100 μL) and was then added to a solution containing amine-modified DNA (0.42 μmol) in the presence of hydroxybenzotriazole (HOBT, 1 mg, 7.4 μmol) and *N,N,N′,N′*-tetramethyl-*O*-(1*H*-benzotriazol-1-yl)uronium hexafluorophosphate (HBTU, 1 mg, 2.6 μmol) in sodium bicarbonate solution (200 μL, pH 8, 0.1 M) overnight in the dark with the 1.5 mL Eppendorf tube wrapped in aluminum foil and mixed thoroughly using the shake function of a benchtop vortexer. The 1.5 mL tube secured using a clip to avoid spilling. The crude product was then buffer exchanged using a NAP-5 size-exclusion column into phosphate buffer (pH 7.0, 5 mM NaH_2PO_4, 50 mM NaCl). The treated product was

subsequently purified using HPLC on a reverse-phase PLRP-S column with a gradient of acetonitrile and 50 mM ammonium acetate (5-15% ammonium acetate over 35 minutes) while monitoring 252, 260, 280, 354, and 365 nm simultaneously. Pale yellow liquid fractions were collected and freeze-dried on a lyophilizer (Labconco). The resulting yellow dried smear was resuspended in minimal MQ H_2O and was subsequently analyzed by MALDI-TOF-MS.

Formation of double-stranded DNA duplexes

The two strands of a duplex are synthesized separately, purified, desalted, EtOH precipitated, and stored frozen at -20 °C. Prior to electrochemical experiments, the two strands of a duplex were mixed in equimolar (50 μM) in 200 μL phosphate buffer (pH 7.0, 5 mM NaH_2PO_4, 50 mM NaCl). The DNA solution was deoxygenated by bubbling Ar for at least 5 minutes per mL, and then annealed on a thermocycler (Beckman Instruments) by initial heating to 90°C followed by slow cooling over a span of 90 min.

Preparation of DNA-modified electrodes

Multiplexed chips are gently cleaned by sonicating with acetone once, then with isopropanol three times before drying with Ar. They are then cleaned with UV/Ozone using a UVO cleaner for 20 minutes. Immediately after cleaning the surface, a plastic clamp and rubber gasket (Buna-N) were affixed to the Au surface to create a well for liquid and 50 μM duplex DNA in phosphate buffer (5 mM phosphate, pH 7, 50 mM NaCl) to make ds DNA-modified surfaces. The ds DNA was incubated on the surface for 18-24 h in the absence of light. Once the ds DNA is affixed to the surface, it cannot be dried without compromising the structure and subsequently the measured properties of the ds DNA-modified surfaces. The solution was then exchanged 3× with phosphate buffer (pH 7, 5 mM phosphate, 50 mM NaCl, 5% glycerol) and incubated with 1 mM mercaptohexanol in phosphate buffer (pH 7, 5 mM phosphate, 50 mM NaCl, 5% glycerol) for 45 minutes. Lastly, the surface was rinsed at least 5× with phosphate buffer (pH 7, 5 mM phosphate, 50 mM NaCl) that was degassed by leaving it open in an anaerobic chamber (Coy Lab Products) for at least 3 days.

Multiplexed chip electrochemical measurements

Experiments performed were replicated at least three times using different samples, and data presented are from representative trials. Cyclic voltammetry (CV), square wave voltammetry (SWV), and differential pulse voltammetry (DPV) were carried out using a 620D Electrochemical Workstation (CH Instruments) at room temperature inside an anaerobic chamber. The atmosphere of the anaerobic chamber (< 1 ppm O_2, ca. 3.4% H_2) was monitored using a CAM-12 O_2 and H_2 sensor (Coy Lab Products). The chamber was maintained O_2-free by using two ventilated Pd catalyst packs (Coy Lab Products).

Electrochemical experiments were carried out in a three-electrode set-up under an anaerobic atmosphere. CV was conducted at a scan rate of 100 mV/s unless otherwise specified. The central well around the multiplexed electrode surfaces created by the plastic clamp was filled with aqueous buffer containing degassed phosphate buffer (pH 7, 5 mM phosphate, 50 mM NaCl). An Ag/AgCl reference electrode (BASi) was coated with a solidified mixture of 1% agarose and NaCl (3 M) in water inside a long, thin pipette tip. The tip was cut so that the salt bridge could connect the electrode to the buffer from the top of the well. A freshly-polished Pt wire used as an auxiliary electrode was also submerged in the buffer from the top of the well. The working electrode contacted a dry part of unmodified gold surface. Scan rate dependence studies (10-5000 mV/s) were carried out to determine whether the phenazine moiety was covalently attached to the DNA-modified electrodes. A linear relationship between scan rates and measured peak currents signified that phenazine was covalently attached. For O_2 electrocatalysis studies, CV was conducted in open air in O_2-saturated phosphate buffer (pH 7, 5 mM phosphate, 50 mM NaCl). Hexaammineruthenium(III) chloride (RuHex, 1-500 μM in pH 7, 5 mM phosphate, 50 mM NaCl) was used in control experiments to probe whether electron transfer occurred between the Au electrode and the covalently attached PCN through DNA.

Time resolved spectroscopy with metal complexes

Colony biofilms (Δ*phz**) were grown and suspensions were prepared in 500 μL PBS, as described above for the LC-MS and eDNA measurements. 400 μL of the suspension was

transferred to a clean quartz cuvette. Time-resolved emission measurements utilized a YAG laser (λ_{exc} = 532 nm), with laser powers of ~2 mJ per pulse. A colored-glass longpass filter (λ > 600 nm) was used to minimize scattered laser light and the emission of the $Ru(phen)_2dppz^{2+}$ complex was monitored at 620 nm. An excitation pulse (532 nm) was delivered and emission was recorded at 620 nm for 1.9 μs and each timepoint was 0.2 ns. A background scan was acquired with only the biofilm suspension. Then 5 μM $Ru(phen)_2dppz^{2+}$ was added and a scan was recorded. Subsequently, 5 μM $Rh(phi)_2bpy^{3+}$ was added after each scan to acquire the 1, 2, 3, and 4 quencher equivalent datasets. This process was repeated for multiple biofilms and a liquid Δ*phz** culture that was concentrated to the same optical density (500 nm) as the biofilm suspensions. Datasets were background subtracted from the biofilm-only background scan and were fit with biexponential decay models.

IDA biofilms

Electrode and reactor preparation

Gold IDA electrodes were prepared as previously described (Boyd et al., 2015). IDAs fabricated on glass substrate were ordered from CH Instruments (#012125). A passivation membrane covered the working electrodes except for the overlapping regions that form the 5 μm gap and where the leads were attached. Insulated wires (Digi-Key #W7-ND) were attached to the two working electrodes of the IDA with a conductive epoxy (Electron Microscopy Sciences #12670-EE) that was cured at 80°C for 1 hour. A shell for the IDA construct was constructed from 15 mL conical vials that were sawed off at the 2.5 mL mark. Rough edges were smoothed with a razor blade, and two holes were poked in the bottom of the vial. The IDA with attached wires was placed inside the conical vial and the wires were threaded through the holes at the bottom. A nonconductive epoxy (Amron International #2131-B) was carefully pipetted into the vial with the IDA until it was full to the rim. The epoxy was allowed to set at room temperature in a fume hood for 24-48 hours. IDA constructs were then used immediately or stored in petri dishes and covered to protect from light and dust.

Reactors (Pine Instruments, 265 mL water-jacketed electrochemical reactor) used to grow biofilms on the IDA were cleaned thoroughly and autoclaved between uses. For gas control, the ports were stoppered or sealed with o-rings and screw clamps. Gas inflow and outflow lines were attached via 6 in gassing needles and 16g 1.5 in needles, respectively, pierced through separate stoppers. Gas outflow was attached to a liquid overflow vessel, a 500 mL Erlenmeyer flask that also had 16g needles as inflow and outflows. The water jacket of each reactor was connected in series to a water chiller (Lytron) to heat the vessels to ~31°C. Each reactor was filled with 180 mL of sterile medium and the IDA construct was suspended from a stopper (size 4) by threading the wires through 16g needles and then removing the needles, so that the electrode was fully submerged in the liquid. IDAs were sterilized in 10% bleach for 30 seconds, then rinsed in sterile medium before submerging in the reactor.

Biofilm growth

Biofilms were grown in a minimal medium (MM) with succinate as the carbon source (14.15 mM KH_2PO_4, 38.85 mM K_2HPO_4, 42.8 mM NaCl, 9.3 mM NH_4Cl, 40 mM Na-succinate, adjusted to pH 7.2, autoclaved, then 1x SL-10 trace element solution (Atlas, 2004) and 1 mM $MgSO_4$ were added).

From a stationary phase MM culture, the reactors with 180 mL MM were inoculated to an OD_{500} of 0.005. The medium was exchanged every 24 hours, and biofilms were grown on the IDA for 3 or 4 days in this fashion. During growth, constant temperature was maintained at ~31°C, reactors were stirred at 250 rpm (VWR #58948-138), and air was bubbled into two reactors at a time with a small aquarium bubbler (Tetra #77851).

Depending on the experiment, biofilms were grown with or without the full electrochemical setup described below. At a minimum, biofilms were grown with the IDA working electrode (disconnected from potentiostat).

Electrochemical setup

Electrochemistry was performed using a three-electrode setup and CHI 760b or CHI 760e bi-potentiostats. The working electrode(s) were on the IDA and connected to wires as

described above. The counter electrode was a separate graphite rod (Alfa Aesar #14738) and the reference electrode was a separate Ag/AgCl electrode (BASi #MW-2030 or #MF-2079) assembled as described in the above DNA CT section. Before measurements were made in a reactor, the medium was sparged with N_2 for at least 10 min. Reactors were gently bubbled with N_2 throughout the measurements. Unless otherwise noted, Generator-Collector scans were acquired at 3 mV/s, with the collector held at 0 mV. Square wave voltammetry was performed at 300 Hz with an amplitude of 25 mV and an increment of 1 mV. Chronoamperometry of metabolic current was acquired at +100 mV.

Measurement scheme

For experiments where biofilms were soaked in synthetic PYO, biofilms were soaked for at least 10 min. To transfer the IDA biofilm, the potentiostat leads were removed and the reference and counter leads were attached to the transfer reactor electrodes. The IDA biofilm was dipped in fresh medium to remove solution PYO and then submerged in the transfer reactor. The working electrodes were attached and the open circuit potential was measured to ensure proper connections – this took roughly 30 seconds. For time sensitive experiments, SWVs were immediately recorded. For biofilm D_{ap} and D_{loss} measurements, SWV and GC scans were taken consecutively (manually or with a macro) until 15 of each scan had been acquired. For blank D_{loss} measurements, rapid consecutive SWV scans were taken in an automated fashion using the "repeated runs" option in the CHI software. For blank D_{ap} measurements, the blank IDA was incubated with increasing concentrations of PYO in the soak reactor.

Fluorescence Imaging

IDA biofilms were prepared for imaging by removing the biofilm coated region of the IDA from the epoxy encased shell. The exposed region of the glass substrate near the epoxy interface was scored with a diamond-tipped scribe, and then it was snapped off from the rest of the vial/epoxy assembly. With tweezers, the IDA fragment was transferred to a slide with a multi-well silicone spacer and dye mixture was added with a pipette directly to the edge of the IDA fragment until it was fully coated. The dye mixture was 10 μM Syto60 (Invitrogen

#S11342) and 1 or 2 μM TOTO-1 (Invitrogen T3600) in PBS. Coverslips (#1.5) were added directly on top of the mixture and sealed with clear nail polish to the spacer.

Slides were then imaged on a confocal microscope. Most imaging was done using an upright Zeiss LSM 880 with Fast Airyscan. Syto60 was excited with a 633 nm laser and emission was typically recorded with a bandpass filter from 650 to 750 nm. TOTO-1 was excited with a 488 or 514 nm laser and emission was typically recorded with a bandpass filter from 530 to 630 nm. Tile scans were taken using a 10x objective and high magnification images were taken with a 63x objective. Several images were taken at 63x magnification using the Airyscan module with superresolution settings. For Airyscan images, the appropriate filter cubes were used.

Other imaging was done on an inverted confocal Leica model TCS SPE with a 10x objective for tile scanning. Syto60 was excited with a 633 nm laser, TOTO-1 was excited with a 488 nm laser, and emissions were set by bandpass filters as above.

Abiotic IDA measurements with Nafion

Electrochemical experiments were recorded with a bi-potentiostat (CHI, Model #760) in a Teflon cell designed in-house to mount gold interdigitated array (IDA) electrodes from CHI. The counter and reference electrodes were a Pt coiled wire and an Ag/AgCl reference electrode. All measurements were recorded at room temperature in 0.2 M Na_2SO_4 as the electrolyte purged with Argon. The IDA electrodes were modified with Nafion film by pipetting 20 μL of a 5% by weight Nafion solution (Sigma Aldrich) onto the IDA electrodes, and allowing a film to form as the solution dried at room temperature. After 2 hours, the modified IDAs were rinsed with ethanol and DI water, and then mounted into the base of the Teflon cell.

The Nafion films on the IDAs mounted in the Teflon cell were loaded with various amounts of $Ru(NH_3)_6^{3+}$ by either exposing the films to a 10 mM solution of $Ru(NH_3)_6Cl_3$ (Sigma Aldrich) in 0.2 M Na_2SO_4 at time points from several minutes to several hours or by allowing $Ru(NH_3)_6^{3+}$ in the films to diffuse out into bulk electrolyte for several hours. The Nafion

films were loaded with Ferrocenemethanol (Fc-OH) by exposing the films to a 250 μM solution of Fc-OH in 0.2 M Na_2SO_4 for several hours. To decrease the amount of Fc-OH in loaded films, the films were allowed to have the Fc-OH in the films to diffuse out into bulk electrolyte for several hours. For each electrochemical measurement after loading or depleting the film, the cell was rinsed with DI water and 2 mL of fresh electrolyte was added. The counter and reference electrodes were position above the IDA electrodes in a Teflon lid, and the electrolyte were purged with Argon for 15 minutes with a blanket of Argon maintained in the head space of the Teflon cell. Three conditions were measured with the Fc-OH: (i) Fc-OH in solution with naked IDAs, (ii) Fc-OH in solution at IDAs modified with Nafion, and (iii) Fc-OH loaded into the Nafion modified IDAs.

For the SWV vs. GC method, SWV and GC scans were acquired as described above, and equation 5 (Supp. Text) was used to calculate D_{ap} with the following parameters: A = 0.0213 cm^2, $\psi = 0.505$, S = 18.4 cm, t_p = 1/600 s. For chronocoulometry, voltage was stepped from 0 mV to -500 mV vs. Ag/AgCl. From the slope of plots of charge vs. $(time)^{1/2}$, D_{ap} was calculated from the following equation:

$$D = \left(\frac{S\pi^{1/2}}{2FC}\right)^2 = \left(\frac{S\Phi\pi^{1/2}}{2F\Gamma}\right)^2$$

where S is the chronocoulometric slope (C cm^{-2} $s^{-1/2}$), Φ is the film thickness (cm), Γ is the total quantity of Ferrocenemethanol in the film (mol cm^2), F is the Faraday constant, and C is concentration in moles/cm^3 (C = 2.5 x 10^{-7} moles/cm^3). A film thickness of 10 μm was estimated from the reported density of casted Nafion films by knowing the amount of Nafion deposited and the area covered by the film.

Scanning electron microscopy (SEM)

IDA and colony biofilms were prepared for SEM using the following protocol. Delicate samples were gently transferred between solutions using metal spatulas or plastic grids as supports. Material was fixed in 4% paraformaldehyde in PBS for 2 hours or overnight, then washed twice with PBS. Material was then fixed in 1% OsO_4 in water for 1 hour, then washed

twice with PBS. Next, the samples were dehydrated by sequentially immersing in 50, 70, 90, 95, and 100% ethanol (EtOH) solutions for 10 min, and then again in 100% EtOH for 1 hour. Samples were then transferred to hexamethyldisilazane (HMDS) solutions of 1:2, then 2:1 HMDS:EtOH for 20 min each, followed by two incubations in 100% HMDS for 20 min each. Samples were then removed from the solution and air-dried before attaching to imaging stubs with conductive tape. Imaging stubs were then sputter-coated with 10 nm of palladium before being loaded into the SEM. Imaging was done with a Zeiss 1550VP field emission SEM using the SE2 detector.

Data analysis

Nearly all data processing and analysis was done in R (R Core Team, 2018) using tidyverse packages including ggplot2, dplyr, readr (Wickham, 2017), broom (Robinson and Hayes, 2018), and hms (Müller, 2018). The nonlinear least squares ('nls') function in base R was used for D_{loss} fits and the linear model ('lm') function was used for D_{ap} fits. Electrochemical data was exported from CHI software as text files with raw data, acquisition parameters, and timestamps, and then imported into R. Confocal images were stitched (for tilescans) and processed into z-slices or maximum intensity projections using the Zeiss Zen Black software and Fiji (Schindelin et al., 2012).

All code used for data processing and analysis is available in a GitHub repository (github.com/DKN-lab/phz_eDNA_2019). Html versions of the Rmarkdown notebooks are also available as a website (DKN-lab.github.io/phz_eDNA_2019).

Supplementary Text

DNA modified electrode controls

The purpose of carrying out the control experiments shown in Fig. S4 using electrodes modified using self-assembled monolayers (SAMs) of double-stranded DNA (ds DNA) was to probe the electron transfer mechanism between the redox probe and the electrode surface. Four sets of control experiments were conducted to probe whether DNA-mediated charge transport (DNA CT) occurs between PCN and the electrode via the base stack of ds DNA: (i) WM- vs. MM-DNA, (ii) high- vs. low-density monolayers, (iii) PCN vs. RuHex, and (iv) scan rate dependence studies.

(i) WM- vs. MM-DNA: Electrodes modified using SAMs of ds DNA that are well-matched (WM) or contain a single base pair mismatch (MM) were prepared under identical conditions. WM-DNA electrodes and MM-DNA electrodes have similar physical properties, but exhibit different charge transfer properties that occur through the aromatic base stacks of DNA. If the electron transfer process between the redox probe and the electrode occurs via DNA CT, then a decrease in the yield of DNA CT is expected due to the perturbation to the base stack introduced by the MM lesion. If the electron transfer process occurs via other modes such as physical diffusion of a charge carrier or physical contact between the redox probe and the electrode surface, then no difference in the current measured would be expected.

(ii) High- vs. low-density monolayers: Electrodes modified using high- and low-density SAMs of ds DNA were used to probe the effect of the number of ds DNA on the charge transport mechanism. A low-density ds DNA monolayer promotes electron transport within one ds DNA, but ds DNA may adopt various conformations because the individual ds DNA molecules are more distantly spaced. A high-density ds DNA monolayer encourages ds DNA to align with each other in a more orderly fashion due to more ds DNA present in a confined space. Regardless of a high- or low- density monolayer, for the case of PCN-modified DNA-SAM, MM discrimination was observed, suggesting that DNA CT is the major mode of electron transport between the electrode and the redox probe.

(iii) PCN vs. RuHex: RuHex is a positively-charged species that binds electrostatically to the negatively-charged phosphate backbone. RuHex also associates to the OH groups at the terminus of the SAM surface passivated by backfilling using mercaptohexanol. Electrons tunnel through the SAM from the electrode to the RuHex situated at the SAM terminus. Electrons can then be transferred and be distributed among the Ruhex bound to the SAM surface and on the DNA phosphate backbone. Residual RuHex present in solution could help with ET through hopping and diffusion in solution, and the contribution of solution-based ET to the current measured depends on the concentration of RuHex used. Therefore, a number of RuHex concentrations were screened in order to optimize the conditions for this measurement. For species that do not participate in DNA CT, no MM discrimination will be observed. The RuHex experiments show that the number of ds DNA on the SAM-modified electrodes is similar for both the WM and MM cases. The observation of a sizable MM discrimination demonstrates that PCN bound on DNA participates in DNA CT.

(iv) Scan rate dependence studies (10-5000 mV/s) were carried out to determine whether the phenazine moiety was covalently attached to the DNA-modified electrodes. A linear relationship between scan rates and measured peak currents signified that phenazine was covalently attached.

D_{ap} measurement theory

To measure D_{ap}, we compared two electrochemical measurements that depend on D_{ap} in different ways. By performing this comparison at multiple concentrations, we could fit the data points to a line whose slope can be defined by known parameters, yielding D_{ap}. *Δphz** biofilms were soaked in 75 μM of PYO, and then transferred to fresh medium lacking PYO. The biofilm PYO concentration dropped over the course of 45 min as equilibration with the medium occurred. Approximately 15 sets of scans were taken during this time period.

The first measurement was square wave voltammetry (SWV) (Fig. 5B). The SWV peak current (I_{swv}) is defined in terms of concentration of redox molecules (C) reacting directly (by physical diffusion) or indirectly (through electron self-exchange reactions) with the electrode (D_{ap}), the area of the electrode (A), the number of electrons per redox reaction (n),

the Faraday constant (F), the pulse width (t_p), and a normalization constant (φ). Note that I_{swv} depends on the square root of D_{ap}.

$$I_{swv} = \frac{nFAC\sqrt{D_{ap}}}{\sqrt{\pi t_p}}\varphi \quad (eq.1)$$

The second measurement was a generator-collector (GC) measurement (Figure 5C). The maximum GC current (I_{gc}) is also defined in terms of C, D_{ap}, n, and F, but depends on a geometric factor (S) (Boyd et al., 2015) as opposed to the electrode area. Note that I_{gc} depends directly on D_{ap}.

$$I_{gc} = nFSCD_{ap} \quad (eq.2)$$

A plot of experimentally determined I_{gc} vs. I_{swv} values yields linear relationships for PYO in biofilms and in solution (i.e., blank IDA) (Fig. 5D, S6), with slope (m) that can be defined in terms I_{gc} and I_{swv}:

$$m = \frac{I_{gc}}{I_{swv}} = \frac{nFSCD_{ap}}{\frac{nFAC\sqrt{D_{ap}}}{\sqrt{\pi t_p}}\varphi} \quad (eq.3)$$

$$m = \frac{S\sqrt{\pi t_p D_{ap}}}{A\varphi} \quad (eq.4)$$

This relationship enables determination of D_{ap} from the experimentally determined dependency of I_{gc} to I_{swv} (i.e., m) in terms of known experimental parameters (Fig. 5F). Importantly, it provides a means of determining D_{ap} that is not dependent on knowing C, which for our system is unknown and changes over time as PYO diffuses out of the biofilm.

$$D_{ap} = \frac{(mA\varphi)^2}{S^2\pi t_p} \quad (eq.5)$$

Note that because the slope of these plots is linear, it suggests that D_{ap} is constant for a biofilm despite how the concentration of PYO changes as it diffuses. We assume a constant D_{ap} by fitting the data with a linear model.

D_{loss} measurement theory

In order to measure the physical diffusion coefficient of PYO molecules lost from the IDA-grown biofilms, we monitored the loss of biofilm PYO over time as it equilibrated with the fresh medium similar to an approach taken with polymer films (White et al., 1982a). To quantify this process, we used successive SWV scans acquired over 45min following transfer to fresh medium (the SWV subset of the D_{ap} data). A 1-dimensional diffusion model was then applied to fit the decay of I_{swv} yielding an estimate of D_{loss}.

Considering 1-dimensional diffusion of an initial mass (M_0) of a substance from a point source, the solution of Fick's second law describing the time-dependent concentration gradient is given by eq. 6 where x is distance normal from the source, A is the cross-sectional area in 3D space, and D_{loss} is the physical diffusion coefficient.

$$C(x,t) = \frac{M_0}{A\sqrt{4\pi D_{loss} t}} e^{-\frac{x^2}{4D_{loss}t}} \quad (eq.6)$$

When the source is located at no-flux boundary such that the mass diffuses only to one side,

$$C(x=0,t) = \frac{2M_0}{A\sqrt{4\pi D_{loss} t}} \quad (eq.7)$$

where $C(x = 0, t)$ is the time dependent concentration at the surface of the no-flux boundary (e.g. the IDA surface).

To connect this model to the data, the concentration and initial mass can be defined in terms of the measured SWV current (I_{swv}). For SWV, the concentration, C, is given by:

$$C(t) = \frac{I_{swv}(t)\sqrt{\pi t_p}}{nFA\sqrt{D_{ap}}\varphi} \quad (eq.8)$$

Concentration can be defined as the mass per volume, so the initial mass, M_0, can be expressed in terms of the effective volume probed by the electrode (V):

$$M_0 = \frac{VI_0\sqrt{\pi t_p}}{nFA\sqrt{D_{ap}}\varphi} \quad (eq. 9)$$

The initial current is defined as I_{swv} (t = 0) = I_0, which is experimentally estimated from the last I_{swv} in the PYO soak, before transfer to PYO-free medium. This is a conservative overestimate because some of the soak signal comes from the solution PYO. Substituting the values for *C* (eq. 8) and M_0 (eq. 9) into equation 7 yields:

$$I_{swv}(t) = \frac{2I_0V}{A\sqrt{4\pi D_{loss}t}} \quad (eq. 10)$$

The term *V* refers to the biofilm volume from which the mass of PYO was detected by the electrode. For a 1D electrode process, the concentration gradient extends from the electrode-solution interface ($C = 0$) to the edge of the diffusion layer, δ ($C = C_{bulk}$) in a near linear fashion (Bard et al., 1980). There is no region where all of the mass is detected, but the electrode has detected one half of the mass in the volume $A \times \delta$, therefore the effective *V* can be defined:

$$V = \frac{A\delta}{2} \quad (eq. 11)$$

The diffusion layer, δ, for a single potential step can be estimated by:

$$\delta = 2\sqrt{D_{ap}t_s} \quad (eq. 12)$$

where t_s is the amount of time that the driving potential is held. SWV is a series of forward and reverse potential steps for which we could not unequivocally define an equivalent t_s value, however, we discuss reasonable bounds in the assumptions section below. Substituting into equation 11 yields $V = A\sqrt{D_{ap}t_s}$, therefore equation 10 can be written as:

$$I_{swv}(t) = \frac{I_0\sqrt{D_{ap}t_s}}{\sqrt{\pi D_{loss}t}} \quad (eq. 13)$$

and with that expression, we can fit the decay of I_{swv}(t) to a model of the form:

$$y = \frac{b}{\sqrt{t}} + a \quad (eq. 14)$$

where the coefficient, b, is described in known variables except for D_{loss} and where a accounts for any constant background signal.

$$b = \frac{I_0 \sqrt{D_{ap} t_s}}{\sqrt{\pi D_{loss}}} \quad (eq. 15)$$

Therefore, D_{loss} can be calculated from the fit data as (Fig. 5F, S7):

$$D_{loss} = \frac{{I_0}^2 D_{ap} t_s}{\pi b^2} \quad (eq. 16)$$

Model assumptions

The D_{loss} analysis described above is based on a number of assumptions. It assumes, for example, that the biofilms are homogeneous. In reality, they are heterogeneous, containing many voids and obstacles (e.g., cells and exopolysaccharides) through which diffusion would not occur. We contend that heterogeneity would affect D_{loss} and D_{ap} in a similar manner, as it reduces the biofilm volume in which PYO resides. As such, we don't expect biofilm heterogeneity to greatly affect the determination of D_{loss} from D_{ap}. Importantly, our analysis assumes a single infinitely thick phase described by a single D_{loss}. In reality, there are at least two phases, a thin biofilm adjoining an infinitely thick solution. If D_{loss} in solution is greater than in the biofilm, then at any instance the concentration gradient of PYO across the biofilm will be steeper than predicted by the model. Since the flux of PYO out of the biofilm at any instance is proportional to the product of the gradient and D_{loss}, as the model fits the rate of change of PYO in the biofilm, the assumption of a shallower gradient than the actual gradient is expected to result in a calculated D_{loss} that is higher than the actual D_{loss}.

To estimate the scan time parameter, t_s, we assumed that for the blank IDA $D_{ap} = D_{loss}$ and solved for t_s that best fit the I_{swv} decay for the blank IDA. We then used this value, $t_s = 21$ ms, to calculate D_{loss} for the biofilm IDAs. The scan time parameter is intended to estimate the thickness of the diffusion layer that is formed during a single potential step that drives

the flux of the electrode reactant resulting in the observed current. SWV is, however, a series of forward and reverse potential steps superimposed on a series of forward potential steps. Therefore, determining the effective scan time that describes the change in thickness of the diffusion layer that occurs during the forward pulse contributing to I_{swv} is nontrivial (we only consider the forward pulse as the reverse scan partially replenishes the electrode reactant that is depleted during the forward scan). One approach to estimate t_s is setting the SWV expression equal to twice the Cottrell equation (eqs. 17 & 18), since I_{swv} is the net current from the forward and reverse pulses. For a pulse amplitude of 0.025 V and step increment of 0.001 V as used here, each potential step is effectively 0.05 V. The potential at which the I_{swv} occurs is the formal potential of the electrode reactant and applying the Nernst equation, the fraction of electrode reactant in the oxidized state at the electrode surface at the start of the forward potential step generating I_{swv} (E = Eo'+ 0.025 V) is 82.6% and at the end (E = Eo -0.025 V) is 17.4%. The Cottrell equation assumes that the potential step drives a redox reaction in which 100% of the electrode accessible redox molecules at the electrode go from oxidized to reduced (or vice versa). Replacing C in the Cottrell equation with 0.655 x C to reflect the fraction of PYO at the electrode surface that changes oxidation state during the forward potential step of the SWV yields an estimate $t_s \approx 6$ ms.

$$I_{swv} = \frac{nFAC\sqrt{D_{ap}}}{\sqrt{\pi t_p}}\varphi = 2I_{ps} = \frac{nFA\ 0.655 \times C\sqrt{D_{ap}}}{\sqrt{\pi t_s}} \quad (eq.17)$$

$$t_s = \frac{t_p\ (2 \times 0.655)^2}{\varphi^2} \quad (eq.18)$$

As such, our t_s estimate (21 ms) based on the blank $D_{ap} = D_{loss}$ used to estimate D_{loss} for the biofilm may be an overestimate. Noting that D_{loss} scales linearly with t_s (eq. 16), this would conservatively underestimate the difference between biofilm D_{ap} and D_{loss}.

Parameters for electrochemical calculations

The surface area of the electrode for SWV, A = 0.025 cm^2, and the geometric factor for GC, S = 18.4 cm, were calculated for a blank IDA using the known concentration and D_{ap} for ferrocene methanol (Boyd et al., 2015). All quantified SWVs were acquired with a pulse

amplitude of 25 mV at a frequency of 300 Hz and an increment of 1 mV. The SWV pulse time, t_p, is one half the square wave period (½ * 1/300 = 1/600 sec). Peak separation from CV of PYO in solution indicated that it did not undergo the full 2 electron reduction, but on average underwent electron transfer with $n \approx 1.8$. From these acquisition parameters, $\varphi = 0.7$ was inferred from a table of existing values (Lovrić, 2010). For the D_{loss} estimate, it was assumed that I_0 was the soak SWV peak current. The equivalent scan time, t_s, for the D_{loss} calculation is discussed above.

Supplemental Figures

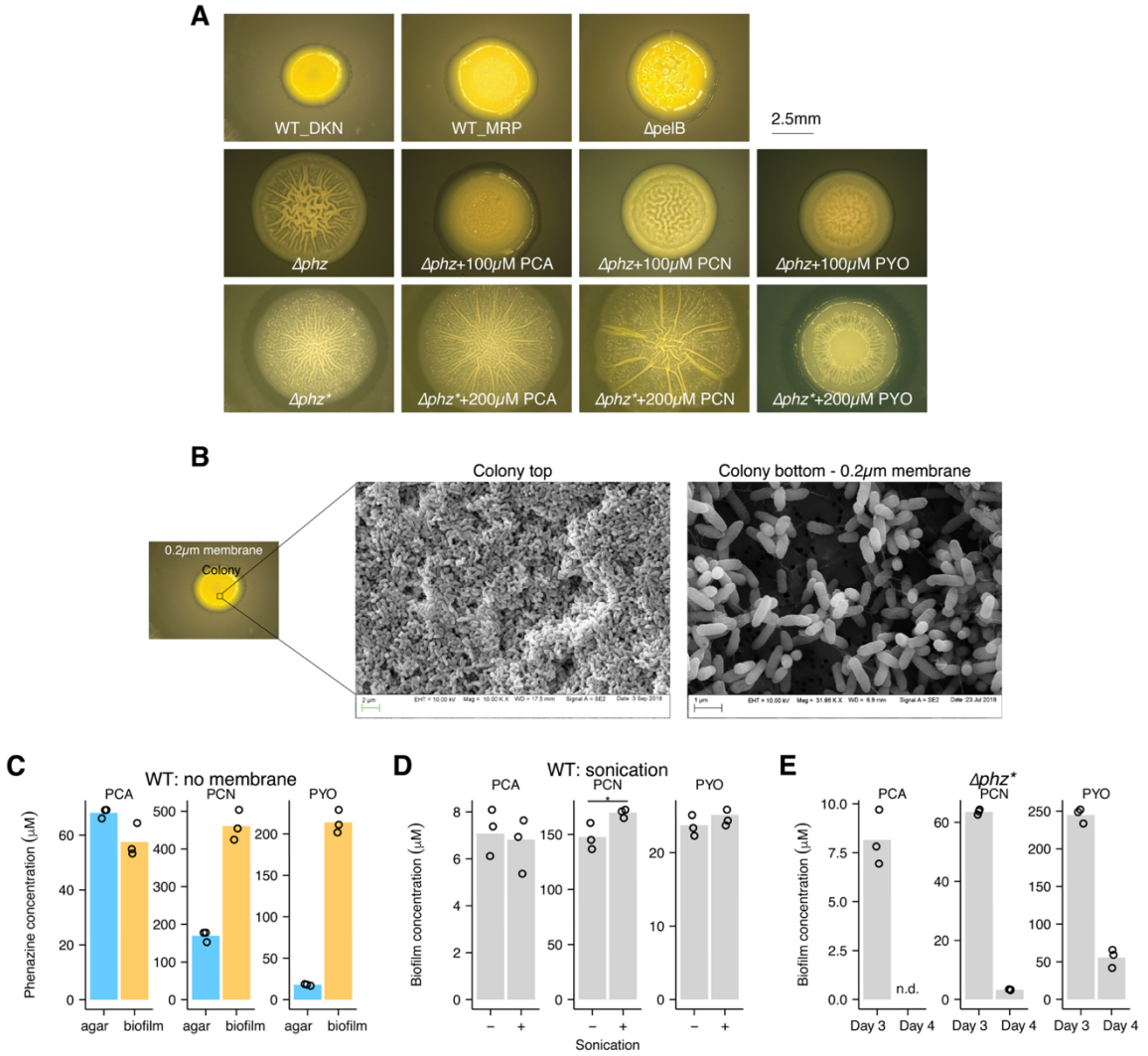

Figure S1. Colony biofilm images and controls.

(A) Representative images of colony biofilms formed by WT-DKN, WT-MRP, *ΔpelB*, and *Δphz* and *Δphz** grown with each phenazine. (B) SEM image of cells at the top and bottom (attached to the 0.2 μm membrane) of the colony biofilm. (C) LC-MS quantification of phenazines from colony biofilms grown without an underlying membrane. (D) Comparison of phenazines from WT colonies that were lysed with sonication or not. Statistical test was a Welch's single tailed t-test and the star denotes $p<0.05$. (E) Accumulated phenazine from three *Δphz** colony biofilms following three days of growth with synthetic phenazine (Day 3), and one day later after transfer to fresh agar (Day 4). PCA was not detected on Day 4. Same data are shown in Fig. 1 H.

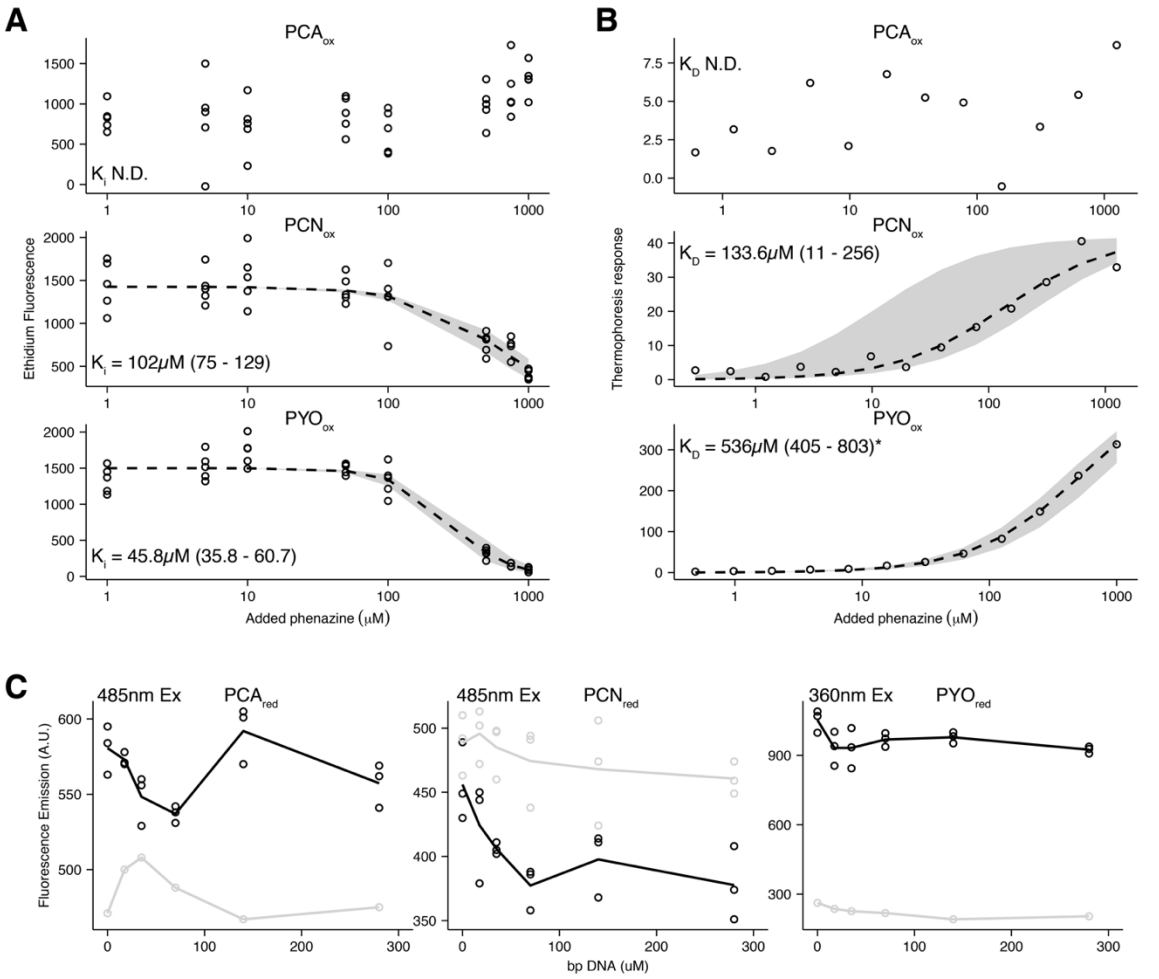

Figure S2. Phenazine – DNA binding assays.

(A-B) Dotted lines show best fit Hill equations with shaded regions showing curves from the 95% confidence intervals for IC50 or K_D. (A) Ethidium bromide displacement from 1 μM 30 bp ds DNA by oxidized phenazines, as measured by change in ethidium fluorescence before and after incubation with DNA. Assays were done with 5 μM ethidium, which has a K_D of 1 μM under these conditions. K_i for phenazines was calculated from the relationship $K_i = IC50/(1 + [EtBr]/K_D)$. (B) Microscale thermophoresis binding assay of three oxidized phenazine derivatives with 50 nM 80 bp cy3 tagged ds DNA. *PYO elicited a strong thermophoresis response that did not saturate, therefore the calculated K_D is likely not relevant. (C) Endogenous fluorescence of reduced phenazines at increasing DNA concentrations. Black lines show experimental conditions and gray lines show buffer-only control wells. PCN_{red} did not show fluorescence above background, but the values were reported to show that adding DNA did not facilitate fluorescence emission.

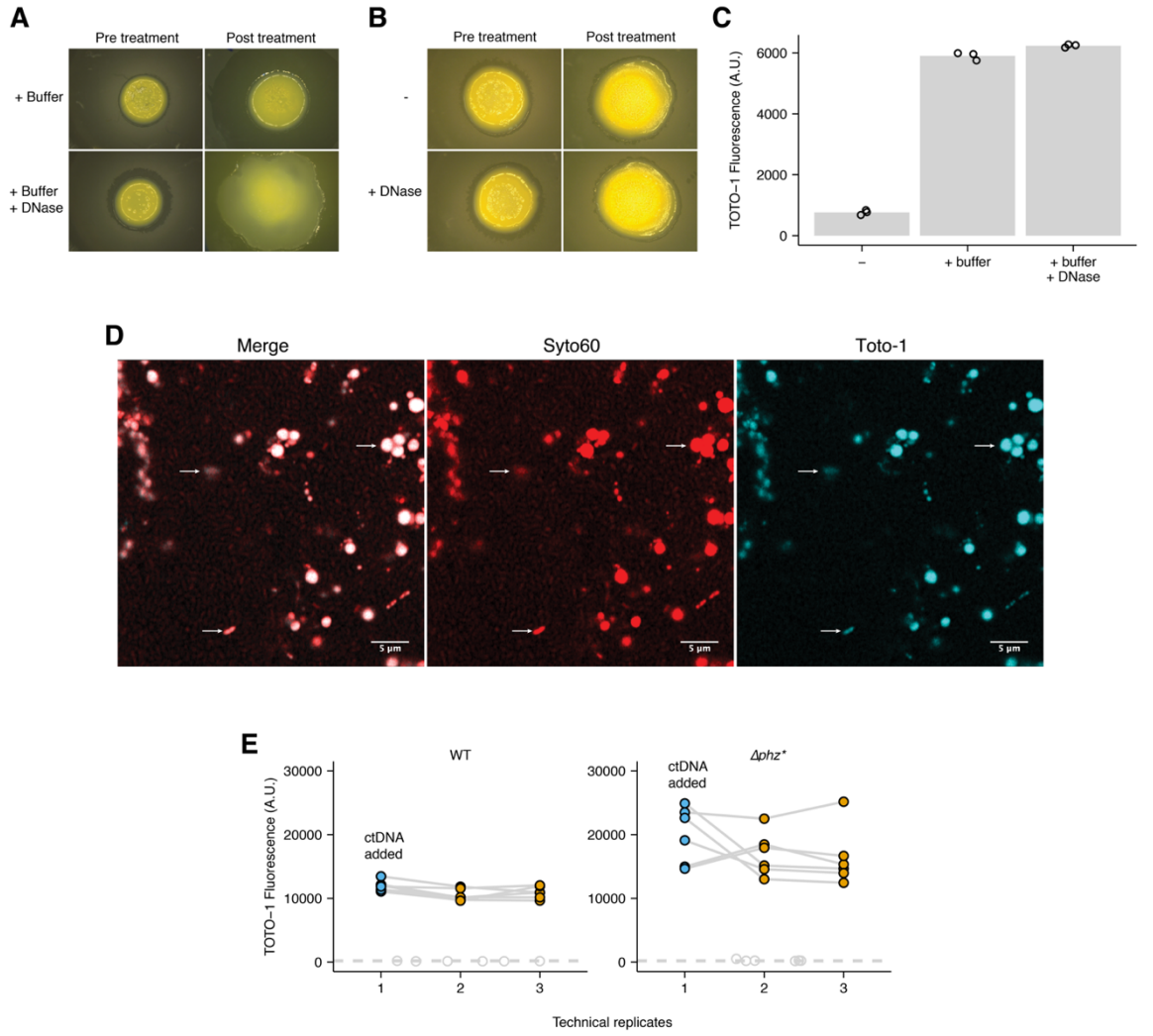

Figure S3. eDNA in colony biofilms.

(A) Images show representative WT colony biofilms on Day 3 (pre-treatment) and Day 4 (post treatment) with DNase and buffer or only buffer (NEB Buffer 4). (B) DNase treatment of colonies without buffer corresponding to phenazine measurements shown in Fig. 2B. (C) Quantification of eDNA (i.e. cell death) in colony biofilm extracts from A measured by TOTO-1 fluorescence in a plate reader. (D) A high magnification confocal image showing different eDNA structures at the surface of a colony biofilm (white arrows). (E) TOTO-1 measurements of WT and Δ*phz** colony biofilm suspensions. Blue dots show technical replicates where 160 ng of calf thymus DNA were added to assess the sensitivity of the assay. Dotted lines and gray dots show background fluorescence values of technical replicates acquired without the dye.

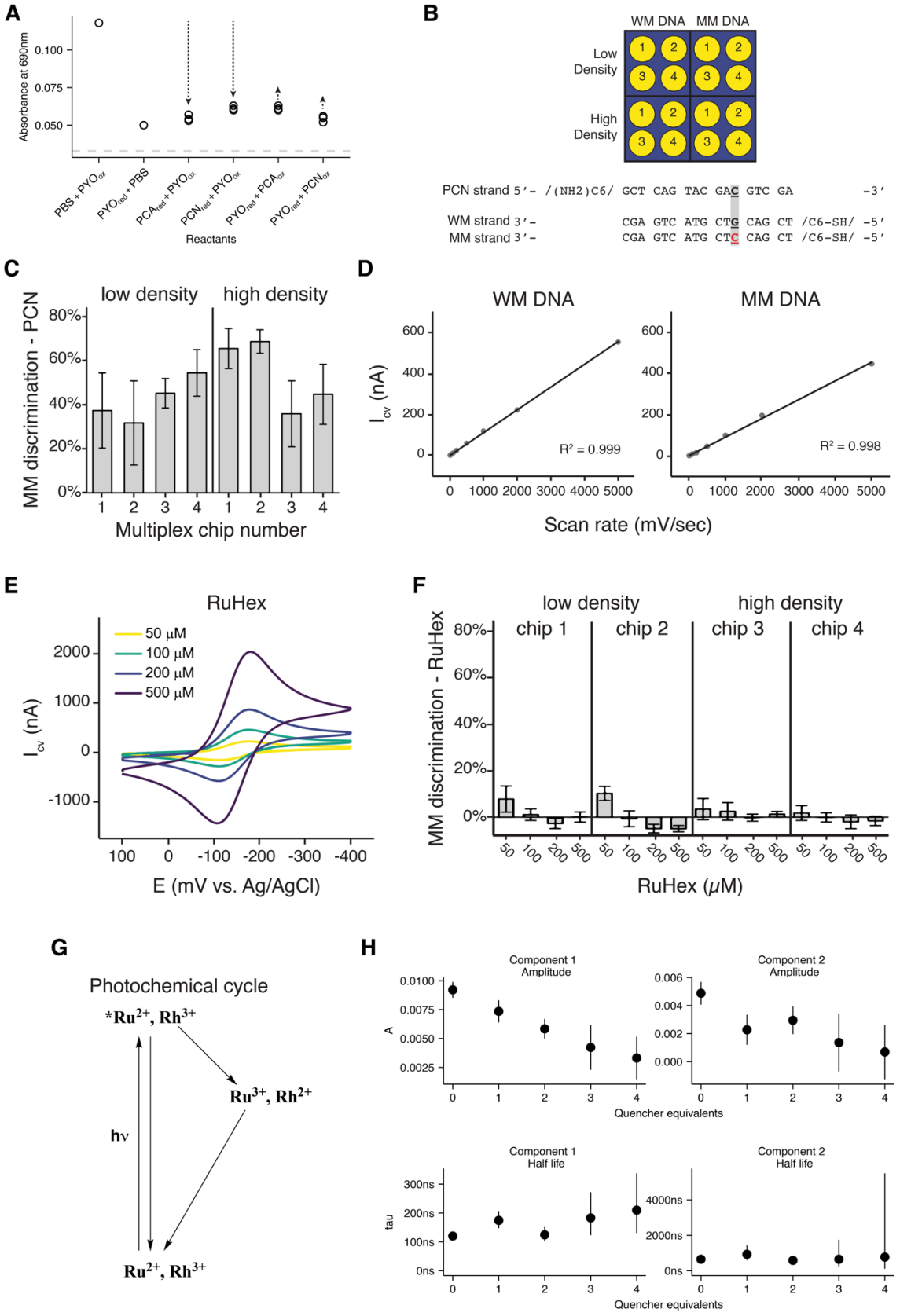
A
Absorbance at 690nm
0.100
0.075
0.050
PBS + PYOox
PYOred + PBS
PCAred + PYOox
PCNred + PYOox
PYOred + PCAox
PYOred + PCNox
Reactants
B
WM DNA
MM DNA
Low Density
High Density
PCN strand 5′- /(NH2)C6/ GCT CAG TAC GAC GTC GA -3′
WM strand 3′- CGA GTC ATG CTG CAG CT /C6-SH/ -5′
MM strand 3′- CGA GTC ATG CTC CAG CT /C6-SH/ -5′
C
low density
high density
MM discrimination - PCN
80%
60%
40%
20%
0%
1 2 3 4 1 2 3 4
Multiplex chip number
D
WM DNA
MM DNA
I_cv (nA)
600
400
200
0
R² = 0.999
R² = 0.998
0 1000 2000 3000 4000 5000
Scan rate (mV/sec)
E
RuHex
50 μM
100 μM
200 μM
500 μM
I_cv (nA)
2000
1000
0
-1000
100 0 -100 -200 -300 -400
E (mV vs. Ag/AgCl)
F
low density
high density
chip 1
chip 2
chip 3
chip 4
MM discrimination - RuHex
80%
60%
40%
20%
0%
50 100 200 500
RuHex (μM)
G
Photochemical cycle
*Ru2+, Rh3+
Ru3+, Rh2+
hν
Ru2+, Rh3+
H
Component 1 Amplitude
Component 2 Amplitude
A
0.0100
0.0075
0.0050
0.0025
0.006
0.004
0.002
0.000
0 1 2 3 4
Quencher equivalents
Component 1 Half life
Component 2 Half life
tau
300ns
200ns
100ns
0ns
4000ns
2000ns
0ns
0 1 2 3 4
Quencher equivalents

Figure S4. DNA modified electrode details.

(A) Inter-phenazine electron transfer reactions in solution, including PYO as the reductant for PCA_{ox} and PCN_{ox}. Dashed line shows the background signal from PBS alone or with PCN or PCA. (B) Top – layout of the multiplex chip electrodes used for the measurements. Bottom – the oligomer sequences used to assemble the PCN and thiol-modified ds DNA monolayers. (C) Mismatch (MM) discrimination for the high density and low density DNA monolayers from four multiplex chips of the layout shown in B. MM discrimination was calculated by comparing peak integrations from WM and MM electrodes using the formula 1 – (avg. MM/avg. WM) × 100%. Error bars are standard error propagated from the four WM and four MM electrodes. (D) Scan rate dependence of both the well-matched and mismatched surfaces showed linear dependence with increasing scan rate, consistent with a bound redox species. (E) Cyclic voltammetry of hexaammineruthenium(III) chloride (RuHex), which does not participate in DNA CT. Signal is proportional to DNA surface concentration. (F) MM discrimination for different RuHex concentrations calculated in the same way as C. (G) The detailed photochemical cycle referred to in Fig. 3G. (H) The bi-exponential fit coefficients from Fig. 3I. Error bars show two standard deviations.

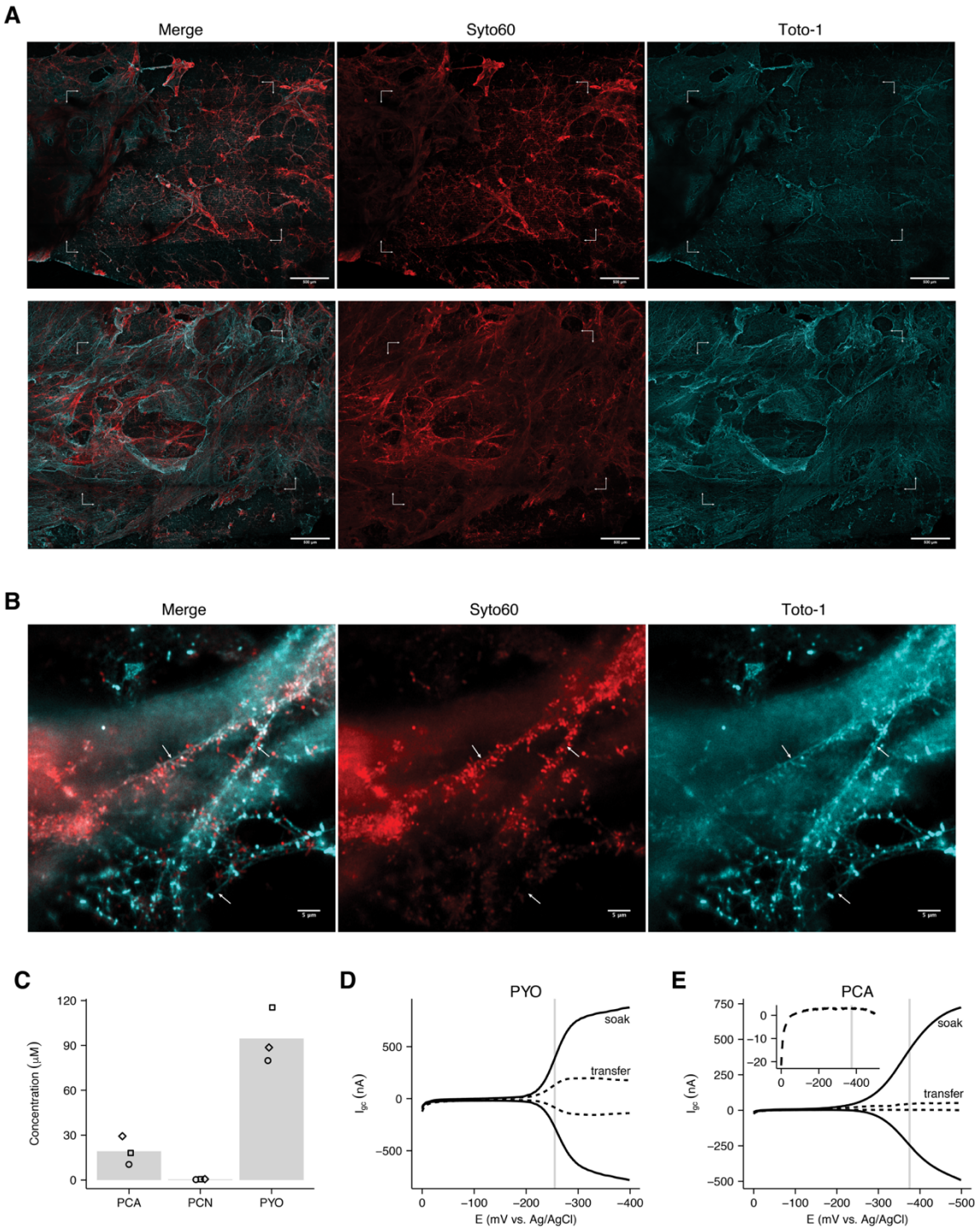

Figure S5. IDA biofilm characterization.

(A) Confocal microscopy tilescan images of the two IDA Δ*phz** biofilms used for D_{ap} and D_{loss} analysis. Brackets show the bounds of the IDA working electrode array. Images were

acquired at 10x magnification as a tilescan zstack. The stitched maximum intensity projections are shown. (B) Images show individual cells and fine eDNA structures (arrows) at high magnification (63x with digital zoom and airyscan processing). Images are from a single slice of a zstack. (C) LC-MS quantification of WT culture supernatant from an IDA reactor on three consecutive days before medium exchange. (D) Generator collector measurements of Δ*phz** biofilms soaked with PYO. Measurements were acquired during the soak and immediately following transfer to a reactor with fresh medium. (E) Same measurements as D, except the Δ*phz** biofilm was soaked in PCA. The inset figure shows as the collector current with more detail.

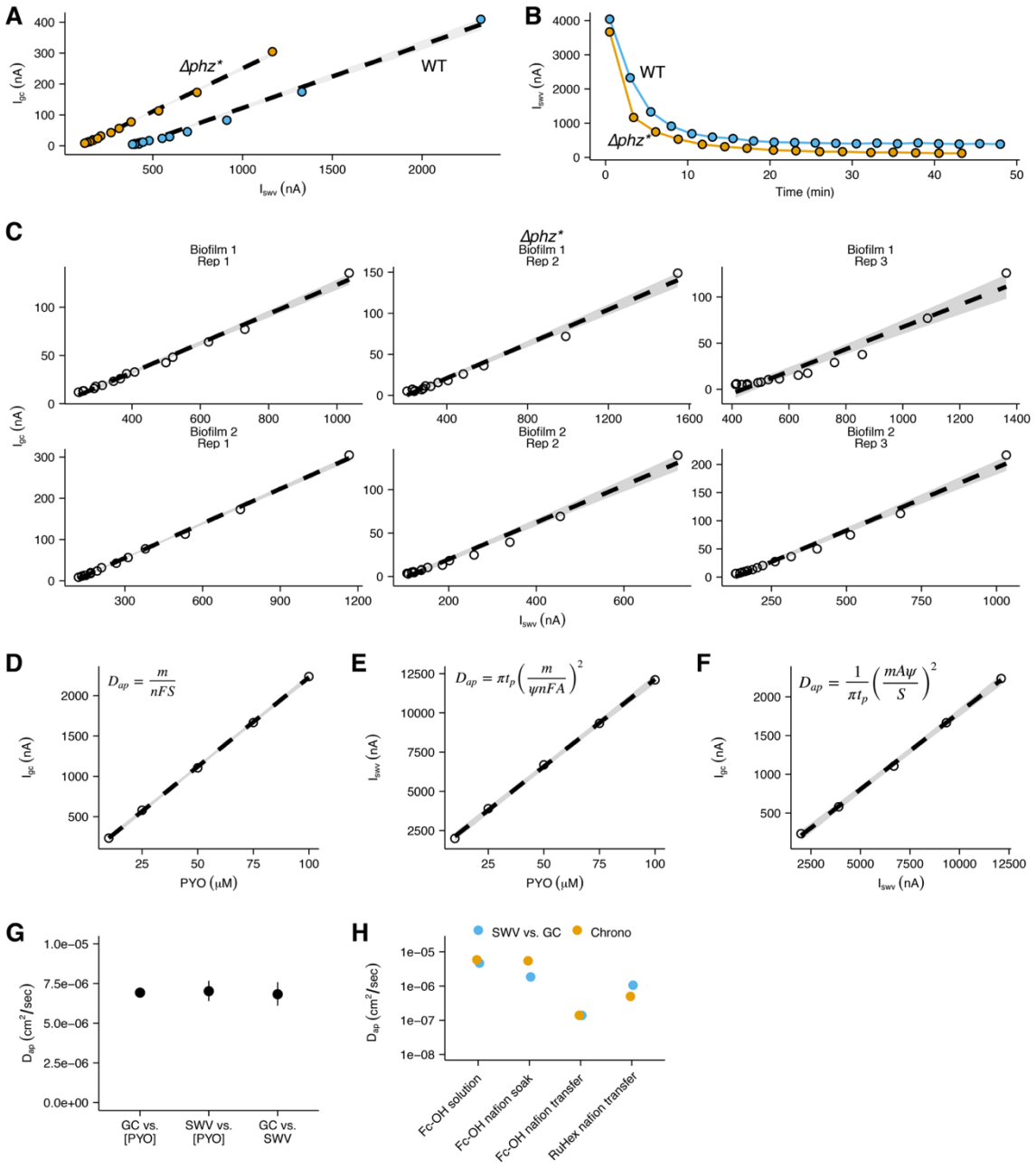

Figure S6. IDA D_{ap} measurements.

(A) Comparison of WT and Δ*phz** + PYO IDA measurements used to determine D_{ap}. (B) Comparison of WT and Δ*phz** retention of PYO signal over time. (C) Linear fits for D_{ap} analysis for two Δ*phz** IDA biofilms. Dashed lines show best fit linear models for each subset of data. Shaded regions show 95% confidence intervals from the linear models. (D) GC peak current vs. PYO concentration. The slope, *m*, is used to define D_{ap} as shown in the expression. The dashed line is a linear fit through the data points and the gray region is a 95% confidence

interval. (E) SWV peak current vs. PYO concentration in the same format as D. (F) GC peak current vs. SWV peak current in the same format as D. (G) Estimates of D_{ap} from the three methods shown in D-F with 95% confidence intervals. See supplemental text for the parameter values used. (H) D_{ap} estimates from abiotic IDA experiments with or without the polymer, Nafion, and RuHex or Fc-OH redox molecules.

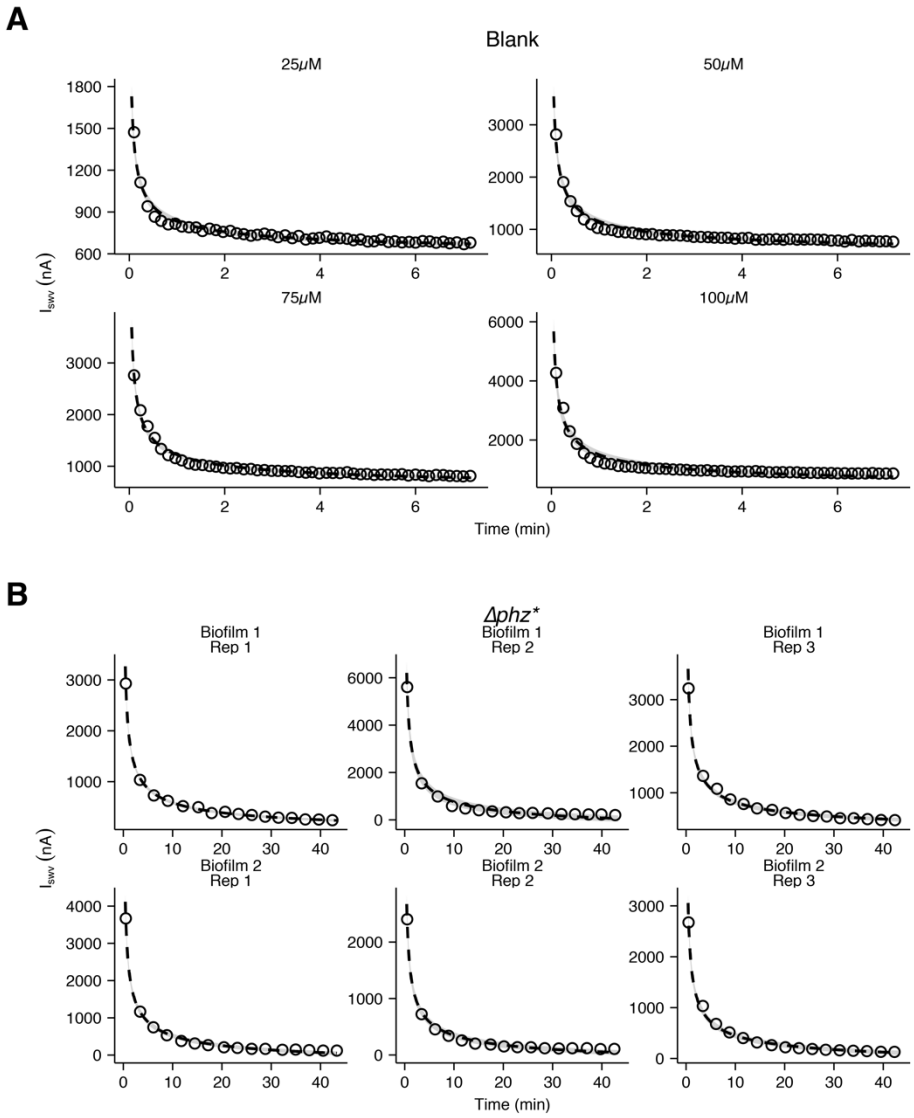

Figure S7. IDA D_{loss} measurements.

(A) Nonlinear fits for D_{loss} analysis of the blank IDA with different concentrations of PYO. Dashed lines are best fit models. Shaded regions show curves generated from the 95% confidence intervals for the parameter estimates. (B) Nonlinear fits for D_{loss} analysis of two Δ*phz** biofilms (three technical replicates each). Dashed lines are best fit models. Lines and shaded regions same as above.

Strain name	Genotype	Description
WT_DKN		*Pa* PA14 WT from Newman Lab.
Δ*phz*	Δ*phzA1-G1* Δ*phzA2-G2*	Mutant incapable of synthesizing PCA. Derivative of WT_DKN.
Δ*phz**	Δ*phzA1-G1* Δ*phzA2-G2* Δ*phzMS* Δ*phzH*	Mutant incapable of synthesizing PCA or modifying exogenous PCA. Derivative of WT_DKN, from Dietrich lab.
WT_MRP		*Pa* PA14 WT from Parsek Lab.
Δ*pel*	Δ*pelB*	Mutant incapable of synthesizing Pel polysaccharide. Derivative of WT_MRP.

Strains are all derivatives of *Pseudomonas aeruginosa* UCBPP-PA14 (Schroth et al., 2018).

Table S1. Strains used in this study.

Assay	Description	Sequence (5' – 3')
ITC 29bp duplex	Top	GTGGCAGGTCAGTCAAGTATACTGCACTA
	Bottom	TAGTGCAGTATACTTGACTGACCTGCCAC
MST PCR 80bp fragment	Forward primer	Cy3/AGAGCAGTTGGTCAAGGC
	Reverse primer	GAAAATAACGCTTGACGGAA
DNA mod electrode duplex	Top - PCN	$(NH_2)-C_6$/GCTCAGTACGACGTCGA
	Bottom WM	$(SH)-C_6$/TCGACGTCGTACTGAGC
	Bottom MM	$(SH)-C_6$/TCGACCTCGTACTGAGC

Table S2. DNA sequences used in this study.

CONCLUSIONS

In this thesis, I have tried to understand the concepts of electron shuttling broadly, and also examine the specifics of *P. aeruginosa* and phenazines in great detail. Chapter 1 discussed the vast diversity of bacterial redox molecules and the phylogenetic diversity of a particular redox-sensing transcription factor. This review suggested that despite the biosynthetic costs, electron shuttles would likely pay off for producer cells if they provide access to a limiting electron acceptor. A simple model also demonstrated that flux of small molecule electron shuttles, driven purely by their physical diffusion, would be sufficient to support survival of cells. Chapter 2 examined the well-studied *P. aeruginosa* and phenazine system where the broad questions addressed in Chapter 1 have (mostly) already been tested experimentally. This paper sought to push this understanding further by examining how the multi-phenazine electron shuttle system operates extracellularly in a complicated biofilm system. It established that certain phenazines are retained in the biofilm matrix via a binding interaction with extracellular DNA. This result along with a better understanding of phenazine based electron transfer in vivo and in vitro led to the proposal of a more detailed model of phenazine electron shuttling. Below, I will focus on a few in vitro and in vivo questions surrounding phenazine EET that may be interesting future directions.

How do phenazines function independently and/or together to achieve electron transfer from donor to acceptor? Much of my work has focused on experiments with simplified systems that contain only one phenazine at a time. Moving forward, I think it will be important to explicitly look at multi-phenazine systems. In Chapter 2, I proposed one multi-phenazine model of EET, and I believe an important step in testing this model will require some type of well-designed in vitro system coupled to theory and modeling. As mentioned at the end of the manuscript, ideally this in vitro system would be a "physicochemically well-defined matrix." Perhaps this system could be composed of agarose blocks, a series of electrodes, or a microfluidic chamber? No matter the details, it would be useful to spatially separate an electron donor and acceptor with phenazines in the intervening space. It would be valuable

to measure the overall electron transfer flux from the donor to the acceptor, and direct optical detection (absorbance, fluorescence, or Raman) of different phenazines over time would truly allow for the dissection of a complex multi-phenazine system. Such a system would be able to test interesting questions raised by the proposed model. What combination of phenazines maximizes electron transfer to O_2? How mobile is PYO in a matrix containing DNA? Does inter-phenazine electron transfer promote significant back diffusion towards the anoxic region? Maybe this perfect in vitro system will never exist, but aspects of this setup are already achievable. Importantly, these types of experiments could bridge the gap between extremely simple in vitro experiments and very complicated biofilm observations.

Where are phenazines produced and used in a biofilm? There are pieces of data that start to answer this question but building an understanding of what phenazines do where in different biofilms remains a challenging and worthy goal. Direct fluorescence measurements of phenazines in biofilms have long been a goal of the Newman lab. These measurements are complicated by high background signals from NADH and siderophores, closely overlapping spectra, and somewhat weak fluorescence. Besides some technical issues, it should be noted that only reduced phenazines are fluorescent, and PCN is not fluorescent at all. We should remain optimistic that technical issues can be overcome, and beyond fluorescence there are also new imaging modalities that may soon enable phenazine detection (e.g. Raman spectroscopy, Mass spectrometry). Direct fluorescence imaging of the different phenazines in different oxidation states would not only show where phenazines are, but it would open up a variety of modern microscopy techniques that could shed light on the proposed model from Chapter 2. For example, FRAP or FCS could be used to quantify diffusion or eDNA binding in vivo. Further, fluorescent dyes (e.g. voltage sensors) and fluorescent protein sensors (e.g. intracellular NADH) may allow microscopy to answer sophisticated physiologically questions surrounding phenazines. Without direct detection of phenazines progress could likely be made by simply using transcriptional reporters with fluorescent proteins under the control of the individual phenazine promoters (e.g. for genes *phz1*, *phz2*, *phzH*, *phzS*). Ultimately, the potential of biofilm microscopy for the study of simple and complex phenazine related questions is promising.

How are phenazines regulated and utilized by cells in biofilms? The study of phenazine EET would be greatly enhanced by a better understanding of the mechanisms cells use to regulate and cycle phenazines. Many conditions and perturbations are known to affect various aspects of phenazine production, but it is not known comprehensively what genes control the expression of which phenazine biosynthetic pathways. One approach to address this area would be to perform a genetic screen where mutant fitness (or quantification) in liquid medium is tied to the ability to express a reporter (e.g. antibiotic resistance or GFP) under the control of a phenazine promoter. Such a screen should demonstrate the effect of each mutated gene on expression from the assayed phenazine promoter. Knowledge of this regulation could generate new hypotheses about the functions or relevant conditions for certain phenazines and provide useful handles to dissect phenazine pathways in biofilms genetically or microscopically (see above). The appendix of this thesis discusses a first attempt to genetically screen for PCA cycling mechanisms in a liquid culture system. Future attempts to screen for phenazine interactions could consider other phenazines (PYO, PCN) or genetic interactions by comparing mutant libraries in WT and Δ*phz1/2* (or Δ*phzMSH* for individual phenazines) backgrounds. Perhaps it may even be possible for these screens to be performed in colony biofilms either as cells growing together or separate colonies growing individually and later pooled. Such phenazine genetic interactors could include directly interacting cellular machinery, as well as complex indirect interactions from connected cellular pathways. The study of cellular phenazine machinery will require targeted genetic and biochemical studies, but well-designed screens may yield new targets for these studies.

Despite the remaining unknowns, phenazines are a relatively convenient model system for the study of electron shuttles. However, to understand electron shuttles more broadly will require careful characterization of new redox metabolites with their associated producers. Perhaps the most valuable and most uncertain future direction is to take on this challenge. Maybe electron shuttles are only used by the few organisms we already know about. Maybe they are the tip of the iceberg. Good luck!

-Scott Saunders

A p p e n d i x

IDENTIFYING MECHANISMS OF PHENAZINE CYCLING WITH TN-SEQ

A version of this work first appeared as a written candidacy proposal from May, 2016.

Background

Pseudomonas aeruginosa is an effective chronic pathogen that forms recalcitrant biofilms. This gram-negative bacterium infects ~51,000 (CDC report 2013) hospital patients every year (nosocomial infections), and it is particularly infamous for residing in the lungs of cystic fibrosis patients where it can cause lung function decline and ultimately death. This organism is difficult to treat because it forms heterogeneous biofilms that resist desiccation, antibiotic treatment, and nutrient limitation. Biofilms are groups of cells attached to a surface, encapsulated in matrix composed of extracellular polymeric substances (EPS) such as extracellular DNA (eDNA), polysaccharides, lipids, and proteins (Flemming 2010). This biofilm lifestyle confers many advantages, but cells must also cope with the metabolic challenges of living in dense, sessile communities. Even in human lungs, evidence suggests that *P. aeruginosa* biofilms actually use anaerobic metabolisms to survive (Cowley 2015). Despite an atmosphere of 21% O_2, a steep oxygen gradient forms as cells at the periphery of the biofilm respire faster than the gas can diffuse to the center of the community, leaving oxygen levels below ~8 μM required for aerobic respiration (Wimpenny 1979, Glasser 2014, Kempes 2014). Consequently, cells use alternative metabolisms, such as nitrate respiration, pyruvate fermentation, and a poorly understood strategy called electron shuttling to survive.

Phenazines are redox-active metabolites produced by *P. aeruginosa* that serve as electron shuttles, enabling survival during electron acceptor limitation. Pyocyanin, phenazine-1-carboxylate (PCA), phenazine-1-carboxamide (PCN), and 1-hydroxyphenazine (1-OHPHZ) are the four phenazines produced by *P. aeruginosa*, and their distribution is tightly regulated by environmental conditions. These molecules are heterocyclic aromatic rings with two nitrogens in the center ring that undergo redox reactions accepting up to two electrons and

two protons. They have variable midpoint potentials and reactivities dependent on their side groups, for example, pyocyanin has a midpoint potential -40mV (vs. NHE at pH 7) and reacts fastest with O_2 (Wang 2008). This redox activity is central to phenazines' role as electron shuttles that transfer metabolic electrons to external electron acceptors. The conceptual model of electron shuttling involves four cyclical steps (see Figure 1A-B): 1) Oxidized shuttle (phenazine) is reduced intracellularly, which is coupled to substrate oxidation and energy generation, 2) Reduced shuttles are expelled from the cell into the biofilm matrix, 3) A reduced shuttle reacts with an electron acceptor (*e.g.* oxygen) abiotically, 4) The cell uptakes an oxidized shuttle, which can now accept more metabolic electrons.

This electron shuttling model has been supported by two key experiments with *P. aeruginosa* and its phenazine metabolites. The first experiment uses the colony biofilm as a model system, where cells are grown as colonies on agar plates containing a red dye. Wildtype (WT) and a mutant in phenazine biosynthesis (Δ*phz*) exhibit dramatically different colony morphologies in this assay, where WT is relatively thick and smooth, while Δ*phz* is thin and wrinkles drastically (Dietrich 2013). It was shown that WT biofilms have a steep oxygen gradient, but Δ*phz* biofilms are thin enough to allow oxygen to diffuse relatively uniformly. An analogous experiment called the Phenazine Cycling Survival Assay (PCSA), approximated the conditions of a biofilm, but used liquid media and allowed for control and measurement of several key parameters. The PCSA forces all cells to use an electron shuttling metabolism, since the only electron acceptor is exogenous phenazine and an electrode reoxidizes phenazine (Glasser 2014, Wang 2010). In this highly controlled system, cells can survive for 2-3 days independent of phenazine cycling, and then exhibit phenazine-dependent survival for several weeks (see Figure 1C). These results show that phenazine electron shuttling plays important roles in biofilm development and anaerobic survival.

This study seeks to leverage the significant advantages of working with the model organism *Pseudomonas aeruginosa*, but also to elucidate a broader electron shuttling paradigm that may apply to the shocking variety of microorganisms that exist. Over 36,000 microbial

isolates have sequenced genomes available on the Integrated Microbial Genomes database, and these genomes are predicted to contain more than 600,000 biosynthetic clusters encoding capabilities to synthesize 'secondary metabolites' (Hadjithomas 2016). For many years, people believed that phenazines were merely 'secondary metabolites' of lesser importance than other metabolites used by the cell for energy generation. It is clear that these molecules are essential for bacteria in the environment, and it is very likely that diverse secondary metabolites in other organisms play critical physiological roles for their producers. Perhaps even some of them are electron shuttles too.

Approach

To efficiently shuttle electrons, phenazines must be reduced and transported across the cell membrane, but the molecular mechanisms underpinning these activities are almost entirely unknown. A major challenge to identifying such genes has been the inability to perform a genetic screen specific for phenazine cycling. This was because of the technical complexity of the PCSA, and the fact that phenazine cycling only supports survival, not growth. During my first year in the Newman Lab, I planned and executed a method to genetically screen for genes involved in phenazine cycling.

Because survival requires efficient phenazine cycling in the PCSA, knocking out genes important for the process should cause cells to die, even when phenazine and electrode are both present. Several mutants have been characterized individually in this manner, and Glasser et al. showed that certain metabolic genes are required to couple phenazine cycling to energy generation (Glasser 2014). I performed a high throughput genetic screen using the PCSA and a method known as Tn-seq (Opijnen 2014). This method makes use of a highly saturated transposon library and Illumina sequencing libraries to simultaneously track transposon mutants' relative abundance under a condition of interest in a single vessel. This method is described in detail in the paper and thesis by David Basta (Basta 2017 & 2019) and the same wildtype transposon library was used. I compared samples from the phenazine-dependent survival phase to the control condition (phenazine-independent survival), see Figure 1C. Illumina libraries from transposon–genome junctions were sequenced, and reads

were processed bioinformatically, yielding a relative abundance of individual transposon mutants falling in each gene. Adjusted p-values were calculated using DeSeq.

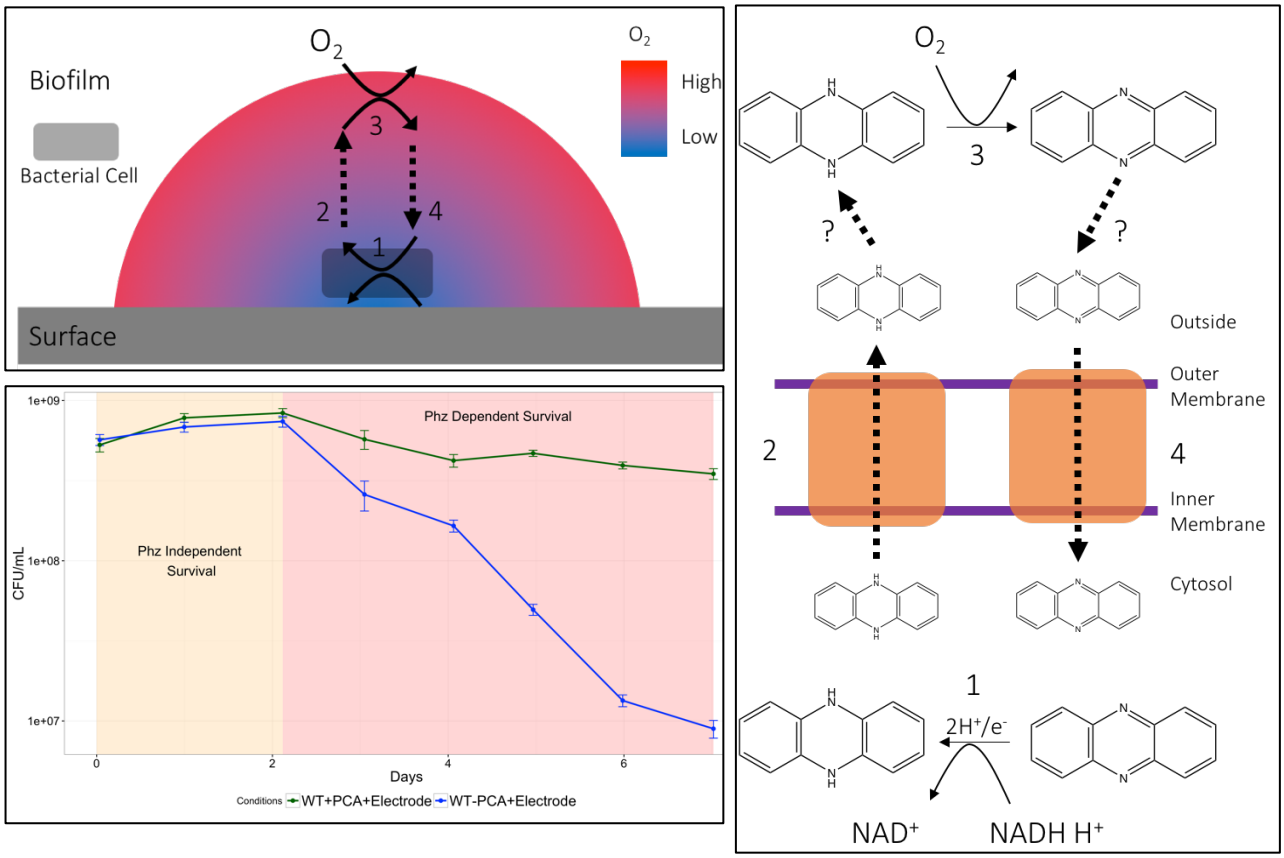

Figure 1. Phenazine cycling and survival. (A) (Top left). Electron shuttling in an oxygen-limited biofilm. (B) (Right). Electron shuttling conceptual model at the molecular level. Orange figures represent putative transporters. (C) (Bottom left). PCSA results showing phases of survival from single chambers. Error bars are standard error of CFU counts. Arrows indicate times when Tn-seq samples were taken.

Results

The Tn-seq screen recapitulated previously known phenotypes and successfully quantified relative abundance of nearly all non-essential *P. aeruginosa* genes. With clean deletions, Glasser et al. showed that *ackA* and *pta* play essential roles in energy generation coupled to phenazine cycling (Glasser 2014). In my preliminary Tn-seq screen, the corresponding Tn-seq mutants had strong disadvantages as expected (Fig. 2). Over 5200 genes had transposon

mutants in the population with more than 100 reads at Day 0. Of those, mutants in 68 genes showed decreases in relative abundance by more than two-fold and mutants in 51 genes showed increases greater than two-fold (comparing day 2 to day 7). These data suggest that the screen was effective and specific, and it is exciting to think that the dataset may contain many of the phenazine cycling mechanisms outlined in Figure 1.

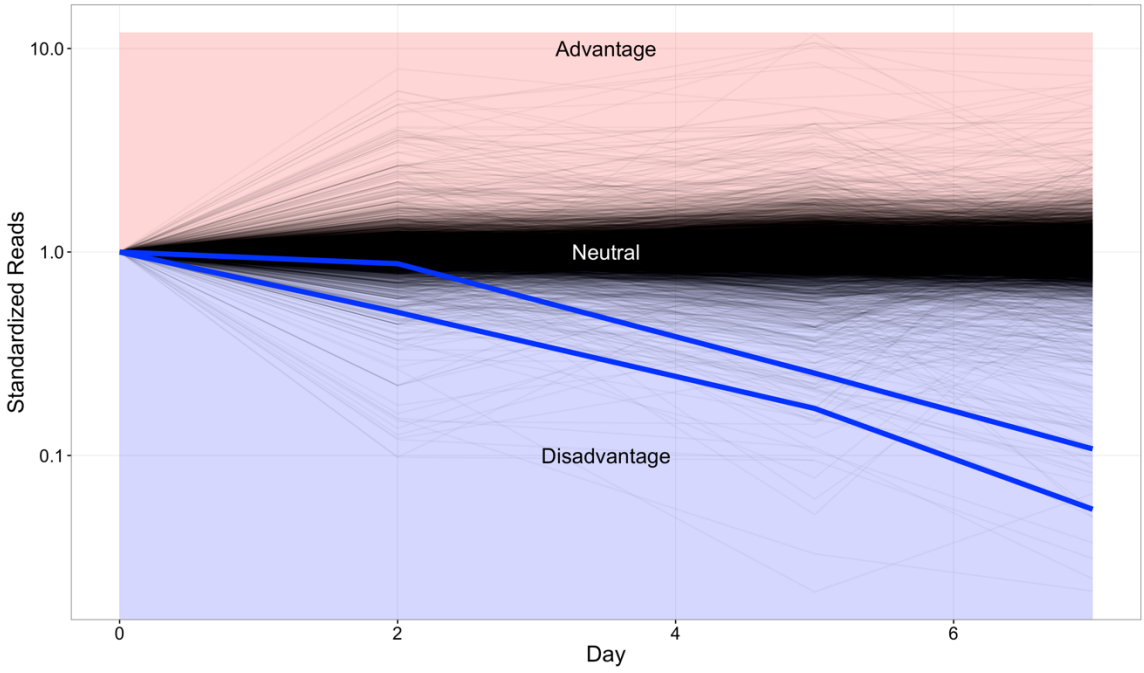

Figure 2. Tn-seq read counts for every gene. Blue lines show positive control genes *ackA* and *pta.*

The tables below show some of the strongest effects observed in the screen. Table 1 reports transposon mutants that had at least 4-fold disadvantages from day 2 to day 7 with high enough read counts to yield low adjusted p-values. There are many other genes that had at least 2-fold advantages. Please refer to the supplemental data files to fully explore the data. Table 2 reports transposon mutants that had at least a 2-fold statistically significant advantage. As suggested by Figure 2 and Table 2, more mutants had disadvantages than advantages, although most mutants have no effect (neutral). For each entry in the table, there is a PA14 locus number that can be searched in various databases by appending the number (e.g. 'PA14_00000'). Next, there is a product name which may be useful for well

characterized genes. For poorly characterized genes, these descriptions are less useful, but with some basic searches more specific information can often be found. There are also raw read counts for the four different time point libraries. Total read counts were similar between libraries, so no normalization was performed.

There are countless interesting hits in this screen that are worth exploring, but we can try to make sense of the effects broadly as a starting point. Besides the known phenazine-dependent survival metabolism genes, *ackA* and *pta*, there are many genes that are likely connected to central metabolism. The PCSA is well documented in Suzanne Kern's thesis (Kern 2013) and it requires cells to metabolize glucose. This condition might explain the effect of mutants in glucokinase (PA14_22930), transaldolase B (PA14_27960), phosphoenolpyruvate synthase (PA14_41670), glyceraldehyde-3-phosphate (PA14_25250), aldolase (PA14_23090), ribose-5-phosphate isomerase (PA14_04310), and others with weaker disadvantages. Simple realities of the medium condition may explain other genes in these lists, for example. The putative ABC transporter (PA14_69060-69090) also showed up in David Basta's pyruvate survival Tn-seq (Basta 2017 & 2019) and may transport a carbon compound or do something entirely different. Argininosuccinate lyase (PA14_69500) may be important for synthesizing arginine (which can also be used for survival), but it may be an ammonia detoxification mechanism, since the PCSA is done at high ammonium concentrations. Similarly, the sulfate transporter (PA14_43200) and phosphate uptake regulator *phoU* (PA14_70800) may affect cell's ability to utilize sulfur and phosphorus sources effectively.

There are well-known broad effectors that could control many relevant genes – *fleN* (PA14_45640), *anr* (PA14_44490), *lasR* (PA14_45960), *ftsH* (PA14_62860), *lon* protease (PA14_41220), pseudomonas quinolone signal *pqsA-E,* and others. However, more specifically there are two repressors of efflux pumps *nfxB* (PA14_60860), *mexR* (PA14_05520) and a transporter associated oxidoreductase, *mexS* (PA14_32420). Phenazines are likely pumped by many redundant RND efflux pumps (*mex* prefixes), so it seems possible that mutation of these repressors either overexpresses the pumps that do not

actually affect phenazines or overexpresses the cognate pumps at such high levels that the phenazines cannot be effectively reduced for metabolism. It is also possible that there is simply a high burden of expressing these efflux systems. Lastly, there are poorly characterized transcriptional regulators that may be interesting if they are specific to this condition.

Perhaps the most exciting hits in the screen are the hypotheticals. There are many, but one set is particularly compelling: PA14_17550, 17570, 17580. These mutants are all in table 1 below and therefore have very strong, statistically significant disadvantages. Their annotations are relatively vague, but PA14_17550 does have ortholog group members that are annotated as ubiquinol oxidase subunits. PA14_17570 has a beta lactamase domain among others. PA14_17580 may bind thiamine and be involved in carbohydrate metabolism. There is no obvious connection, but maybe one day their strong effects will be clear.

In pursuing specific hits from this screen to look for phenazine-related genes, I would suggest a few general strategies. First, look for strong effects with >100 reads. One simple way to do this is to color-code the effect size and the adjusted p-value. Furthermore, promising hits' read counts should follow the phenazine dependence of survival, where counts remain similar from day 0 to 2, and then decline successively on days 5 and 7. Second, look for multiple genes in an operon. This is simple by sorting the supplemental spreadsheet by locus number. Certainly, there are real effects on just one gene of an operon, but higher confidence can be placed on entire operons that have significant effects for every gene. Third and most important, compare this Tn-seq dataset to David Basta's Tn-seq datasets. (Basta 2017). In particular, his pyruvate survival is quite similar to the PCSA. Therefore, genes that are specific to this dataset are more likely to be specific to phenazines. Related to this suggestion, this Tn-seq dataset can also be compared to other genome-wide datasets acquired in the Newman Lab: colony biofilm morphology screen, phenazine reduction screen (Price-Whelan 2009), RNAseq.

Locus	Product_Name	time_0	time_2	time_5	time_7	log2 fold change	p-value
17570	hypothetical_protein_beta_lactamase	589	421	149	34	-3.66	1.20E-16
05520	multidrug_resistance_operon_repressor_MexR	7822	6114	1616	508	-3.62	3.29E-50
45640	flagellar_synthesis_regulator_FleN	186	77	23	8	-3.30	1.02E-03
44490	transcriptional_regulator_Anr	257	288	109	30	-3.29	1.40E-09
17550	hypothetical_protein_cytochrome D ubiquinol oxidase subunit II	582	519	140	55	-3.27	1.89E-15
00210	lysin_domain-containing_protein	2086	1753	514	189	-3.24	3.16E-30
53470	acetate_kinase	1575	902	314	99	-3.22	1.22E-23
07730	dimethyladenosine_transferase	3639	3992	1040	477	-3.09	6.69E-35
53480	phosphate_acetyltransferase	3848	3817	1144	479	-3.02	1.08E-33
25050	hypothetical_protein	144	176	35	23	-2.96	8.01E-05
27960	transaldolase_B	768	867	291	124	-2.83	1.20E-16
69060	ABC_transporter_permease	883	151	34	22	-2.81	6.12E-08
62860	cell_division_protein_FtsH	3718	2275	966	354	-2.71	8.74E-26
65750	outer_membrane_efflux_protein	1325	952	232	151	-2.69	3.45E-17
16790	TetR_family_transcriptional_regulator	424	578	179	93	-2.66	4.01E-11
69090	hypothetical_protein	1992	344	256	57	-2.62	2.48E-13
17580	hypothetical_protein	2250	1341	497	235	-2.54	3.00E-19
22930	glucokinase	1379	938	391	169	-2.50	1.17E-15
41670	phosphoenolpyruvate_synthase	486	388	185	72	-2.46	1.56E-08
18080	TetR_family_transcriptional_regulator	8825	7897	3385	1623	-2.31	6.14E-24
60860	transcriptional_regulator_NfxB	1122	451	200	95	-2.28	6.48E-10
45960	transcriptional_regulator_LasR	1371	1317	772	278	-2.27	4.77E-15
69500	argininosuccinate_lyase	1711	1194	422	268	-2.18	1.00E-13
32420	oxidoreductase mexS	78803	78471	34437	18479	-2.12	1.39E-22
04310	ribose-5-phosphate_isomerase_A	240	241	118	57	-2.11	3.57E-04
43200	sulfate_transporter	423	273	117	67	-2.06	5.54E-05
25250	glyceraldehyde-3-phosphate_dehydrogenase	164	158	98	40	-2.01	1.13E-02

Table 1. Transposon mutants with disadvantages. Entries contain PA14 locus numbers, putative product names, read counts from each timepoint, log2 transformed fold changes from days 2 to 7, and adjusted p-values for multiple testing.

Locus	Product_Name	time_0	time_2	time_5	time_7	log2 fold change	p-value
23090	keto-hydroxyglutarate-aldolase/keto-deoxy-_phosphogluconate_aldolase	259	398	782	1225	1.59	1.37E-06
15830	GntR_family_transcriptional_regulator	587	814	1537	2432	1.55	2.01E-08
47540	outer_membrane_protein	428	926	1630	2520	1.42	4.61E-07
41680	hypothetical_protein	194	205	452	528	1.34	5.77E-03
18230	DNA-binding_transcriptional_regulator_FruR	446	636	1061	1545	1.25	1.06E-04
44470	coproporphyrinogen_III_oxidase	768	1047	1986	2517	1.24	1.47E-05
70800	phosphate_uptake_regulatory_protein_PhoU	152	265	440	626	1.21	1.37E-02
23060	DNA-binding_transcriptional_regulator_HexR	706	802	1221	1741	1.09	8.83E-04
41220	Lon_protease	744	757	1390	1528	0.98	5.77E-03

Table 2. Transposon mutants with advantages. Entries contain PA14 locus numbers, putative product names, read counts from each timepoint, log2 transformed fold changes from days 2 to 7 and adjusted p-values for multiple testing.

One interesting gene from the Tn-seq screen is *hemN1*, which codes for a coproporphyrinogen oxidase in heme biosynthesis (see Figure 3). Heme is of particular interest because it is known to play an essential role in extracellular electron transfer via multiheme cytochromes that transport electrons across membranes in *Geobacter* and *Shewanella* (Snider 2012). Transposon mutations in *hemN1* conferred a strong fitness advantage, while most other mutants in the heme biosynthesis pathway had few reads or were disadvantageous, see *hemC* in Table 1. *hemN1* is redundant, so it is expected that the mutation would increase flux to a heme precursor, coproporphyrin III without totally eliminating heme production (Rompf 1998). Coproporphyrin is known to bind bacterioferritin in rare cases, which scavenges iron (Ramao 2000). However, it is unclear how this change affects heme biosynthesis or other processes.

As an example workflow, the *hemN1* gene and the importance of heme more broadly can be characterized by many techniques already available in the Newman lab. 1)Transposon mutants from an existing library can be used to quickly confirm phenotypes. 2) Clean deletions can be made to avoid unintended transposon effects, such as polarity on downstream genes. 3) Whole cell phenazine reduction rate can be quantified. 4) Intracellular redox pools can be quantified by measuring the NAD^+/NADH ratio. 5) Porphyrins and heme

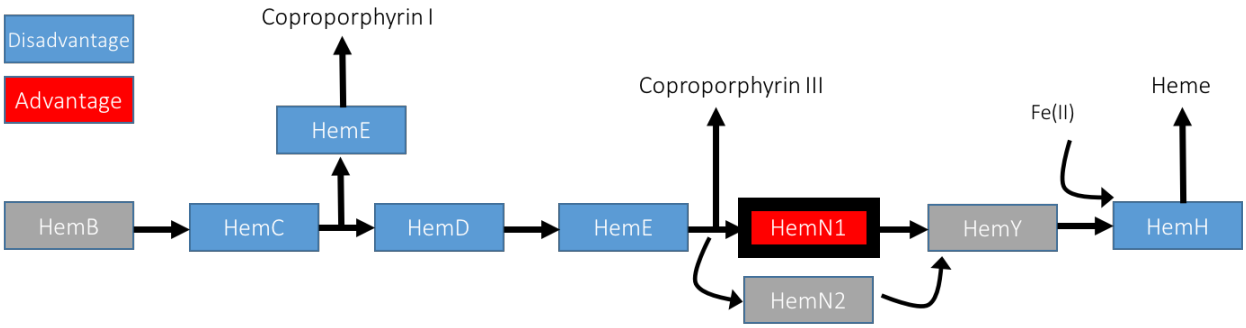

Figure 3. Heme biosynthetic pathway of *P. aeruginosa* with Tn-seq data color-coded. Grey boxes indicate that there was a neutral or undetermined effect of the transposons.

can be quantified spectrophotometrically by HPLC and staining of cell lysate. These assays would indicate whether heme proteins are responsible for phenazine reduction activity and coupled to intracellular redox pools, and would determine whether a strategy to identify specific porphyrin-binding proteins is warranted. It is reasonable to look at the heme cofactor because past genetic and biochemical evidence from the Newman lab suggests that multiple proteins could play a role in phenazine reduction (Glasser 2017).

Conclusion

P. aeruginosa and other microorganisms evolved to live in biofilm communities where they can masterfully survive in an unpredictable world. By characterizing the cellular mechanisms and extracellular electrochemistry of phenazine cycling, paradigms of electron shuttling will be concretely developed. This mode of anaerobic metabolism could be an important mechanism by which this opportunistic pathogen survives, and knowledge from this project could directly inform clinical studies. Lastly, the protein sequences of cycling mechanisms and chemical properties of phenazines will lay the foundation for the exploration of the diverse microbial world for this amazing metabolism.

Data availability

Supplemental files are included in this thesis containing tables with read counts. Raw sequencing data is available on the Newman Lab NAS.

Acknowledgements

Thank you to Dianne Newman and the entire Newman lab for providing a supportive, collaborative research environment. Specifically, this work would not have been possible without David Basta who created the transposon library for Tn-seq, Megan Bergkessel who helped with the Tn-seq library preparation and data analysis, and Nate Glasser who taught me the PCSA.

References

Hadjithomas, M. et al. IMG-ABC: A knowledge base to fuel discovery of biosynthetic gene clusters and novel secondary metabolites. mBio 6, e00932–15 (2015).

Glasser, N., Kern, S. & Newman, D. Phenazine redox cycling enhances anaerobic survival in *Pseudomonas aeruginosa* by facilitating generation of ATP and a proton-motive force. Molecular Microbiology 92, 399–412 (2014).

Wang, Y., Kern, S. & Newman, D. Endogenous phenazine antibiotics promote anaerobic survival of *Pseudomonas aeruginosa* via extracellular electron transfer. Journal of Bacteriology 192, 365–369 (2010).

Flemming, H.-C. & Wingender, J. The biofilm matrix. Nature Reviews Microbiology (2010). doi:10.1038/nrmicro2415

Wang, Y. & Newman, D. Redox reactions of phenazine antibiotics with ferric (hydr)oxides and molecular oxygen. Environmental Science & Technology 42, 2380–2386 (2008).

Van Opijnen, T. & Lazinski, D.W. Genome-wide fitness and genetic interactions determined by Tn-seq, a high-throughput massively parallel sequencing method for microorganisms. Current Protocols in Microbiology (2014). doi:10.1002/0471142727.mb0716s106

Wimpenny, J. & Parr, J.A. Biochemical differentiation in large colonies of Enterobacter cloacae. Microbiology (1979).

Deng, X. et al. Proteome-wide quantification and characterization of oxidation-sensitive cysteines in pathogenic bacteria. Cell Host & Microbe 13, 358–370 (2013).

Romão, C. et al. Iron-coproporphyrin III is a natural cofactor in bacterioferritin from the anaerobic bacterium Desulfovibrio desulfuricans. FEBS Letters 480, 213–216 (2000).

Rompf, A. et al. Regulation of *Pseudomonas aeruginosa* hemF and hemN by the dual action of the redox response regulators Anr and Dnr. Molecular microbiology 29, 985–997 (1998).

CDC threat report. (2013). http://www.cdc.gov/drugresistance/threat-report-2013/pdf/ar-threats-2013-508.pdf#page=69

Kempes, C. P., Okegbe, C., Mears-Clarke, Z., Follows, M. J., & Dietrich, L. E. Morphological optimization for access to dual oxidants in biofilms. Proceedings of the National Academy of Sciences *111*(1), 208-213 (2014).

Dietrich L et al. Bacterial Community morphogenesis is intimately linked to the intracellular redox state. Journal of Bacteriology 195,1371–1380 (2013).

Sullivan NL, Tzeranis DS, Wang Y, So PT, Newman D. Quantifying the dynamics of bacterial secondary metabolites by spectral multiphoton microscopy. ACS Chemical Biology 6,893–9 (2011).

Costa, KC, Bergkessel, M, Saunders, S & Korlach, J. Enzymatic degradation of phenazines can generate energy and protect sensitive organisms from toxicity. mBio (2015).

Shigeta, M., Tanaka, G., Komatsuzawa, H., Sugai, M., Suginaka, H. and Usui, T. Permeation of antimicrobial agents through *Pseudomonas aeruginosa* biofilms: a simple method. Chemotherapy, 43(5), 340-345. (1997).

Hernandez, M. E. & Newman, D. K. Extracellular electron transfer. Cellular and Molecular Life Sciences CMLS 58, 1562–1571 (2001).

Friedheim, E. Pyocyanine, an accessory respiratory enzyme. The Journal of Experimental Medicine (1931).

Price-Whelan, A., Dietrich, L. & Newman, D. Rethinking 'secondary' metabolism: Physiological roles for phenazine antibiotics. Nature Chemical Biology 2, 71–78 (2006).

Bellin, D., Sakhtah, H., Rosenstein, J., Levine, P., Thimot, J., Emmett, K., Dietrich, L. and Shepard, K. Integrated circuit-based electrochemical sensor for spatially resolved detection of redox-active metabolites in biofilms. Nature Communications (2014).

Basta, D.W. Genetic Determinants of Growth Arrest Survival in the Bacterial Pathogen *Pseudomonas aeruginosa* and the Role of Proteases. Dissertation (Ph.D.), California Institute of Technology (2019).

Price-Whelan, A.M. Physiology and Mechanisms of Pyocyanin Reduction in *Pseudomonas aeruginosa*. Dissertation (Ph.D.), California Institute of Technology (2009).

Kern, S.E. Consequences of redox-active phenazines on the physiology of the opportunistic pathogen *Pseudomonas aeruginosa*. Dissertation (Ph.D.), Massachusetts Institute of Technology (2013).

Basta, D. W., Bergkessel, M., & Newman, D. K. Identification of fitness determinants during energy-limited growth arrest in *Pseudomonas aeruginosa*. mBio 8: e01170-17. (2017).

Glasser, N. R., Wang, B. X., Hoy, J. A., & Newman, D. K. The pyruvate and α-ketoglutarate dehydrogenase complexes of *Pseudomonas aeruginosa* catalyze pyocyanin and phenazine-1-carboxylic acid reduction via the subunit dihydrolipoamide dehydrogenase. Journal of Biological Chemistry, *292*(13), 5593-5607. (2017).